การสังเคราะห์และการตรึงโปรตีนของพอลิอะคริลิกแอซิดบรัช
สำหรับการเพาะเลี้ยงเซลล์ต้นกำเนิด

นางสาวศศิธร รอดท่าไม้

SYNTHESIS AND PROTEIN IMMOBILIZATION OF POLY(ACRYLIC ACID) BRUSHES
FOR STEM CELL CULTURE

Miss Sasithon Rodtamai

A Thesis Submitted in Partial Fulfillment of the Requirements

for the Degree of Master of Science Program in Chemistry

Department of Chemistry

Faculty of Science

Chulalongkorn University

Academic Year 2009

Thesis Title   SYNTHESIS AND PROTEIN IMMOBILIZATION OF
                        POLY(ACRYLIC ACID) BRUSHES
                        FOR STEM CELL CULTURE
By   Miss Sasithon Rodtamai

Field of Study   Chemistry

Thesis Advisor   Associate Professor Voravee P. Hoven, Ph.D.

Thesis Co-Advisor   Assistant Professor Nipan Israsena Na Ayudhaya, M.D., Ph.D.

Accepted by the Faculty of Science, Chulalongkorn University in Partial Fulfillment of the Requirements for the Master's Degree

…………………………………………Dean of the Faculty of Science

(Professor Supot Hannongbua, Dr.rer.nat.)

THESIS COMMITTEE

………………………………………….Chairman

(Assistant Professor Warinthorn Chavasiri, Ph.D.)

…………………………………….....Thesis Advisor

(Associate Professor Voravee P. Hoven, Ph.D.)

…………………………………….....Thesis Co-Advisor

(Assistant Professor Nipan Israsena Na Ayudhaya, M.D., Ph.D.)

………………………………………….Examiner

(Assistant Professor Varawut Tangpasuthadol, Ph.D.)

………………………………………….External Examiner

(Assistant Professor Punnama Siriphannon, D.Eng.)

ศศิธร   รอดท่าไม้: การสังเคราะห์และการตรึงโปรตีนของพอลิอะคริลิกแอซิดบรัซสำหรับการเพาะเลี้ยงเซลล์ต้นกำเนิด (SYNTHESIS AND PROTEIN IMMOBILIZATION OF POLY(ACRYLIC ACID) BRUSHES FOR STEM CELL CULTURE.) อ.ที่ปรึกษาวิทยานิพนธ์หลัก: รองศาสตราจารย์ ดร.วรวีร์ โฮเว่น, อ.ที่ปรึกษาวิทยานิพนธ์ร่วม: ผู้ช่วยศาสตราจารย์ นพ.ดร.นิพัญจน์ อิศรเสนา ณ อยุธยา, 108 หน้า.

เตรียมพอลิอะคริลิกแอซิด (พีเอเอ) บรัซที่ตรึงบนพื้นผิวโดยปฏิกิริยาแอคติเวเตอร์รีเจนเนอเรตอิเล็กตรอนทรานส์เฟอร์อะตอมทรานส์เฟอร์แรดิคัลพอลิเมอไรเซชันที่ริเริ่มจากพื้นผิวกระจกของเทอร์เทียรีบิวทิวอะคริเลต ตามด้วยไฮโดรไลซิสด้วยมีเทนซัลโฟนิกแอซิด จากการใช้ภาวะในการทำปฏิกิริยาที่ให้ผลดีที่สุด พอลิ(เทอร์เทียรีบิวทิวอะคริเลต)บรัซที่เตรียมได้มีความหนาแน่นการกราฟต์ประมาณ 0.33 โซ่/ตารางนาโนเมตร ความหนาแน่นของหมู่คาร์บอกซิลของพีเอเอบรัซขึ้นกับความยาวโซ่หรือน้ำหนักโมเลกุล ซึ่งมีค่าอยู่ในช่วง 0.7×10^{-9} to 1.6×10^{-9} โมล/ตารางเซนติเมตร โดยพบว่าหมู่คาร์บอกซิลของพีเอเอบรัซสามารถติดบีเอสเอและเพปไทด์ที่เป็นวงซึ่งเลียนแบบเอ็นแคดฮีรินได้ นอกจากนี้ยังยืนยันการดัดแปรพื้นผิวแต่ละขั้นตอนที่เกี่ยวข้องกับการเกิดพอลิเมอร์บรัซและการตรึงโปรตีน/เพปไทด์ได้โดยการวิเคราะห์ด้วยเอทีอาร์เอฟทีไออาร์และการวัดมุมสัมผัสของน้ำ จากการทดสอบความเป็นพิษกับเซลล์ประสาทของหนูพบว่าพีเอเอบรัซที่ตรึงด้วยเพปไทด์ที่เป็นวงเลียนแบบเอ็นแคดฮีริน ไม่เป็นพิษต่อเซลล์และให้ระดับความเข้ากันได้กับเซลล์เทียบเท่ากับพื้นผิวที่เคลือบด้วยลามินินซึ่งเป็นโปรตีนที่ใช้ในการเพาะเลี้ยงเซลล์ต้นกำเนิด แสดงให้เห็นถึงศักยภาพของวัสดุดังกล่าวในการประยุกต์สำหรับการเพาะเลี้ยงเซลล์ต้นกำเนิด

ภาควิชา	เคมี	ลายมือชื่อนิสิต	
สาขาวิชา	เคมี	ลายมือชื่ออ.ที่ปรึกษาวิทยานิพนธ์หลัก	
ปีการศึกษา	2552	ลายมือชื่ออ.ที่ปรึกษาวิทยานิพนธ์ร่วม	

5072481423 : MAJOR CHEMISTRY

KEYWORDS: PAA / POLYMER BRUSHES / ARGET ATRP / SURFACE MODIFICATION

SASITHON RODTAMAI: SYNTHESIS AND PROTEIN IMMOBILIZATION OF POLY(ACRYLIC ACID) BRUSHES FOR STEM CELL CULTURE. THESIS ADVISOR: ASSOC. PROF. VORAVEE P. HOVEN, Ph.D., THESIS CO-ADVISOR: ASST. PROF. NIPAN ISRASENA NA AYUDHAYA, M.D., Ph.D., 108 pp.

Surface-tethered poly(acrylic acid) (PAA) brushes were prepared by surface initiated polymerization of *tert*-butyl acrylate from glass substrates via activator regenerated by electron transfer atom transfer radical polymerization (ARGET ATRP) followed by hydrolysis using methanesulfonic acid. Upon using an optimized condition, poly(*tert*-butyl acrylate) brushes having a graft density of approximately 0.33 chains/nm^2 were obtained. Carboxyl group density of the PAA brushes can be varied as a function of the chain length or molecular weight ranging from 0.7 x10^{-9} to 1.6 x10^{-9} mol/cm^2. It has been demonstrated that the carboxyl groups of PAA brushes are readily available for attachment of BSA and N-cadherin mimic cyclic peptide. The successive surface modification via polymer brushes formation and protein/peptide immobilization were also verified by ATR-FTIR analysis and water contact angle measurements. According to cytotoxicity test against mouse neural progenitor cell, it was found that the immobilized N-cadherin mimic cyclic peptide on PAA brushes was non toxic and provided a level of cell compatibility equivalent to that of the surface coated with laminin, a commonly used adhesive protein for stem cell culture suggesting its potential in stem cell culture applications.

Department : _____Chemistry_____   Student's Signature _____

Field of Study : _____Chemistry_____   Advisor's Signature _____

Academic Year : _____2009_____   Co- Advisor's Signature _____

ACKNOWLEDGEMENTS

CONTENTS

LIST OF TABLES

LIST OF FIGURES

LIST OF SCHEMES

LIST OF ABBREVIATIONS

AFM : Atomic force microscopy

ATRP : Atom transfer radical polymerization

ARGET ATRP : Activator regenerated by electron transfer for

atom transfer radical polymerization

t-BuA : *tert*-Butyl acrylate

$CDCl_3$: Deuterated chloroform

CuBr : Copper (I) bromide

$CuBr_2$: Copper (II) bromide

°C : Degree Celsius

d : doublet

D_2O : Deuterium oxide

DP : Degree of polymerization

Eq. : Equation

FTIR : Fourier transform infrared

GPC : Gel permeation chromatography

k_{act} : The activation rate parameter

k_{deact} : The deactivation rate parameter

k_{eq} : The equilibrium rate parameter

m : multiplet

m° : millidegree

mg : miligram

min : minute

mL : mililiter

mm	: milimeter
mM	: milimolar
mmol	: milimole
$\overline{M}_n$	: Number average molecular weight
$\overline{M}_w$	: Weight average molecular weight
mNSC	: mouse neural progenitor cell
nm	: nano meter
NMR	: Nuclear magnetic resonance spectroscopy
PAA	: Poly(acrylic acid)
P*t*BuA	: Poly(*tert*-butyl acrylate)
ppm	: part per million
s	: singlet
SPR	: Surface Plasmon Resonance
THF	: Tetrahydrofuran
μL	: microliter
Θ_A	: advancing contact angle
Θ_R	: receding contact angle

CHAPTER I

INTRODUCTION

1.1   Statement of problem

Stem cells are defined as a progeny of cells that are capable of self-renewal and differentiation into a variety of specialized cell types. They are key biological components required for cellular therapies, of which goal is to repair damaged organs and tissues *in vivo* as well as generating tissue constructs *in vitro* for subsequent transplantation. Recently, stem cell treatment has become an alternative medical therapy to conventional treatment methods. Culturing stem cells *in vitro* in order to generate a number of stem cells, especially embryonic stem (ES) cells, to be high enough for practical clinical usage is still not successful. The conventional method usually relies on the mouse embryonic skin cells that have been treated and coated at the bottom of the culture dish. This coating layer or so-called feeder layer provides the inner cell mass of cells a sticky surface to which they can attach. Also, the feeder cells release nutrients into the culture medium. This method possesses a risk that viruses or other macromolecules in the mouse cells may be transmitted to the human cells. And very often, stem cells cannot maintain their characteristics and turn death.

Properties and functions of stem cells are generally governed by a combination of intrinsic determinants and signals from the local microenvironment, or niche. Creating a suitable microenvironment for their growth and differentiation and ultimately mimicking the stem cell niche is a key to the success of stem cell culture. Biomaterials are rapidly being developed to display and deliver stem cell regulatory signals in a precise and near-physiological pattern. Biomaterial-related researches include conductive platform formed by protein-conjugated synthetic polymers that present bioactive ligands and respond to cells.

Surface modification of materials by immobilization of bioactive molecules to increase the interactions between cells and material have been studied to determine how the stem cells attach to the materials for transplantation in tissue defects in patients.

Once the cells are attached to the surface of the material, intracellular signals regulating proliferation and differentiation of cells are generated via interactions between specific receptors and cell signaling molecules adsorbed or expressed on the materials. These materials should be useful for the culture and/or preservation of embryonic stem (ES) cells and various other kinds of stem cells, including hematopoietic stem cells.

Recently, it has been demonstrated that cyclic peptides containing a tandem repeat of the individual motifs to function as N-cadherin agonists. HAVDI and INPISGQ sequences have been identified as functional binding motifs in extracellular domain1 (ECD1) of N-cadherin. When presented to neurons as soluble molecules, the dimeric versions of the motifs stimulate neurite outgrow in a similar manner to native N-cadherin. This novel N-cadherin mimic cyclic peptide should be invaluable for dissecting out those cadherin functions that rely on signaling as opposed to adhesion and clearly have the potential to be developed as therapeutic agents for the promotion of cell survival and axonal regeneration.

Surface-initiated polymerization (SIP) in combination with controlled radical polymerization (CRP) has been recently recognized as an efficient and powerful tool for generating surface-tethered polymer brushes that are potentially useful for a number of high-value technologies, ranging from biotechnology to advanced microelectronics. Due to the versatility of the process towards a wide range of readily available monomers, both chemical and physical properties of surface-tethered polymer brushes can be broadly tailored, in particular, the functional group density of the surface which can be varied as a function of the chain length and molecular weight.

Atom transfer radical polymerization (ATRP) has been regarded as one of the most successful CRP process. Despite its great potential, conventional ATRP still suffers from the demand for rigorously deoxygenated condition as well as the catalyst removal. Such limitation has been recently overcome by an addition of minute quantity of an active copper catalyst with an excess amount of appropriate reducing agent. Since the activators (Cu(I) species) can be continuously regenerated by electron transfer, this approach is thus named activators regenerated by electron transfer for atom transfer radical polymerization (ARGET ATRP). This process is highly desirable for large-scale production because the reaction can be carried out in the presence of limited amount of air so the stringent deoxygenation is no longer necessary. The fact that only small amount of catalyst (at the level of ppm) is required apparently satisfies the bio-related applications of which the trace amount of catalyst may be detrimental.

Herein, we report, for the first time, the synthesis of poly(*t*-butyl acrylate) (P*t*-BA) brushes and its subsequent hydrolyzed form, poly(acrylic acid) (PAA) brushes using the ARGET ATRP. Unlike the previous work reported on the systems of polystyrene and poly (*n*-butyl acylate), Me$_6$TREN, a more reactive ligand for copper catalyst was used. Since our ultimate goal is to employ this surface-functionalized poly(acrylic acid) brushes as substrates for cell culturing and tissue engineering applications, the reactivity of the carboxyl moieties along the chains of the PAA brushes were tested against immobilization of bovine serum albumin (BSA), a model representing biomolecules. The covalent immobilization of N-cadherin mimic cyclic peptide to the carboxyl groups of PAA brushes was subsequently performed in order to determine the applicability of the surface-functionalized PAA brushes towards cell culture applications.

1.2   Objectives

1. To synthesize poly(acrylic acid) brushes via activators regenerated by electron transfer for atom transfer radical polymerization (ARGET ATRP) from glass surface.

2. To attach BSA and N-cadherin mimic cyclic peptide on the carboxyl groups of poly(acrylic acid) brushes.

3. To study stem cell viability, attachment and proliferation on poly(acrylic acid) brushes immobilized N-cadherin mimic cyclic peptide.

1.3   Scope of Investigation

The stepwise investigation was carried out as follows.

1. Literature survey for related research work.

2. To synthesize α-bromoester compound and tris (2-(dimethylamino)ethyl)amine [Me$_6$TREN] to be used as a surface initiator an ligand, respectively

3. To immobilize α-bromoester-containing initiator on glass surfaces.

4. To synthesize P*t*-BA brushes via ARGET ATRP from glass substrate containing a monolayer of α-bromoester groups.

5. To prepare PAA brushes by hydrolysis of P*t*-BA brushes.

6. Characterization of P*t*-BA and PAA brushes attached on glass substrates

7. To determine the reactivity of carboxyl groups of PAA brushes towards BSA attachment.

8. To attach N-cadherin mimic cyclic peptide on carboxyl groups of PAA brushes.

9. To test stem cell viability, attachment and proliferation on N-cadherin mimic cyclic peptide immobilized PAA brushes.

CHAPTER II

THEORY AND LITERATURE REVIEW

2.1 Polymer Brushes

Polymer brushes refer to an assembly of polymer chains which are tethered by one end to a surface or an interface. Tethering is sufficiently dense that the polymer chains are crowded and forced to stretch away from the surface or interface to avoid overlapping, sometimes much further than the typical unstretched size of a chain. These stretched configurations are found under equilibrium conditions; neither a confining geometry nor an external field is required. This situation, in which polymer chains stretch along the direction normal to the grafting surface, is quite different from the typical behavior of flexible polymer chains in solution where chains adopt a random-walk configuration. A series of discoveries show that the deformation of densely tethered chains affects many aspects of their behavior and results in many novel properties of polymer brushes [1].

Polymer brushes are a central model for many practical polymer systems such as polymer micelles, block copolymers at fluid–fluid interfaces (e.g. microemulsions and vesicles), grafted polymers on a solid surface, adsorbed diblock copolymers and graft copolymers at fluid–fluid interfaces. All of these systems, illustrated in Figure 2.1, have a common feature: the polymer chains exhibit deformed configurations. Solvent can be either present or absent in polymer brushes. In the presence of a good solvent, the polymer chains try to avoid contact with each other to maximize contact with solvent molecules. With solvent absent (melt conditions), polymer chains must stretch away from the interface to avoid overfilling incompressible space.

The interface to which polymer chains are tethered in the polymer brushes may be a solid substrate surface or an interface between two liquids, between a liquid and air, or between melts or solutions of homopolymers. Tethering of polymer chains on the surface or interface can be reversible or irreversible. For solid surfaces, the polymer chains can be chemically bonded to the substrate or may be just adsorbed onto the surface. Physisorption on a solid surface is usually achieved by block copolymers with

one block interacting strongly with the substrate and another block interacting weakly. For interfaces between fluids, the attachment may be achieved by similar adsorption mechanisms in which one part of the chain prefers one medium and the rest of the chain prefers the other.
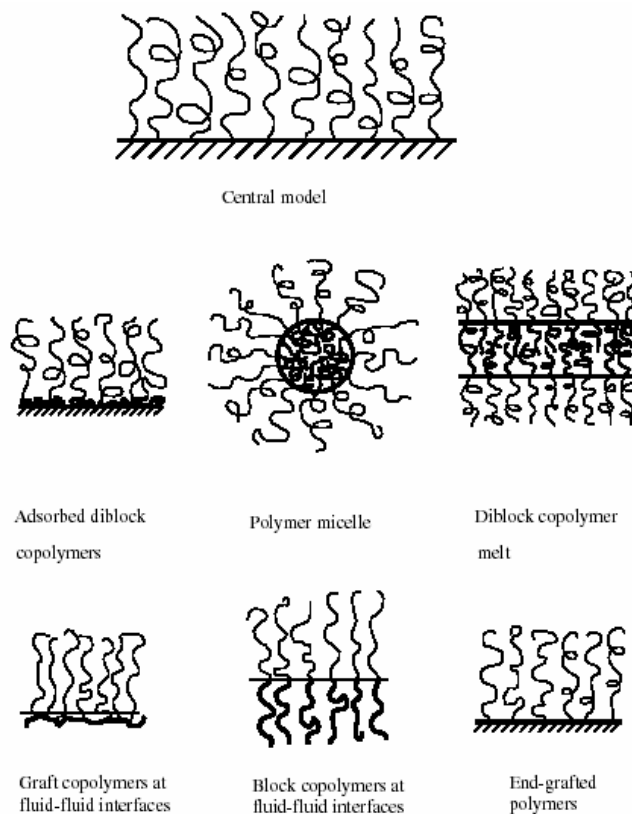
Figure 2.1 Examples of polymer systems comprising polymer brushes [1]

Polymer brushes (or tethered polymers) attracted attention in 1950s when it was found that grafting polymer molecules to colloidal particles was a very effective way to prevent flocculation [1]. In other words, one can attach polymer chains which prefer the suspension solvent to the colloidal particle surface; the brushes of two approaching particles resist overlapping and colloidal stabilization is achieved. The repulsive force between brushes arises ultimately from the high osmotic pressure inside the brushes. Subsequently, it was found that polymer brushes can be useful in other applications such as new adhesive materials [2, 3], protein-resistant biosurfaces [4], chromotographic devices [4], lubricants [5], polymer surfactants [1] and polymer compatibilizers [1]. Tethered polymers which possess low critical solution temperature (LCST) properties exhibit different wetting properties above and below LCST temperature [6]. A very promising field that has been extensively investigated is using

polymer brushes as chemical gates. Ito and coworkers [7],[8],[9] have reported pH sensitive, photosensitive, oxidoreduction sensitive polymer brushes covalently tethered on porous membranes, which are used to regulate the liquid flowing rate through porous membranes. Suter and coworkers [10],[11] have prepared polystyrene brushes on high surface area mica for the fabrication of organic–inorganic hybrids. Cation-bearing peroxide free-radical initiators were attached to mica surfaces via ion exchange and used to polymerize styrene. This process is important in the field of nanocomposites. Patterned thin organic films could be useful in microelectrics [12], cell growth control [13], biomimetic material fabrication [14], microreaction vessel and drug delivery [15].

In terms of polymer chemical compositions, polymer brushes tethered on a solid substrate surface can be divided into homopolymer brushes, mixed homopolymer brushes, random copolymer brushes and block copolymer brushes. Homopolymer brushes refer to an assembly of tethered polymer chains consisting of one type of repeat unit. Mixed homopolymer brushes are composed of two or more types of homopolymer chains [16]. Random copolymer brushes refer to an assembly of tethered polymer chains consisting of two different repeat units which are randomly distributed along the polymer chain [17]. Block copolymer brushes refer to an assembly of tethered polymer chains consisting of two or more homopolymer chains covalently connected to each other at one end [18]. Homopolymer brushes can be further divided into neutral polymer brushes and charged polymer brushes. They may also be classified in terms of rigidity of the polymer chain and would include flexible polymer brushes, semiflexible polymer brushes and liquid crystalline polymer brushes. These different polymer brushes are illustrated in Figure 2.2.
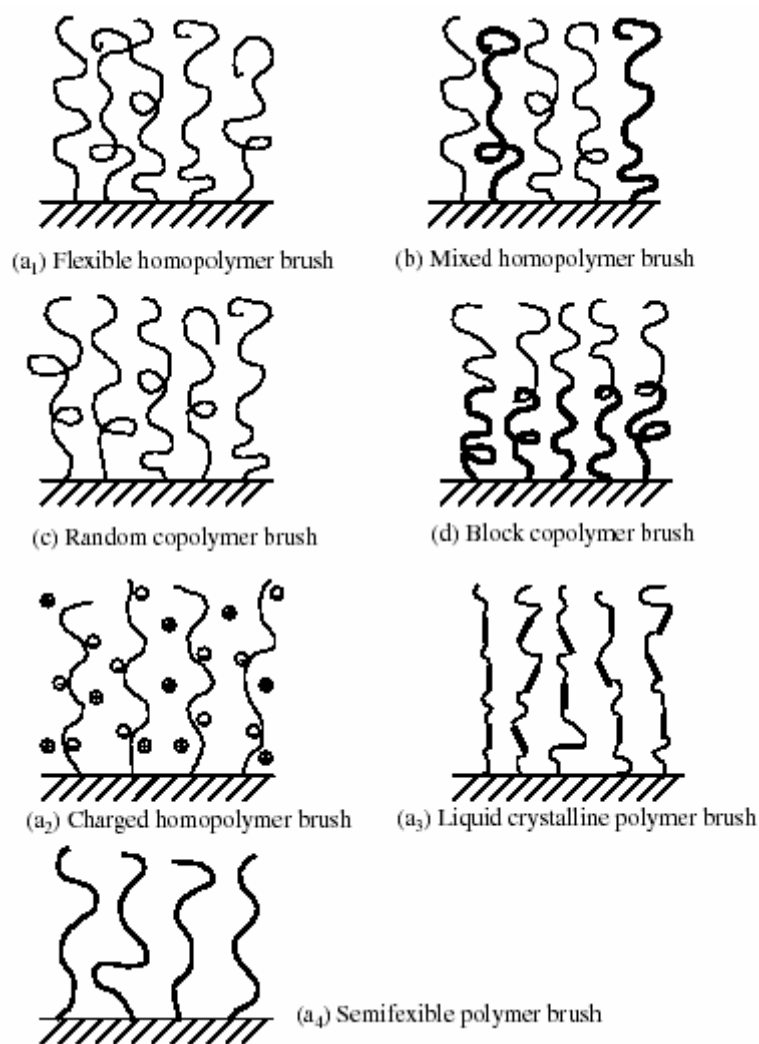
Figure 2.2 Classification of linear polymer brushes, (a₁–a₄) homopolymer brushes; (b) mixed homopolymer brush; (c) random copolymer brush; (d) block copolymer brush [1]

Generally, there are two ways to fabricate polymer brushes: physisorption and covalent attachment (Figure 2.3). For polymer physisorption, block copolymers adsorb onto a suitable substrate with one block interacting strongly with the surface and the other block interacting weakly with the substrate. The disadvantages of physisorption include thermal and solvolytic instabilities due to the non-covalent nature of the grafting, poor control over polymer chain density and complications in synthesis of suitable block copolymers. Tethering of the polymer chains to the surface is one way to surmount some of these disadvantages. Covalent attachment of polymer brushes can be accomplished by either "grafting to" or "grafting from" approaches. In a "grafting to" approach, preformed end-functionalized polymer molecules react with an appropriate

substrate to form polymer brushes. This technique often leads to low grafting density and low film thickness, as the polymer molecules must diffuse through the existing polymer film to reach the reactive sites on the surface. The steric hindrance for surface attachment increases as the tethered polymer film thickness increases. The "grafting from" approach is a more promising method in the synthesis of polymer brushes with a high grafting density. "Grafting from" can be accomplished by treating a substrate with plasma or glow-discharge to generate immobilized initiators onto the substrate followed by in situ surface-initiated polymerization. However "grafting from" well-defined self-assembled monolayers (SAMs) is more attractive due to a high density of initiators on the surface and a well-defined initiation mechanism. Also progress in polymer synthesis techniques makes it possible to produce polymer chains with controllable lengths. Polymerization methods that have been used to synthesize polymer brushes include cationic, anionic, TEMPO-mediated radical, atom transfer radical polymerization (ATRP), activators regenerated by electron transfer atom transfer radical polymerization (ARGET ATRP) and ring opening polymerization.
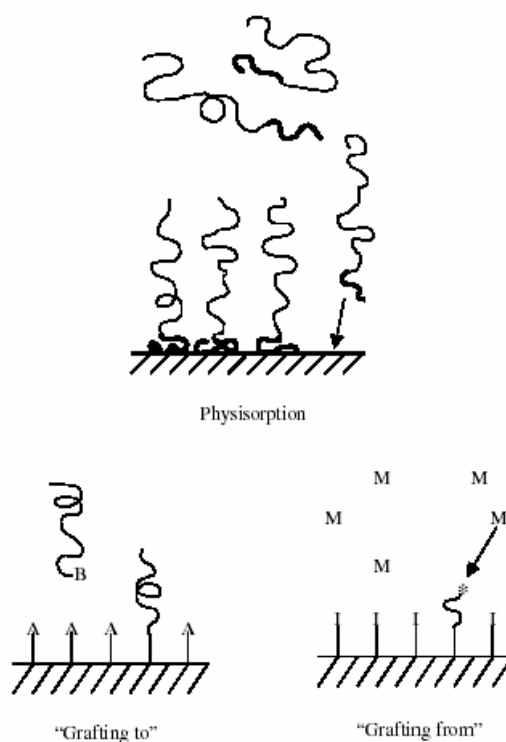
Figure 2.3 Preparation of polymer brushes by "physisorption", "grafting to" and "grafting from" [1]

In order to achieve a better control of molecular weight and molecular weight distribution and to obtain novel polymer brushes like block copolymer brushes, controlled radical polymerizations including ATRP, reverse ATRP, TEMPO-mediated and iniferter radical polymerizations have been used to synthesize tethered polymer brushes on solid substrate surfaces [19, 20].

ATRP has been the most widely empoyled technique for the formation of polymer brushes *via* surface initiated polymerization. ATRP is compatible with a variety of functionalised monomers. The living/controlled character of the ATRP process yields polymers with a low polydispersity ($\overline{M}_w/\overline{M}_n$) that are end-functionalized and so can be used as macroinitiators for the formation of di- and triblock copolymers. Although highly successful, ATRP has some drawbacks. Firstly, relatively high concentrations of catalyst are needed to control the polymerization. Secondly, the catalyst must be removed in order to achieve polymers with high purity and avoid possible issues of toxicity.

In recent years, activator regenerated by electron transfer atom transfer radical polymerization (ARGET ATRP) has been developed. This new system improves the ATRP process. Reducing agent was added in reaction to constantly regenerate the catalyst from deactive species to active species (Scheme 2.1). An added advantage of ARGET ATRP [21-23] is that the polymerization can be carried out in the presence of air and reduced concentration of catalyst. Moreover, this system can be used for high surface area of materials.
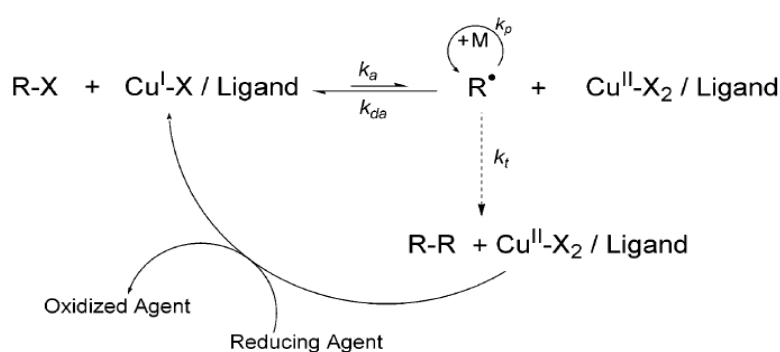
Scheme 2.1 Mechanism of ARGET ATRP process [24]

In 2007, Matyjaszewaski et al. [25] reported that ARGET ATRP can be successfully carried out in the presence of limited amounts of air and control is essentially unaffected by excess reducing agent. Reactions can be carried out without

any deoxygenation, in flasks fitted with rubber septa or even in simple jars (Figure 2.4). This technique has been successfully applied to the preparation of densely grafted polymer brushes, poly (*n*-butyl acrylate) homopolymer, and poly(*n*-butyl acrylate)-block-polystyrene copolymer from silicon wafers (0.4 chains/nm^2) that used a small amount of Cu(II) as 0.00053 mmol. This simple new method of grafting well-defined polymers does not require any special equipment and can be carried out in vials or jars without deoxygenation. The grafting for "everyone" technique is especially useful for wafers and other large objects and may be also applied for molecular hybrids and bioconjugates.
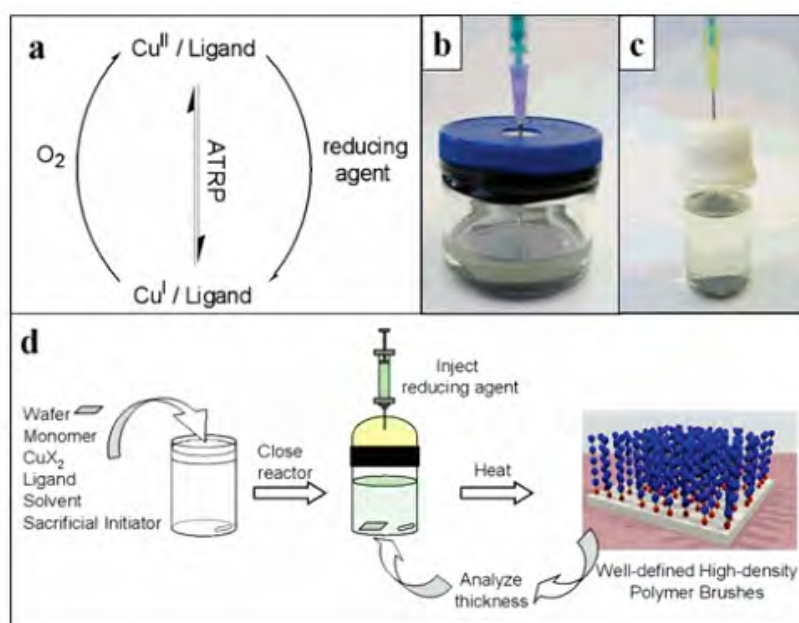
Figure 2.4 ARGET ATRP of *n*-butyl acrylate in the presence of limited amounts of air. (a) Proposed mechanism. Typical setup with silicon wafers for ARGET ATRP with limited air (b) in a large jar and (c) in a sample vial. (d) Illustration of procedures for surface-initiated ARGET ATRP with limited air [25]

In 2010, Cao et al.[26] synthesized poly(methyl methacrylate) (PMMA) and polystyrene (PS) *via* ARGET ATRP on SBA-15 silicas with cylindrical pores of diameter 22 and 14 nm as the nanoporous supports. The grafted layer thicknesses of up to at least 2 nm were achieved in the polymerization process carried out in small vials without using a vacuum line. Due to its simplicity, ARGET ATRP emerges as a powerful and yet surprisingly straightforward way to synthesize well-defined polymer

brushes in nanopores, opening a convenient avenue to a wide range of porous high-surface-area silica-polymer composites.

2.2   Living Polymerization

Synthetic polymers are long-chain molecules possessing uniform repeat units (mers). The chains are not all the same length. These giant molecules are of interest because of their physical properties, in contrast to low molecular weight molecules, which are of interest due to their chemical properties. Possibly the most useful physical property of polymers is their low density versus strength.

When synthetic polymers were first introduced, they were made by free radical initiation of single vinyl monomers or by chemical condensation of small difunctional molecules. The range of their properties was understandably merger. Random copolymers are greatly expanding in the range of useful physical properties such as toughness, hardness, elasticity, compressibility, and strength, however, polymer chemists realized that their materials could not compare with the properties of natural polymers, such as wool, silk, cotton, rubber, tendons and spider webbing. The natural polymers are generally condensation polymers made by addition of monomer units one at a time to the ends of growing polymer chains. Polymerization of all chains stops at identical molecular weights. For some time, polymer chemists have realized that to approach nature's degree of sophistication, new synthetic techniques would be needed.

Conventional chain-growth polymerizations, for example, free radical synthesis, consist of four elementary steps: initiation, propagation, chain transfer, and termination. As early as 1936, Ziegler proposed that anionic polymerization of styrene and butadiene, consecutive addition of monomer to an alkyl lithium initiator occured without chain transfer or termination. During transferless polymerization, the number of polymer molecules remains contant. Since there is no termination, active anionic chain ends remain after all of the monomer has been polymerized. When fresh monomer is added, polymerization resumes. The name "living polymerization" was coined for the method by Szwarc [27] because the chain ends remain active until killed. The term has nothing to do with living in the biological sense. Before Szwarc's classic work, Flory [28] had described the properties associated with living polymerization of ethylene oxide initiated with alkoxides. Flory noted that since all of the chain ends grow at the same rate, the molecular weight is determined by the amount of initiator used versus monomer (Eq. 2.1).

$$\text{Degree of polymerization} = [\text{monomer}]/[\text{initiator}] \qquad (2.1)$$

Another property of polymers produced by living polymerization is the very narrow molecular weight distribution. The polydispersity (D) has a Poisson distribution, $D = \overline{M}_w/\overline{M}_n = 1 + (1/dp)$; $\overline{M}_w$ is the average molecular weight determined by light scattering, $\overline{M}_n$ is the average molecular weight determined by osmometry, and dp is the degree of polymerization (the number of monomer units per chain). The values of $\overline{M}_w$ and $\overline{M}_n$ can also be determined by gel permeation chromatography (GPC). A living polymerization can be distinguished from free radical polymerization or from a condensation polymerization by plotting the molecular weight of the polymer versus conversion. In a living polymerization, the molecular weight is directly proportional to conversion (Figure 2.5, line A). In a free radical or other nonliving polymerization, high molecular weight polymer is formed in the initial stages (line B), and in a condensation polymerization, high molecular weight polymer is formed only as the conversion approaches 100% (line C).
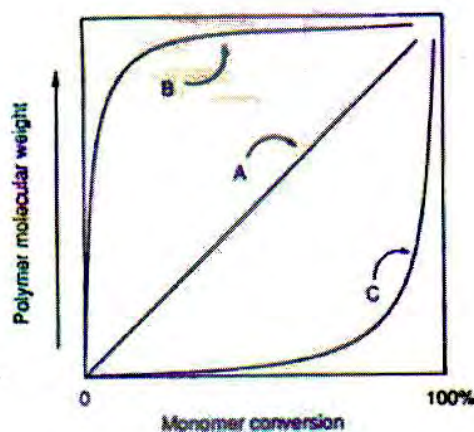
Figure 2.5 Molecular weight conversion curves for various kinds of polymerization methods: (A) living polymerization; (B) free radical polymerization; and (C) condensation polymerization [28]

Living polymerization techniques give the synthetic chemist two particularly powerful tools for polymer chain design: the synthesis of block copolymers by sequential addition of monomers and the synthesis of functional-ended polymers by

selective termination of living ends with appropriate reagents. The main architectural features available starting with these two basic themes are listed in Figure 2.6 along with applications for the various polymer types. Although living polymerization of only a few monomers is nearly perfect, a large number of other systems fit theory close enough to be useful for synthesis of the wide variety of different polymer chain structures. In general, the well-behaved living systems need only an initiator and monomer, as occurs in the anionic polymerization of styrene, dienes, and ethylene oxide.

For an increasing number of monomers, more complex processes are needed to retard chain transfer and termination. These systems use initiators, catalysts, and sometimes chain-end stabilizers. The initiator begins chain growth and in all systems is attached (or part of it, at least) to the nongrowing chain end. The catalyst is necessary for initiation and propagation but is not consumed. The chain-end stabilizer usually decreases the polymerization rate. When the catalyst is a Lewis acid (electron-pair acceptor), the stabilizer will likely be a Lewis base (electron-pair donor), and vice versa. In all systems, the initiation step must be faster than or the same rate as chain propagation to obtain molecular weight control. If the initiation rate is slower than the propagation rate, the first chains formed will be longer than the last chains formed. If an initiator with a structure similar to that of the growing chain is chosen, the initiation rate is assured of being comparable to the propagation rate. A number of living systems operate better if excess monomer is present. A possible explanation is that the living end is stabilized by complexation with monomer [29]. Large counterions tend to be more effective than small counterions in living polymerization systems even when the ionic center is only indirectly involved.

Figure 2.6 Architectural forms of polymers available by living polymerization techniques[24]

In this research, free radical process for living polymerization is selected and described. The concept of using stable free radicals, such as nitroxides, to reversibly react with the growing polymer radical chain end can be traced back to the pioneering work of Rizzardo and Mozd [30]. After further refinement by Georges [31], the basic blueprint for all subsequent work in the area of "living" free radical polymerization was developed. Subsequently, the groups of Sawamoto [32], Matyjaszewski [33], Percec [34] and others [35] have replaced the stable nitroxide free radical with transition metal species to obtain a variety of copper-, nickel-, or ruthenium-mediated "living" free radical systems. These systems were called atom transfer radical polymerization (ATRP). Subsequently, Jakubowski and co-worker [36] developed ATRP system. The new system was called activator regenerated by electron transfer atom transfer radical polymerization (ARGET ATRP). The new system can reduce the drawback of ATRP system. The reducing agent that continually reduced deactivated catalyst to activated catalyst was added in ARGET ATRP system (Scheme 2.1). The ARGET ATRP mechanism is similar to ATRP but ARGET ATRP was added the reduction step.

Considering conventional ATRP, the mechanism is developed based on a method known for carbon-carbon bond formation in organic synthesis. In some of these reactions, a transition-metal catalyst acts as a carrier of the halogen atom in a reversible redox process (Scheme 2.2). Initially, the transition-metal species, M_t^n, abstracts halogen atom X from the organic halide, RX, to form the oxidized species, $M_t^{n+1}X$, and

the carbon-centered radical $R^\bullet$. In the subsequent step, the radical $R^\bullet$ participates in an inter- or intramolecular radical addition to alkene, Y, with the formation of the intermediate radical species, $RY^\bullet$. The reaction between $M_t^{n+1}X$ and $RY^\bullet$ results in a target product, RYX, and regenerates the reduced transition-metal species, M_t^n, which further promotes a new redox process. The fast reaction between $RY^\bullet$ and $M_t^{n+1}X$ apparently suppresses biomolecular termination between alkyl radicals and efficiently introduces a halogen functional group X into the final product in good to excellent yields.
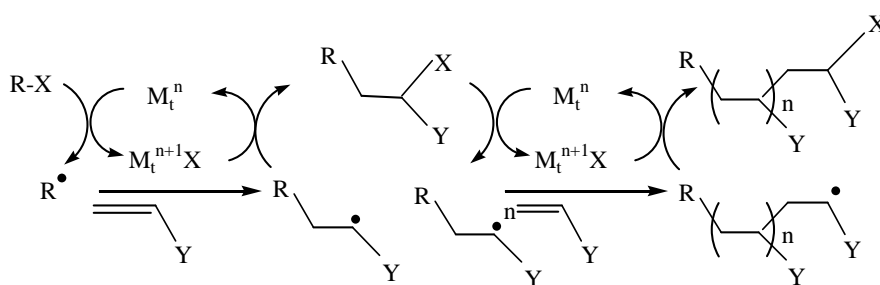
Scheme 2.2 Mechanism of ATRP [29]

The ATRP system relies on one equilibrium reaction in addition to the classical free-radical polymerization scheme (Scheme 2.3). In this equilibrium, a dormant species, RX, reacts with the activator, M_t^n, to form a radical $R^\bullet$ and deactivating species, $M_t^{n+1}X$. The activation and deactivation rate parameters are k_{act} and k_{deact}, respectively. Since deactivation of growing radicals is reversible, control over the molecular weight distribution and, in the case of copolymers, over chemical composition can be obtained if the equilibrium meets several requirements [37, 38].

1. The equilibrium constant, k_{act}/k_{deact}, must be low in order to maintain a low stationary concentration of radicals. A high value would result in a high stationary radical concentration, and as a result, termination would prevail over reversible deactivation.

2. The dynamics of the equilibrium must be fast; i.e. deactivation must be fast compared to propagation in order to ensure fast interchange of radicals in order to maintain a narrow molecular weight distribution.

$$R\text{-}X \quad + \quad M_t^n \quad \xrightleftharpoons[k_{deact}]{k_{act}} \quad R^\bullet \quad + \quad M_t^{n+1}X$$
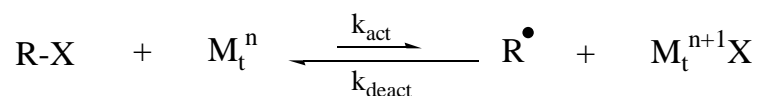
Scheme 2.3 Equilibrium reaction in ATRP [39]

In addition, the reduction step in ARGET ATRP system was studied by Jakubowski and co-workers [36]. The reduction step began in polymerization reaction of ARGET ATRP system. In our studies, tin(II)2-ethylhexanoate(Sn(EH)$_2$) or glucose and was used. Sn(EH)$_2$ and glucose are examples of several possible reducing agents which can be used for *in situ* reduction of Cu-(II) to Cu(I) (Scheme 2.4), without formation of radicals or radical precursors, that can initiate new chains. The reducing agent also allows starting an ATRP with the oxidatively stable Cu(II) species. It may further allow to tolerate a limited amount of air or other radical traps in the system. This significantly simplifies the steps required for pre-purification of ATRP systems.

$$\underset{(II)}{Sn(EH)_2} \quad + \quad \underset{(II)}{2(CuCl_2)/Ligand} \quad \xrightleftharpoons{K_{eq}} \quad \underset{(IV)}{Sn(EH)_2Cl_2} \quad + \quad \underset{(I)}{2CuCl/Ligand}$$
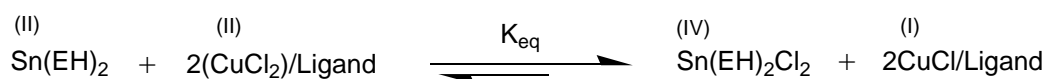
Scheme 2.4 Reduction of Cu (II) to Cu (I) by tin(II)2-ethylhexanoate [36]

Although, ARGET ATRP has reduction step, the catalyst system was yet similar to ATRP. Transition metal complexes (catalyst) are perhaps the most important components of ATRP. It is the key to ATRP since it determines the position of the atom transfer equilibrium and the dynamics of exchange between the dormant and active species. There are several prerequisites for an efficient transition metal catalyst. First, the metal center must have at least two readily accessible oxidation states separated by one electron. Second, the metal center should have reasonable affinity toward a halogen. Third, the coordination sphere around the metal should be expandable upon oxidation to selectively accommodate a (pseudo)-halogen. Fourth, the ligand should complex the metal relatively strongly. Eventually, the position and dynamics of the ATRP equilibrium should be appropriate for the particular system. A variety of transition-metal complexes have been studied as ATRP catalysts.

Copper catalysts are superior in ATRP in terms of versatility and cost. Styrenes, (methyl)acrylate esters and amides, and acrylonitrile have been successfully

polymerized using copper-mediated ATRP. Examples of copper complexes used in ATRP are shown in Figure 2.7.
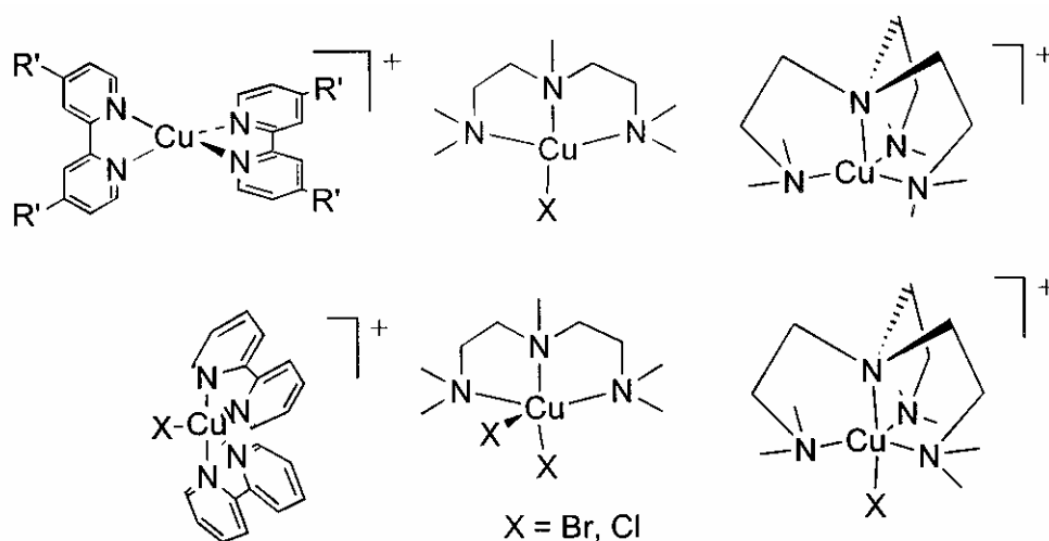
Figure 2.7 Copper complexes used as ATRP catalysts [40]

Nitrogen ligands have been used in copper-mediated ATRP. The monodentate (e.g., N(nBu)3), bidentate(e.g., dNbpy), and multidentate nitrogen ligands have been applied to copper-based ATRP. The electronic and steric effects of the ligands are important. Reduced catalytic activity or efficiency is observed when there is excessive steric hindrance around the metal center or the ligand has strongly electron-withdrawing substituents. A recent survey summarized different ligands employed in copper-mediated ATRP. The effect of the ligands and guidelines for ligand design were reviewed. Activity of N-based ligands in ATRP decreases with the number of coordinating sites N4 > N3 >N2, N1 and with the number of linking C-atoms C2 > C3, C4. It also decreases in the order R_2N- ≈ PyrEnDash-> R-N= > Ph-N=> Ph-NR-. Activity is usually higher for bridged and cyclic systems than for linear analogues. Examples of some N-based ligands used successfully in Cu-based ATRP are shown in Figure 2.8.
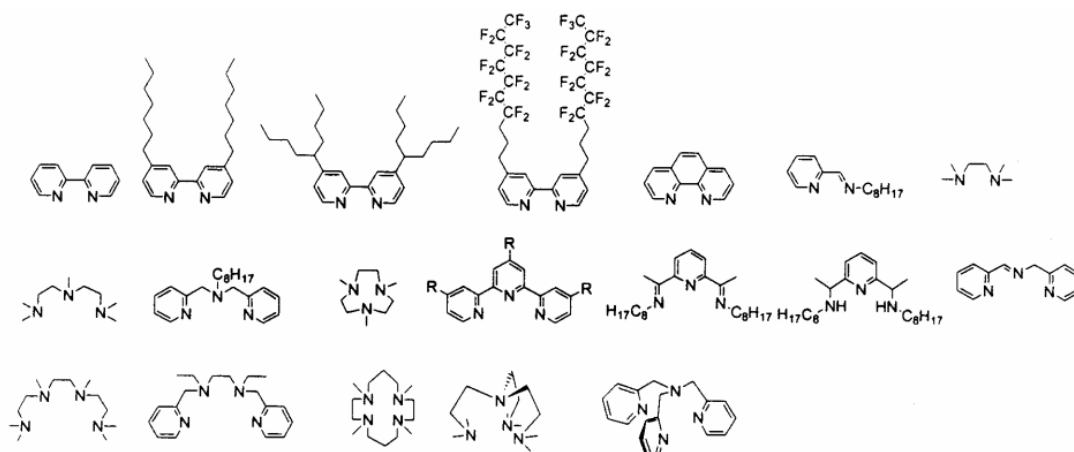
Figure 2.8 Example of ligands used in copper-mediated ATRP [40]

In 1995, Wang and Matyjaszewski has described the use of Cu^IX (X = Br, Cl) with 2,2'-bipyridine (bpy) as a "solubilizing" ligand. The active species has been described as "CuBr·bpy". This system is active toward styrene, acrylates, and methacrylates under the appropriate condition [33]. Percec has also described the role of bpy as partially solubilizing the Cu(I)/Cu(II) catalyst [41]. The role of the bpy is to co-ordinate to Cu(I) to give a *pseudo*-tetrahedral Cu(I) center in solution (Scheme 2.5).
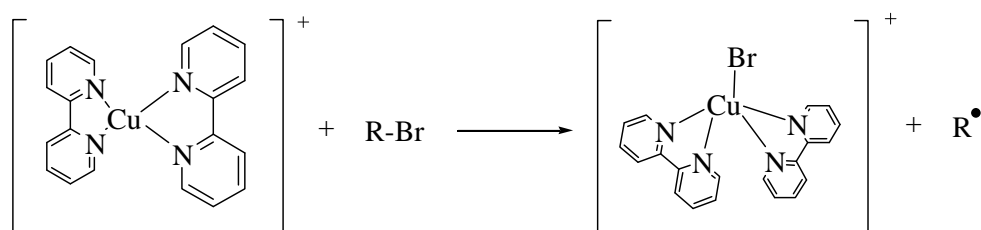
Scheme 2.5 Rotation of the bpy ligands from the tetrahedral and co-ordination of halide at the Cu center [41]

In 1997, Matyjaszewski and coworkers [42] have described the use of simple amines as ligands for the copper mediated atom transfer radical polymerization (ATRP) of styrene, methyl acrylate and methyl methacrylate. The simple amines are of interest in ATRP for three general reasons. First, most of the simple amines are less expensive, more accessible and more tunable than 2,2'-bipyridine (bpy) ligands. Second, due to the absence of the extensive π-bonding in the simple amines, the subsequent copper complexes are less colored. Third, since the coordination complexes between copper and simple amines tend to have lower redox potentials than the copper-bpy complex,

the employment of simple amines as the ligand in ATRP may lead to faster polymerization rates. The example of simple amine ligand is *N,N,N',N'',N''-* pentamethyldiethylenetriamine (PMDETA). When this ligand was empolyed in ATRP, all the polymerizations were well controlled with a linear increase of molecular weights with conversion and relatively low polydispersities throughout the reactions. The rate of polymerization showed a significant increase, as compared to the corresponding bpy system. The higher polymerization rate of PMDETA as the ligand is partially attributed to the lower redox potential of the copper(I)-PMDETA complex than the copper(I)-bipy complex, which shifts the equilibrium from the dormant species toward the active species resulting in the generation of more radicals in the system. The structure of copper complex using PMDETA as the ligand is shown in Scheme 2.6.
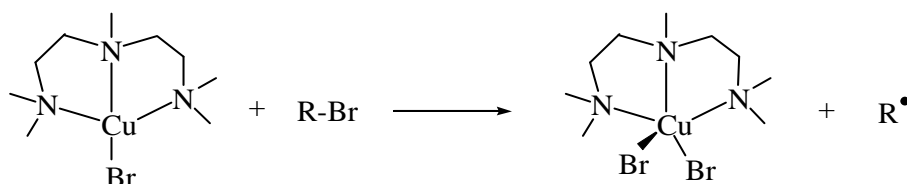
Scheme 2.6 Proposed Cu(I) and Cu(II) species using PMDETA as a ligand [40]

In 1998, Xia and coworkers [43] studied catalyst system that used tris (2-(dimethylamino)ethyl)amine [Me$_6$TREN] (Figure 2.9) as ligand in PMA polymerization *via* ATRP. This system can be reacted at room temperature. Me$_6$-TREN is tridentate ligands so that it is more reactive. The polymerization of methyl acrylate is extremely fast and even at room temperature.
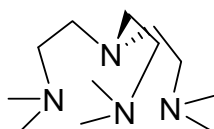
Figure 2.9 Structure of Me$_6$-TREN [43]

2.3 Poly(acrylic acid)

Poly(acrylic acid) (PAA) is a weak polyelectrolyte, in which the degree of ionization is governed by the pH and ionic strength of aqueous solution. PAA has been extensively investigated, owing to many scientific and industrial applications, such as intelligent environment-responsive surface optical chemical sensing and biomaterial

carriers [44-46]. PAA can be covalently modified with a broad range of functional groups, such as fluorophores, electroactive groups, dyes and other biomolecules [47, 48]. Recent advances of the controlled/living polymerization techniques made it possible to produce well-defined polymer structures, such as graft copolymers, star polymers, polymer brushes, etc. The interest in synthesis and characterization of such complex polymer systems containing acrylic acid segments has increased enormously.

For the synthesis of well-defined polymers, controlled/living polymerization techniques have been traditionally employed where the polymerizations proceed in the absence of irreversible chain transfer and chain termination. Controlled/living polymerization of acrylic acid by ATRP presents a challenging problem because the acid monomer can poison the catalysts in system of ATRP by coordinating to the transition metal. In addition, nitrogen containing ligands can be protonated, which interferes with the metal complexation ability. Thus, typically, protected monomers have been employed, followed by a polymer-analogous deprotection, e.g. hydrolysis of protecting ester groups. Protected monomers with masked acid groups involve *tert*-butyl acrylate (*t*-BA), *tert*-butyl methacrylate (*t*BuMA), trimethylsilyl methacrylate (TMSMA), benzyl methacrylate (BzMA), 2-tetrahydropyranyl methacrylate (THPMA) and *p*-nitrophenyl methacrylate (PNPMA) (Figure 2.10). After acid hydrolysis, thermolysis, or catalytic hydrogenolysis, these protective groups liberate their original acid functionality. Essential prerequisites for the protected monomer are good 'livingness' under each polymerization condition and selective deprotection under mild conditions.
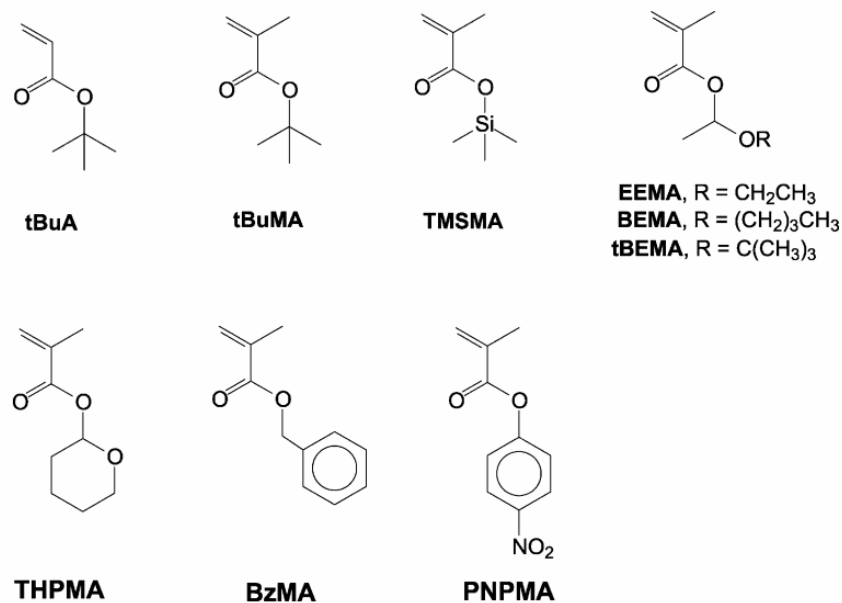
Figure 2.10 Representative examples of protected (meth)acrylic acid monomers with masked acid group [49]

The following literatures describe the synthesis of PAA using ATRP process.

In 1999, Matyjaszewski and coworkers [50] synthesized polystyrene and polyacrylates from silicon wafers *via* ATRP that modified with an initiator layer composed of 2-bromoisobutyrate. The thickness of the layer with reaction time and molecular weight were studied. Modification of the hydrophilicity of the surface layer was achieved by hydrolysis of the poly(styrene-b-*tert*-butyl acrylate) to poly(styrene-*b*-acrylic acid) and confirmed by a decrease in water contact angle from 86° to 18°.

In 2000, Davis and coworkers [51, 52] reported controlled polymerization of *tert*-butyl acrylate (*t*-BA) using methyl 2-bromopropionate, as the initiator and CuBr/N,N,N′,N″,N″-pentamethyldiethylenetriamine (PMDETA) as the catalyst system. In most ATRP based syntheses for block and further complex polymer systems, *t*-BA has been employed as a protected monomer, which may be due to the feasibility to control the polymerization and easy hydrolysis.

In 2001, Mori and coworkers [53] have employed surface-initiated self-condensing vinyl polymerization (SCVP) via ATRP as a new method for the synthesis of branched P*t*-BA–silica hybrid nanoparticles. Hydrolysis of the ester functionality created branched PAA grafted on silica nanoparticles.

In 2003, Boyes and coworkers [54] synthesized diblock copolymer polyelectrolyte brushes of either polystyrene (PS) or poly(methyl acrylate) (PMA) and

poly(acrylic acid) (PAA) by ATRP. The polyelectrolyte diblock copolymer brushes were used for the synthesis of metal nanoparticles by treatment the PAA with aqueous metal salt followed by subsequent reduction of the treated PAA.

In 2004, Kong and coworkers [55] presented a novel *in situ* atom transfer radical polymerization (ATRP) "grafting from" approach to functionalize multi walled carbon nanotubes (MWNT) with polystyrene-block-poly(acrylic acid) (PS-b-PAA). Polystyrene can be synthesized by ATRP and followed by poly(*tert*-butyl acrylate) on the modified MWNT followed by hydrolysis of the grafted poly(*tert*-butyl acrylate)(PtBA) blocks. The structure and morphology of the as-prepared hybrid nanomaterials were characterized and confirmed by TEM, SEM, NMR and TGA.

Since immobilized proteins are used in many biomedical and biotechnological applications, there is an intense research effort in finding materials coatings that allow for a better control and optimization of the protein immobilization process [45, 56]. At the same time, surface coatings must provide a mild environment for immobilized protein molecules to maintain their delicate biological functions. The most prominent types of surface coatings for the immobilization of proteins studied [57] functionalized so far include poly(ethyleneoxide) brushes[58, 59] self-assembled monolayers, and polyelectrolyte multilayers, among others. Polymer brushes offer certain advantages over other materials as they are covalently anchored to the substrate providing excellent mechanical stability and present a high surface area template with functionality controllable by monomer type and brush length. Thus, polymer brushes have been the natural choices as templates for immobilization protein. Poly (acrylic acid) (PAA) has been used to immobilize biomolecules by both ionic interactions and covalent attachment.

In 2002, Bisson and coworkers [60] prepared polymer poly(ethyleneterephthalate) (PET) films that were surface modified by graft polymerization of acrylic acid, subsequently, allow collagen (types I and III) immobilization and human smooth muscle cell expansion. This surface favors cell adhesion and growth of smooth muscle cells in culture.

In 2006, Hollmann and coworker [44] investigated The adsorption of two different proteins at a planar poly(acrylic acid) (PAA) brushes. Planar PAA brushes were prepared with a grafting density of 0.11 nm^{-2}. Hen egg-white lysozyme and bovine serum albumin (BSA) were used as model proteins. The PAA brush binds positively charged lysozyme and negatively charged BSA at a low ionic strength of the protein

solutions. A planar PAA brush therefore appears to be a promising materials coating for controlled protein immobilization in biotechnological applications.

In 2007, Dong and coworker [61] reported the synthesis of poly(acrylic acid) (PAA) brushes by the atom transfer radical polymerization(ATRP) of sodium acrylate at room temperature in aqueous media to generate carboxylic acid groups on a silicon surface. After that, avidin was covalently attached to PAA brushes, and biotin-tagged proteins could be immobilized through avidin-biotin interaction through specific recognition of biotin. Thus, this method can be expanded to immobilize a range of antigens or ligands for biosensing applications and to study cell-surface interactions.

In 2008, Cullen and coworker [46] examine the feasibility of using polymeric brushes as 3D scaffolds to covalently immobilize ribonuclease A (R Nase A), which is used in downstream processing of plasmid DNA for removal of RNA, with high relative activity. PAA brushes were synthesized by atom transfer radical polymerization (ATRP) to immobilize RNase A by covalent immobilization and a high-capacity NTA-Cu^{2+} complexation. The effect of binding chemistry and brush length on the surface density of bound enzyme, the kinetics and thermodynamics of binding, and the resulting temperature were investigated. From these studies, polymeric brushes can be effectively used to immobilize over 30 times more proteins than monolayers which may lead to decrease in detection limits of protein microarrays.

2.4 Stem Cell [62, 63]

Stem cells (SC) are unspecialized cells that develop into the specialized cells that make up the different types of tissue in the human body. They are vital to the development, growth, maintenance, and repair of our brains, bones, muscles, nerves, blood, skin, and other organs. In addition, stem cells are defined functionally as cells with the unique capacity to self-renew as well as to give rise to differentiated cells throughout the lifetime of the organism (Figure 2.11). At variance with the large majority of cells of the body that are committed to a specific function, SC are uncommitted and remain as such, until they receive signals from the environment to generate specialized cells.
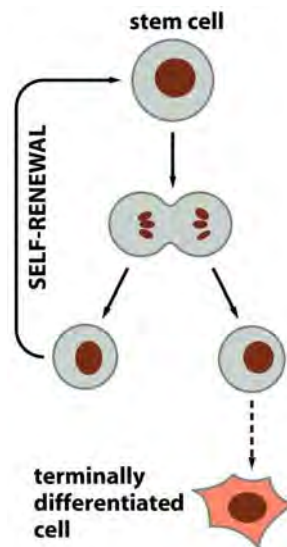
Figure 2.11 Life cycle of stem cell [64]

The type of stem cells is a term to describe precursor cells that can give rise to multiple tissue types. Totipotent stem cells are cells that can give rise to a fully functional organism as well as to every cell type of the body. Pluripotent stem cells are capable of giving rise to virtually any tissue type, but not to a functioning organism. Multipotent stem cells are more differentiated cells (that is, their possible lineages are less plastic/more determined) and thus can give rise only to a limited number of tissues. For example, a specific type of multipotent stem cell called a mesenchymal stem cell has been shown to produce bone, muscle, cartilage, fat, and other connective tissues.

2.4.1   Types of Stem Cells

2.4.1.1   Embryonic Stem Cells

Embryonic stem cells (Figure 2.12) are found in embryos at a very early stage of development. They have the ability to differentiate into any of the over two hundred types of cells that make up the human body.
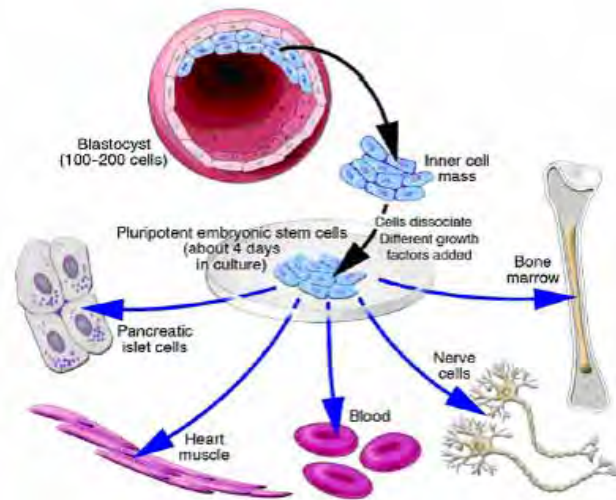
Figure 2.12 Embryonic stem cells [64]

2.4.1.2 Adult Stem Cells

Adult stem cells (Figure 2.13) have the ability to differentiate into varieties of a particular type of cell, determined by the type of tissue in which they are found. For example, blood stem cells found in the bone marrow give rise to red blood cells, white blood cells, and platelets. The term adult is used to indicate that these stem cells are further along the path of differentiation than are embryonic stem cells. Adult stem cells are found in tissues at all but the very earliest stage of human development: in fetal tissues, in children, and in adults. Scientists have thus far been able to isolate adult stem cells from tissues in the eye, skeletal muscle, liver, skin, fat, dental pulp, pancreas, umbilical cord, and the lining of the gastrointestinal tract.
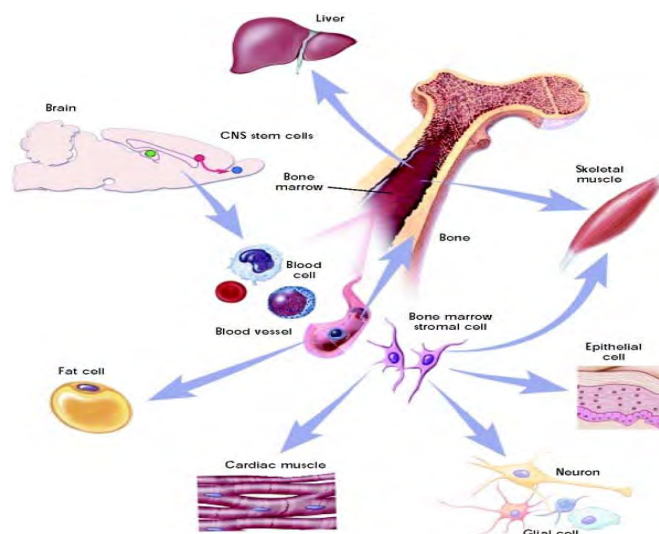
Figure 2.13 Adult stem cells [64]

2.4.2 Stem Cells Culture Method

Stem cells are simply defined as a progeny of cells that have the potential to differentiate into a variety of different lineages. These cells can be isolated from a variety of sources including embryos, umbilical cord blood, as well as from adult tissues, as reviewed previously [65].Since the isolation of mouse embryonic stem cells (mESCs) in 1981 by Davidand Kaufman, and the subsequent isolation of human embryonic stem cells (hESCs) in 1998, their exploration in regenerative medicine have received great interest. Embryonic stem cells (ESCs) are isolated from the inner cell mass of the blastocyst during embryological development [66, 67].Their pluripotent nature gives them the ability to differentiate into anyone of the three germlayers: endoderm, ectoderm, and mesoderm. However, ultimate large scale therapeutic application of these cells necessitates their maintenance in an undifferentiated state *in vitro* so that they can be differentiated into specific lineages on-demand.

It is now well established that adult tissues carry a variety of adult stem cells that are less pluripotent and are more committed than ESCs. Adult stem cells are often referred to as progenitor or multipotent cells since they have limited differentiation potential. These cells have been found in bone marrow, cord blood, adipose tissues, neural tissues etc. This has become attractive cell populations for the field of tissue engineering because of their ability to differentiate into variety of cell types and relative ease in harvest, isolation and expansion *in vitro*.

Growing cells in the laboratory is known as cell culture that grows into a plastic laboratory culture dish that contains a nutrient broth known as culture medium. The culture dish is important for cell grown in the same medium. Thus, materials for stem cell culture have been studied exclusively on the use of biomaterials, both natural and synthetic, to maintain and differentiate stem cells. Both adult and ESCs are cultured. Biomaterial-based scaffolds have been the most important tool in providing a 3-D environment to cells, both in culture or inside the body. Scaffolds for tissue engineering serve numerous functions and their role during tissue development is dependent upon specific properties of the chosen biomaterial. 3-D systems have proven to enhance osteogenic [68], hematopoietic [69], neural [70], and chondrogenic [71] differentiation. Additionally, natural biomaterials used for developing scaffolds can consist of components found in the extracellular matrix (ECM), such as collagen, fibrinogen, hyaluronicacid, glycosaminoglycans (GAGs), hydroxylapatite (HA) etc., and therefore

have the advantage of being bioactive, biocompatible, and of similar mechanical properties as native tissue. Other natural materials include those derived from plants, insects or animal components (e.g. cellulose, chitosan, silk fibroin etc.) with properties to provide favorable microenvironments for stem cell culture. This is comprised of a variety of ECM components including laminin, collagenIV, and heparin sulfate proteoglycans and has been used extensively in cell culture [72]. In addition, fibrinogen and fibrin are another class of tissue-derived natural materials that can be utilized to create 3-D scaffold materials [73]. Disadvantages of using natural materials over synthetic materials include limited control over physico-chemical properties, difficult to modify degradation rates, difficulty in sterilization and purification. Synthetic materials that have been extensively used for cell culture include polymers (poly(glycolic acid) (PGA), poly(lactic acid) (PLA)) [74], ceramics (calcium phosphates, bioactive glasses, and other bioceramics) and metals (titanium) [75].

Conventionally, stem cell culture can be carried out based on human embryonic stem cells that are isolated by transferring the inner cell mass into a plastic laboratory culture dish. The cells divide and spread over the surface of the dish. The inner surface of the culture dish is typically coated with mouse embryonic skin cells that have been treated so they will not divide. This coating layer of cells is called a feeder layer. The mouse cells in the bottom of the culture dish provide the inner cell mass cells a sticky surface to which they can attach. Also, the feeder cells release nutrients into the culture medium.

Studying and developing of condition for cell culture, type, amount of media and materials is critical for supporting cell growth. Researchers have devised ways to grow embryonic stem cells without mouse feeder cells that used in conventional method. This strategy has been recently proposed to avoid the risk that viruses or other macromolecules in the mouse cells may be transmitted to the human cells. However, developing of material surface for cell culture is still a challenge in research. The material surface for cell culture may thus be a need to modify a surface to suppress protein, extracellular matrix and cell adhesion molecule adsorption at this surface and to improve their biocompatibility.

In 2004, Shin and coworkers [76] compared RGD with an osteopontin-derived peptide, and determined that hydrogels modified with the osteopontin-derived peptide triggered significantly higher osteoblast migration than RGD-modified hydrogels. However, RGD remained the dominating peptide for cell-attachment.

In 2006, Higuchi and coworkers [77] prepared bioinert materials on which cell do not proliferate, differentiate, nor de-differentiate to be used for the culture and preservation of stem cells. The PluronicF127, a triblock copolymer of ethylene oxide and propylene oxide was activated using carbonyldiimidazole (CDI), and CDI-activated Pluronic was subsequently immobilized on the surface of a lysine-coated polystyrene tissue culture flask. The hematopoietic stem cells (CD34 and CD133) cultured in the Pluronic-immobilized flask was significantly higher than that in polystyrene tissue culture flask and commercially available bioinert flask.

Recently, Dey and coworkers [78] demonstrated that poly(2-(2-methoxyethoxy)ethyl methacrylate-co-oligo(ethylene glycol) methacrylate) (MEO_2MA-co-OEGMA) copolymer grafted brushes can be grafted onto glass coverslips using ATRP. Feeder free mES adhered and reached confluency on all surfaces; mouse embryonic stem (mES) cell cells also detached from the surface when the temperature was lowered below LCST.

Additionally, the responding of stem cell with the cell adhesion molecule was studied. Cell Adhesion Molecules (CAMs) are proteins located on the cell surface involved with the binding with other cells or with the extracellular matrix (ECM) in the process called cell adhesion (Figure 2.14). Examples of CAMs include cadherins, immunoglobulin-like adhesion molecules, integrins and selectins.
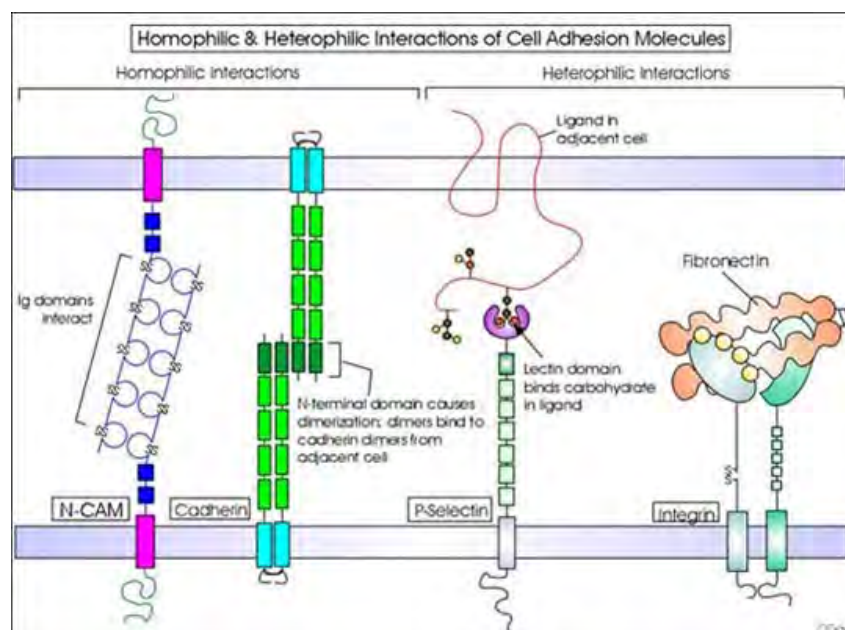
Figure 2.14 Homophilic and heterophilic interactions of cell adhesion molecule [79]

In 2000, Wickenhauser and coworkers [80] analyzed the role of megakaryocyte glycoproteins and selectins regarding their impact on megakaryocyte fribroblast interaction. Selectin-specific antibodies significantly reduced megakaryocyte attachment to fibroblast feeder layers and fibroblast growth in the co-cultures. The effect of CD41a and CD42b specific antibodies was limited to megakaryocyte-dependent fibroblast growth. These results elucidate the involvement of the selectins CD62P and CD62L in the basal activation of megakaryocytes inducing their attachment to bone marrow fibroblasts.

In 2001, Tsuchiya and coworkers [81] studied the effects of various cell adhesion molecules and extra ellular matrices on the initial cellular adhesion properties of articular chondrocytes, ligament cells and mesenchymal stem cells were investigated to target the design of optimal scaffolds for tissue engineering of articular cartilage and ligament. Fibronectin was shown to be most potential to promote cell adhesion.

In 2008, Lu and coworkers [82] investigated the effect of $\beta 1$ integrins to cell-matrix interactions. Human adipose tissue-derived stem cells (ASCs) were encapsulated in collagen type I gels for the induction of chondrogenesis. The effects of $\beta 1$integrins on chondrogenesis were analyzed by blocking ASCs with $\beta 1$integrins neutralizing antibodies. In addition, the effects of $\beta 1$integrins on the gene
expression of the RockI and RockII kinases, which are the most important effectors of prototype GTP ase Rho A, and cell shape of ASCs were also analyzed in order to understand better the mechanisms by which $\beta 1$integrins regulate chondrogenesis.

Recently, cadherins such as N-cadherin (found in neurons), E-cadherin (found in epithelial tissue), P-cadherin (found in the placenta) and T-cadherin were investigated for stem cell responses. The classical cadherins are a family of calcium-binding integral membrane glycoproteins that can account for the ability of cells to segregate from each other during development. The classical cadherins are composed of five extracellular domains, a single transmembrane domain, and two cytoplasmic domains. The first extracellular domain (ECD1) of these cadherins contains an evolutionarily conserved His-Ala-Val (HAV) motif and several lines of evidence suggest that this sequence is critical for function.

In 2000, Williams and coworkers [83] demonstrate that short cyclic HAV peptides can inhibit N-cadherin function. Interestingly, the nature of the amino acids that flank the HAV motif determine both the activity and specificity of the peptides.

When turn the cyclic HAV peptide into an N-cadherin peptide by incorporating flanking amino acids that are specific to N-cadherin, it can substantially increase the antagonistic properties of the peptide. That opposite result when turn the peptide into an E-cadherin peptide. The peptides that contained flanking amino acids from E-cadherin had little or no effect on the N-cadherin response. In summary, a novel family of cyclic peptides containing the HAV motif has been developed as N-cadherin antagonists. The specific N-cadherin antagonists can be developed based on the incorporation of 1or 2 flanking amino acids from native N-cadherin onto the HAV motif.

From the development of N-adherin antagonists described in 2000, the same groups of researchers [84] demonstrated the feasibility of cyclic peptides (Figure 2.15) containing a tandem repeat of the individual motifs to function as N-cadherin agonists. They have identified the HAVDI and INPISGQ sequences as functional binding motifs in extracellular domain1 (ECD1) of N-cadherin. When presented to neurons as soluble molecules, the dimeric versions of the motifs stimulate neurite outgrow in a similar manner to native N-cadherin. The response to the dimeric agonist peptides was inhibited by monomeric versions of the same motif and also by recombinant N-cadherin ECD1 protein. The responses were also inhibited by antibodies to a fibroblast growth factor receptor (FGFR) binding motif in ECD4 of N-cadherin and by a specific FGFR antagonist (PD17304). These data suggest that the peptides function by binding to and clustering N-cadherin in neurons and thereby activating an N-cadherin/FGFR signaling cascade. The novel agonists will be invaluable for dissecting out those cadherin functions that rely on signaling as opposed to adhesion and clearly have the potential to be developed as therapeutic agents for the promotion of cell survival and axonal regeneration.
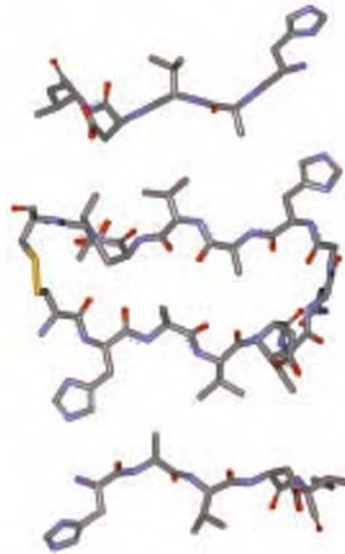
Figure 2.15 The structure above and below as a possible structure for the cyclic *N*-Ac-CHAVDINGHAVDIC-NH$_2$ peptide (middle) [84]

Besides N-cadherin can support axonal regeneration, they can be useful as cell surface marker. In 2006, Honda and coworkers [85] explored the induction of cardiomyocytes from mouse ES cells in chemically defined serum-free medium by using a mesoderm-inducing factor, BMP4. N-cadherin positive cells highly expressed cardiogenic markers, Nkx2.5, Tbx5, and Isl1, and showed a high differentiation rate into cardiomyocyte lineage. Moreover, N-cadherin can be a useful cell surface marker for the progenitors of cardiomyocyte differentiated from ES cells in the serum-free culture.

In 2008, Haug and coworkers [86] examined how N-cadherin expression in hematopoietic stem cell (HSC) relates to their function. Bone marrow (BM) cells highly expressing N-cadherin (N-cadherin^{hi}) are not stem cells, being largely devoid of a Lineage$^-$ Sca1$^+$ cKit$^+$ population and unable to reconstitute hematopoietic lineages in irradiated recipient mice. Instead, long-term HSCs form distinct populations expressing N-cadherin at intermediate (N-cadherin^{int}) or low (N-cadherin^{lo}) levels (Figure 2.16). The minority of N-cadherin population can robustly reconstitute the hematopoietic system, express genes that may prime them to mobilize, and predominate among HSCs mobilized from BM to spleen. The larger N-cadherin^{int} population performs poorly in reconstitution assays when freshly isolated but improves in response to overnight *in vitro* culture. Their expression profile and lower cell-cycle entry rate suggest N-

cadherin^{int} cells are being held in reserve. Thus, differential N-cadherin expression reflects functional distinctions between two HSC sub-populations.
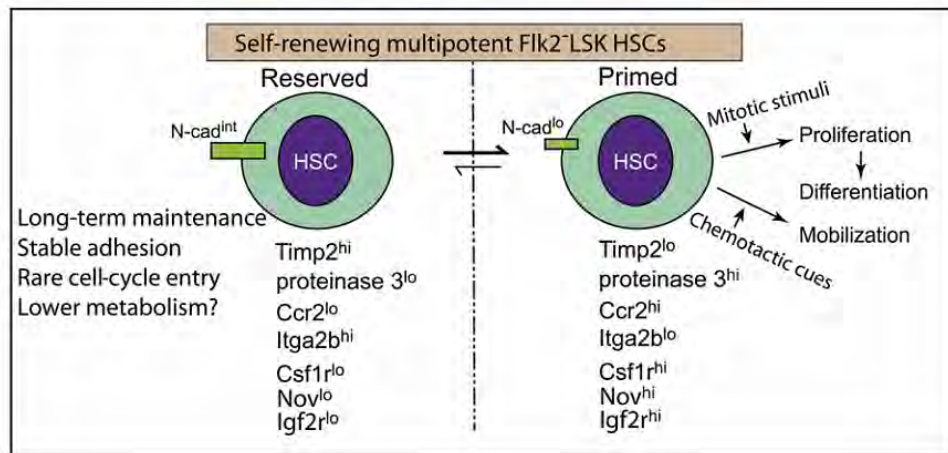
Figure 2.16 Model of reserved and primed HSCs [86]

CHAPTER III

METHODS AND MATERIALS

3.1   Materials

Glass coverslips (diameter = 1.2 cm) were purchased from Thermo Scientific, Thailand. 2-Bromoisobutyryl bromide, dimethychlorosilane, iodine, Toluidine blue O and *tert*-butyl acrylate (*t*-BA) were purchased from Aldrich (USA). Copper(II) bromide ($CuBr_2$), ethyl α-bromoisobutyrate (EBiB), methanesulfonic acid, *N*-hydroxysuccinimide (NHS), *N*-(3-dimethylaminopropyl)-*N*'-ethylcarbodiimide hydrochloride) (EDC) and platinum on activated charcoal (Pt/C (10%Pt)), were purchased from Fluka (Switzerland). Bovine serum albumin (BSA), laminin, phosphate buffer saline (PBS), tin(II)2-ethylhexanoate ($Sn(EH)_2$) and tris(2-(aminoethyl)amine) (TREN) were purchased from Sigma (USA). Acetone, allyl alcohol, ethanol (EtOH), formic acid (98%w/v), hydrochloric acid(HCl), hydrogen peroxide (H_2O_2), methanol (MeOH), 2-propanol, pyridine, sodium hydroxide (NaOH), sodium sulfate (Na_2SO_4), sulfuric acid (H_2SO_4), toluene and triethylamine were purchased from Merck (Germany). Acetic acid (CH_3COOH), dichloromethane and hexane were purchased from Carlo Erba (France). Formaldehyde (35%w/v) and tetrahydrofuran (THF) were purchased from LabScan Asia Co., Ltd.(Thailand). Glutamine, heparin, mouse neural progenitor cells, neurobasal medium, penicillin, streptomycin, trypan blue dye and trypsin were purchased from Gibco (USA). Epithelial growth factor (EGF) and Fibroblast growth factor (FGF) were purchased from R&D system (USA). All reagents and materials are analytical grade and used without further purification. N-cadherin mimic peptide (*N*-CHAVDINGHAVDIC-NH$_2$ sequence) was synthesized from Bio basic Inc. (USA). Distilled water was obtained after purification using a Millipore Milli-Q system (USA) that involves reverse osmosis, ion exchange, and a filtration step.

3.2 Equipments

3.2.1 Nuclear Magnetic Resonance Spectroscopy (NMR)

^{1}H NMR spectra was recorded in $CDCl_3$ and D_2O using Varian, model Mercury-400 nuclear magnetic resonance spectrometer operating at 400 MHz. Chemical shifts (δ) are reported in part per million (ppm) relative to tetramethylsilane (TMS) or using the residual protonated solvent signal as a reference.

3.2.2 Attenuated Total Reflectance - Fourier Transform Infrared Spectroscopy (ATR-FTIR)

ATR-FTIR spectra of the surface-modified silica particles were recorded with a FT-IR spectrometer (Nicolet), model system 6700 with using DLa TGS detector. The spectra were collected at a resolution of 4 cm^{-1} and 16 scans with using diamond ATR IR accessory.

3.2.3 Contact Angle Measurements

Water contact angle were determined with Contact angle goniometer model Ramé-Hart 200-F1 equipped with a Gilmont syringe and a 24–gauge flat-tipped needle (Ramé-Hart, Inc., USA). The measurements were carried out in air at ambient temperature. The tested angle could be measured from a silhouette image of droplet shown on the screen. Dynamic advancing and receding angles were recorded while water was added to and withdrawn from the drop, respectively. The reported angle is an average of 5 measurements on different area of each sample.

3.2.4 Atomic Force Microscopy (AFM)

AFM images were recorded with Scanning Probe Microscope model NanoScope®IV, Veeco, USA. Measurements were performed in air using tapping mode. Silicon nitride tip with a resonance frequency of 267-295 KHz and a spring constant 20-80 N/m were used.

3.2.5 Gel Permeation Chromatography (GPC)

Molecular weight and molecular weight distribution of poly(t-butyl acrylate) (Pt-BA) was determined by gel permeation chromatography obtained from Waters 600 controller chromatograph, connected to the RI detector, equipped with Waters E 600 column at 35 C°. THF was used as eluent with the flow rate of 1 mL/min. Narrow PS standards were used for establishing a calibration curve.

3.3 Synthesis of α-Bromoester Compound

3.3.1 Synthesis of 2-Bromo-2-methylpropionic Acid Allyl Ester (1)
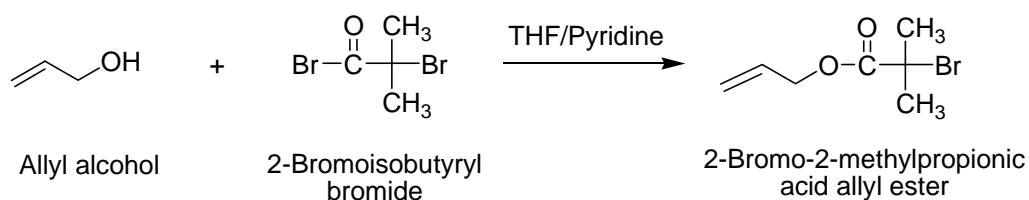
(1)

2-Bromoisobutyryl bromide (6.18 mL, 50 mmol) was added dropwise to a stirred solution of allyl alcohol (2.64 mL, 50 mmol) and pyridine (4.27 ml, 53 mmol) in 50 mL of dry tetrahydrofuran at $0^{\circ}C$. The reaction mixture was stirred at ambient temperature overnight. White precipitated pyridine bromide was then removed by filtration. The mixture was diluted with hexane and then washed once with 2 N HCl and twice with deionized water. The organic phase obtained was dried over sodium sulfate and filtered. The solvent was removed under reduced pressure. After purification by a silica gel column chromatography, colorless oil was obtained as a product in 91% yield.

^{1}H-NMR (CDCl$_3$) of 2-bromo-2-methylpropionic acid allyl ester: δ 1.98 (s, 6H, C(C$\underline{H}_3$)$_2$), 4.65 (d, 2H, OC$\underline{H}_2$, J= 5.46 Hz), 5.2-5.4 (m, 2H, =C$\underline{H}_2$), 5.8-6.0 (m, 1H, =C$\underline{H}$)

3.3.2 Synthesis of 3-(Chlorodimethylsilyl)propyl 2-bromo-2-methylpropanoate (2)
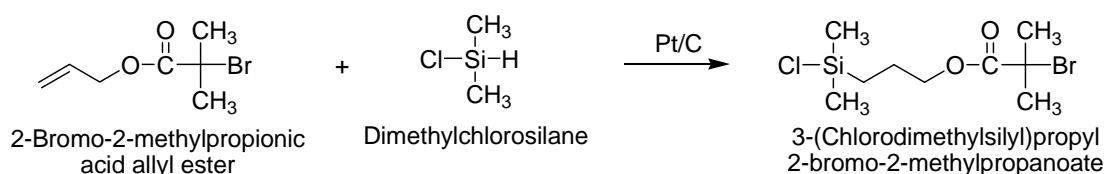
Allylic ester **(1)** (2 mL, 12 mmol) and dimethychlorosilane (20 mL) was added in 50 mL round bottom flask. After that, Pt/C (10%Pt) (20 mg) was added into this mixture. The mixture was refluxed at 45 °C for 24 h. The excess dimethychlorosilane was removed under reduced pressure. The oil residue was filtered through anhydrous

sodium sulfate to remove the catalyst to give chlorosilane initiator (2) as a colorless oil product in 95% yield.

^{1}H-NMR (CDCl$_3$) of 3-(chlorodimethylsilyl)propyl 2-bromo-2-methylpropanoate: δ 4.0-4.2 (t, 2H, -C$\underline{H}_2$O-, J= 13.65 Hz), 1.95 (s, 6H, -C(C$\underline{H}_3$)$_2$), 1.98 (m, 2H, -C$\underline{H}_2$-), 0.5 (m, 2H, -SiC$\underline{H}_2$-), 0.1 (m, 6H, -Si(C$\underline{H}_3$)$_2$-)

3.4 Synthesis of Tris(2-(dimethylamino)ethyl)amine [Me$_6$TREN](3)

Tris(2-aminoethyl)amine   formaldehyde/formic acid   Tris(2-(dimethylamino)ethyl)amine

95°C

(3)
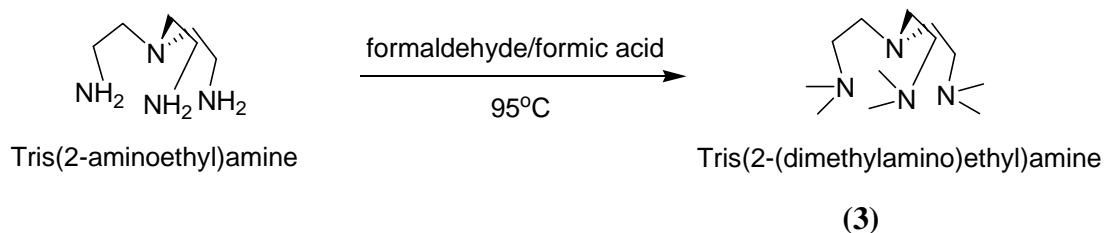
The synthetic method was modified from that reported by Queffelec [87]. A mixture of 35%w/v formaldehyde (12.0 mL, 0.4 mole) and 98%w/v formic acid (36.0 mL, 0.95 mole) was stirred at 0 ^{o}C under nitrogen atmosphere. After 1 h, 0.05 mole of tris(2-(aminoethyl)amine) or TREN was added dropwise via cannula, followed by an addition of deionized water via syringe. A mixture was refluxed for 24 h at 95 ^{o}C. After cooling to room temperature, a red-brown mixture was treated with saturated NaOH until pH reached 12. The resulting brown oil layer was extracted with dichloromethane and washed with saturated NaOH. The organic phase was dried over sodium sulfate before solvent removal under reduced pressure over 3h to give yellow oil as a product in 88% yield.

^{1}H-NMR (CDCl$_3$) of tris(2-(dimethylamino)ethyl)amine: δ 2.2 (s, 6H, -N(C$\underline{H}_3$)$_2$), 2.4 (t, 6H, -(C$\underline{H}_2$N-)$_3$, J= 14.43 Hz), 2.6 (t, 6H, -(C$\underline{H}_2$N)$_3$, J= 14.82 Hz).

3.5 Preparation of Polymer Brushes

3.5.1 Pretreatment of Glass Substrates

Glass coverslips having a diameter of 1.2 cm held in a slotted hollow glass cylinder (custom designed holder) were put a freshly prepared mixture of 7 parts of concentrated sulfuric acid an 3 parts of 30% hydrogen peroxide at ambient temperature for 2.5 h, rinsed with five aliquots of deionized water and placed in a clean oven at 130

°C for 2.5 h. Silanization reaction was carried out immediately after treating the substrates in this fashion.

3.5.2 Preparation of Surface-tethered Initiator (4)

	Glass coverslip	3-(Chlorodimethylsilyl)propyl 2-bromo-2-methylpropanoate	Glass supported 2-bromoisobutyrate monolayer
		(2)	**(4)**
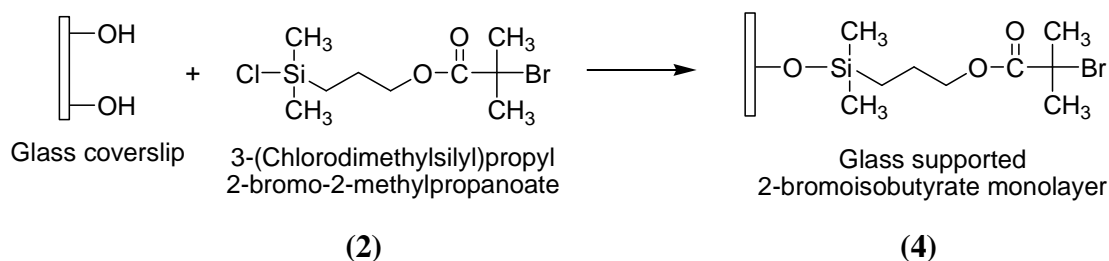
Freshly cleaned glass coverslips held in a slotted hollow glass cylinder were placed into a dried Schlenk flask. Substrates were kept under nitrogen. Triethylamine (60 μL, 0.43 mmol) in anhydrous toluene (20 mL) was transferred to the reactor flask *via* cannula. 3-(Chlorodimethylsilyl)propyl 2-bromo-2-methylpropanoate **(2)** (100 μL, 0.12 g, 0.4 mmol) was added into the reactor flask by a syringe. Reactions were carried out under nitrogen atmosphere at ambient temperature for 18 h. The substrates was rinsed with 1x10 mL of toluene, 2x10 mL of 2-propanol, 2x10 mL of ethanol, 1x10 mL of ethanol-water (1:1), 1x10 mL of water and then dried *in vacuo*.

3.5.3 Surface-initiated Polymerization of *tert*-Butyl Acrylate

(4)

CuBr$_2$ / EBriB

Sn(EH)$_2$

(5)
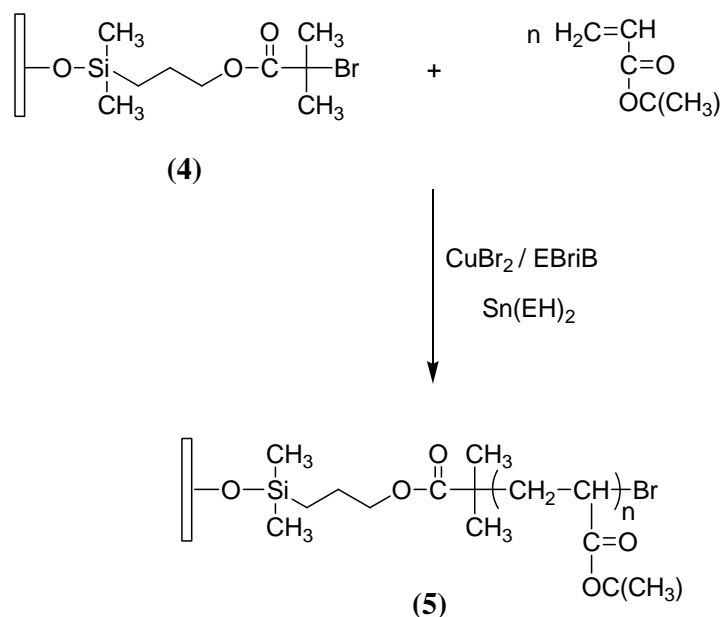
CuBr$_2$ (0.98 mg, 4.39 μmol) and acetone (4 mL) were first mixed in a glass vial having a magnetic stirring bar followed by an addition of Me$_6$TREN **(3)** (4.5 μL) to form a complex with Cu(II). *Tert*-butyl acrylate was added to the vial. The mixture was then stirred at ambient temperature until it became homogeneous (approximately 10 min) followed by an addition of ethyl α-bromoisobutyrate (59.4 μL, 0.399 mmol), the "sacrificial" initiator. The substrates bearing α-bromoisobutyrate monolayer **(4)** held in a slotted hollow glass cylinder was immersed in the vial that was later sealed with a rubber septum. The well-mixed solution of tin(II) 2-ethylhexanoate (194 μL, 0.6 mmol), acetone (1.5 mL) and Me$_6$TREN (11.0 μL) in a separated vial was then added via syringe to the reaction vial carrying the substrates. The volume of air in the reaction vial above the solution was fixed at 10.8 mL. The polymerization was allowed to proceed at ambient temperature. After a set reaction time, the polymerization was stopped by opening the vial and exposing the catalyst to air. And then, the substrates were removed and rinsed with THF. To remove the untethered P(*t*-BA), the substrates were placed in a soxhlet extractor and extracted with THF for 24 h and dried *in vacuo*. The substrates bearing poly(*tert*-butyl acrylate) (P*t*-BA) brushes were then analyzed by contact angle measurements. Free P*t*-BA from the solution was isolated by first evaporating residual monomer and solvent under reduced pressure and dissolving in THF. The polymer solution in THF was then analyzed by GPC.

3.5.4 Preparation of Surface-tethered Poly(acrylic acid) (PAA) Brushes via Hydrolysis of Poly(*tert*-butyl acrylate) Brushes

(5)

methanesulfonic acid
/CH_2Cl_2

(6)
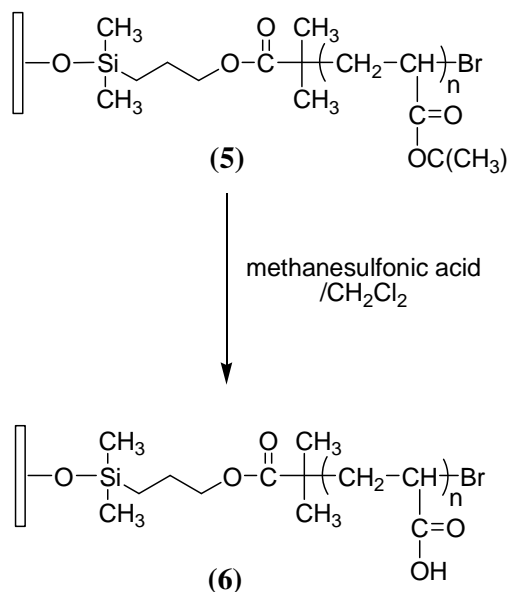
To remove the *t*-butyl groups by hydrolysis, the substrates-tethered P*t*-BA brushes (5) were treated with a mixture of methanesulfonic acid in dichloromethane (0.1 mL: 10 mL) at ambient temperature for 1 h to prepare surface-tethered PAA brushes (6). The substrates were removed, rinsed with dichloromethane (1x10 mL), ethanol (2x10 mL) and water (1x10 mL) and then dried *in vacuo*.

3.6 Determination of Carboxyl Groups of Surface-tethered Poly(acrylic acid) Brushes

Toluidine blue O staining method was employed to determine the amount of carboxyl groups on PAA brushes. A 0.5 mM dye aqueous solution was prepared at pH 10. The substrate-tethered PAA brushes were immersed in the dye solution for 6 h at ambient temperature. The substrates were then removed and thoroughly washed with a sodium hydroxide solution of pH 10 for 2 h to remove any noncomplexed dye adhering to substrates. The dye complexed with carboxyl groups was desorbed from the surface by dipping the substrates in 50% acetic acid solution overnight. The desorbed dye content was obtained by measuring the optical density of the solution at 633 nm with an UV-vis spectrophotometer (model Techna, specgene). The PAA was obtained from a calibration plot of the optical density versus dye solution having known concentration assuming that one carboxyl group reacts with one dye molecule.

3.7 Immobilization of Biomolecules to Carboxyl Groups of Poly(acrylic acid) Brushes

3.7.1 Activation of Carboxyl Groups on Surface-tethered Poly(acrylic acid) Brushes

(6)

(7)
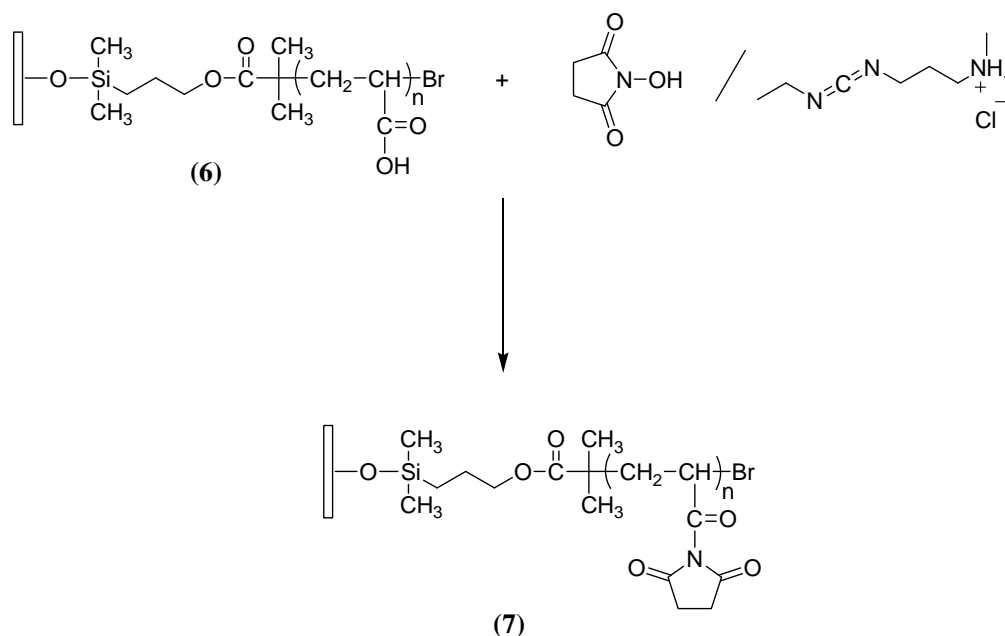
The substrates carrying PAA brushes (6) were immersed in an aqueous solution of EDCI (0.05 M) and NHS (0.1 M) and then stirred for 30 min. The activated PAA brushes-containing substrates (7) were removed from the solution and rinsed with deionized water and then dried *in vacuo*.

3.7.2 Immobilization of BSA on Activated PAA Brushes-Containing Substrates

(7)

(8)
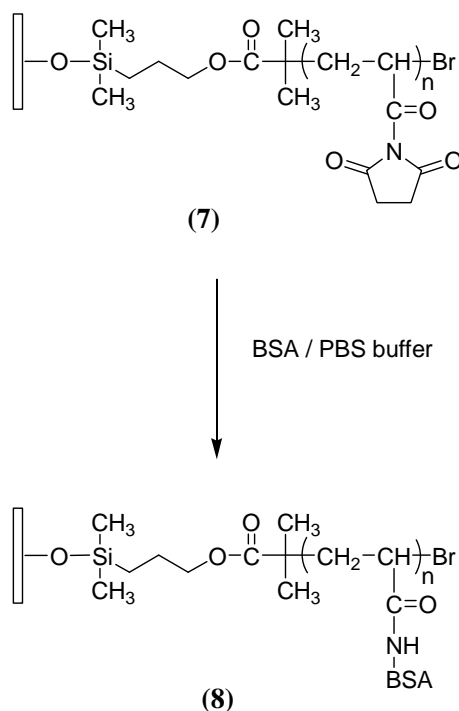
The activated PAA brushes-containing substrates (7) were immersed in a 2 mL of BSA solution (1mg/mL) in phosphate buffer saline (PBS, pH 7.4). After 1 h, the BSA immobilized substrates (8) were thoroughly rinsed with PBS solution and deionized water and then dried *in vacuo*.

3.7.3 Preparation of N-cadherin Mimic Cyclic Peptide
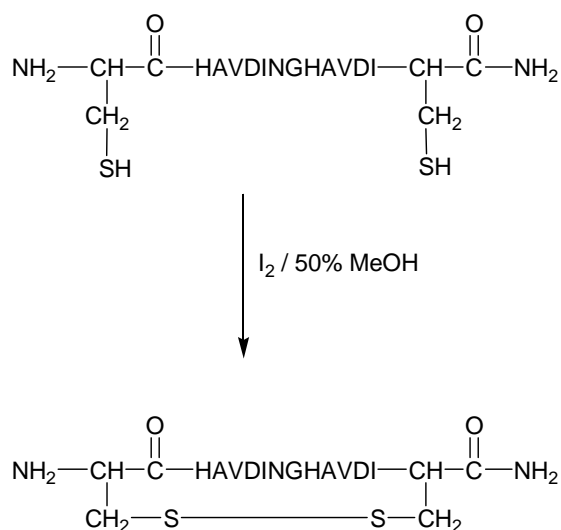
A synthetic N-cadherin mimic peptide has a sequence of *N*-CHAVDINGHAVDIC-NH$_2$. Two thiol groups of cysteine were oxidized by iodine. The peptide was first dissolved in 50% methanol to prepare a 1mg/1mL peptide solution. The peptide solution was added dropwise to a mixed solution of 0.1M I$_2$ (1 mL) and 1M HCL (1 mL) and then centrifuged for 30 min. Excess iodine in the peptide solution was removed by nitrogen blowing. The cyclized product appearing as white powder was obtained after lyophilization. Molecular weight of N-cadherin mimic cyclic peptide was analyzed by Mass spectrometer.

3.7.4 Immobilization of N-cadherin Mimic Cyclic Peptide on PAA Brushes-Containing Substrates

(7)

NH$_2$-*N*-cadherin mimic cyclic peptide/ PBS buffer

(9)
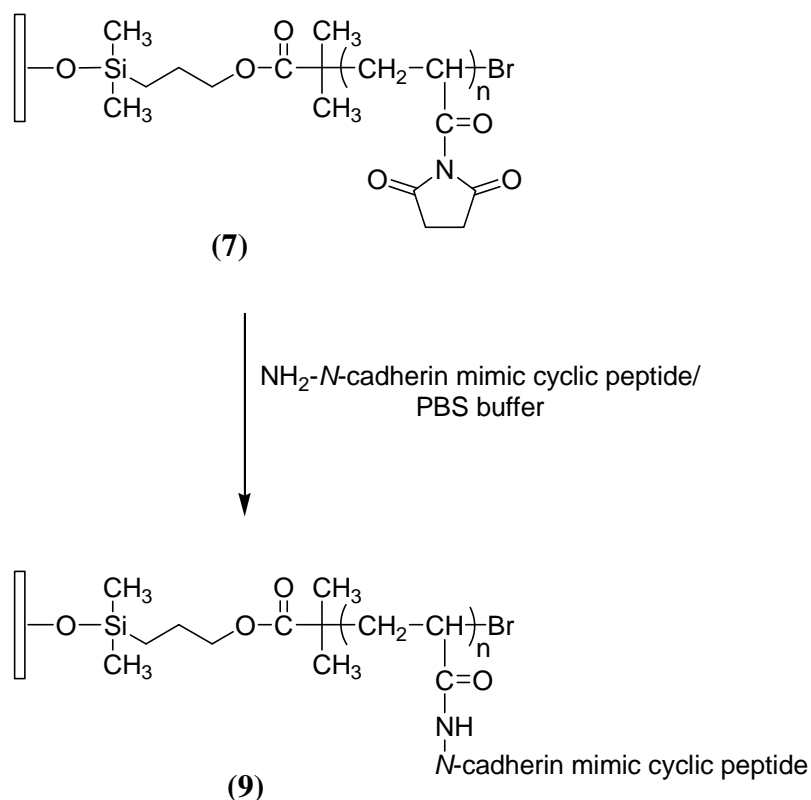
To determine the effect of N-cadherin mimic cyclic peptide concentration and reaction time on the amount of immobilized peptide, Surface plasmon resonance (SPR) technique was employed using a gold-coated SPR disk grafted with PAA brushes having a target DP = 200 as a substrate. SPR assays were conducted using an Autolab SPR procured from the Eco Chemie (Netherlands) at 25°C. The carboxyl groups of

PAA brushes were activated by aqueous solution of EDC/NHS and subsequent coupling with amino groups of-N-cadherin mimic cyclic peptide in PBS buffer..

The activated PAA brushes-containing substrates (7) were immersed in a solution of N-cadherin mimic cyclic peptide in phosphate-buffered saline (PBS, pH 7.4) using the optimized peptide concentration and reaction time identified by SPR. After that the substrates (9) were thoroughly rinsed with PBS buffer solution and deionized water and then dried *in vacuo*.

3.8 Cytotoxicity Test

PAA brushes-containing substrates immobilized with N-cadherin mimic cyclic peptide (9) were sterilized by 70% ethanol solution for 6 h in 24-well tissue culture plate. The substrate were removed from the solution and rinsed with sterile PBS buffer solution. Mouse neural progenitor cells were added in this well plate at a seeding density of 5×10^5 cells/mL in 500 µL Neurobasal medium (serum-free medium) supplemented with 1× B27, 2 mM glutamine, 50 U/mL penicillin/streptomycin, 20 ng/mL Epithelial growth factor (EGF), 20 ng/mL Fibroblast growth factor (FGF) and 2 µg/ml Heparin. The plate was then incubated at 37°C in humidified 5% CO_2 in air for 6 h, 1, 2, and 4 days. Cell morphology was continuously monitored under an optical microscope. After the desired period of time, the cells were harvested by trypsinization and counted after adding Trypan blue dye in cell solution to detect live or dead cells under hemacytometer. The experiments were carried out in triplicate in comparison with laminin-coated substrates.

CHAPTER IV

RESULTS AND DISCUSSION

In this chapter, the results are divided into four sections. The first section, explains the synthesis of reagents to be used for polymerization such as surface initiator and ligand. The second section mainly focuses on polymerization of poly(*tert*-butylacrylate)(P*t*-BA) brushes from surface-tethered α-bromoisobutyrate monolayer via surface-initiated polymerization as activators regenerated by electron transfer (ARGET) of *tert*-butyl acrylate (*t*-BA). Poly(*tert*-butyl acrylate) (P*t*-BA) brushes were converted to poly(acrylic acid)(PAA) brushes by acid hydrolysis. The third section presents reactivity of carboxyl groups towards biomolecule immobilization. The last section addresses cytotoxicity test of mouse neural progenitor cell (mNSC) on surface modified with N-cadherin mimic cyclic peptide.

4.1   Synthesis of α-Bromoester Compound

4.1.1   Synthesis of 2-Bromo-2-methylpropionic Acid Allyl Ester

$$(1)$$
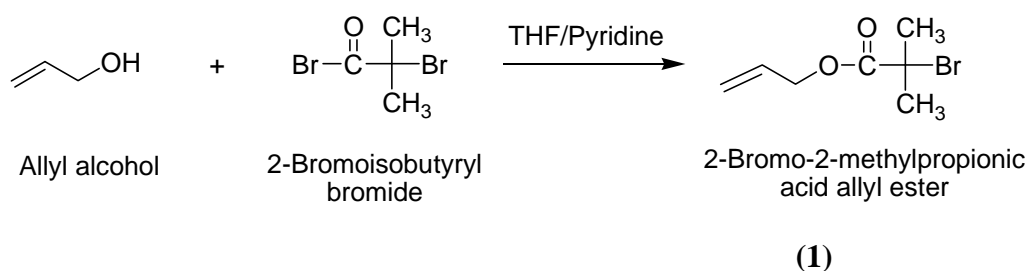
Scheme 4.1 Stepwise synthetic route of 2-bromo-2-methylpropionic acid allyl ester

2-Bromo-2-methylpropionic acid allyl ester (1) as colorless oil was a product obtained from esterification reaction allyl alcohol with 2-bromoisobutyryl bromide (Scheme 4.1). This product was sufficiently pure for the next synthesis after purification by liquid extraction and vacuum distillation. This synthesis gave the product in 91%

yield. The ^{1}H-NMR (Figure A-1) of a 2-bromo-2-methylpropionic acid allyl ester shows a doublet of doublet signal and multiplet signals of alkene protons, (C<u>H</u>$_2$=CH, b) at 5.2-5.4 ppm and (CH$_2$=C<u>H</u>, a) at 5.8-6.0 ppm, a doublet signal of methylene protons (OC<u>H</u>$_2$, c) at 4.7 ppm, and a signal of methyl protons of C(C<u>H</u>$_3$) at 1.9 ppm (d). This spectrum indicates the complete reaction between allyl alcohol and 2-bromo-2-methylpropionyl bromide.

4.1.2 Synthesis of 3-(Chlorodimethylsilyl)propyl 2-bromo-2-methylpropanoate

2-Bromo-2-methylpropionic acid allyl ester **(1)** + Dimethylchlorosilane → [Pt/C] → 3-(Chlorodimethylsilyl)propyl 2-bromo-2-methylpropanoate **(2)**
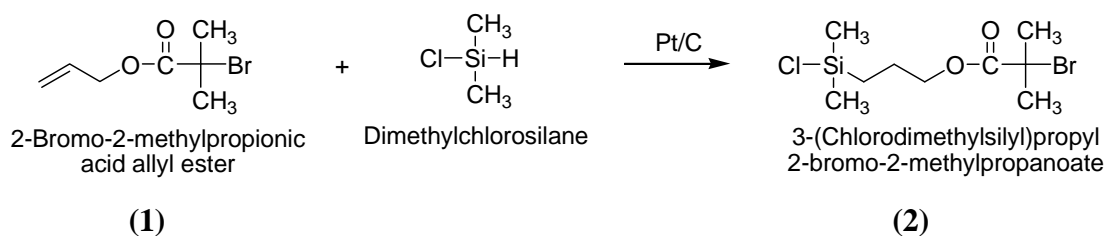
Scheme 4.2 Hydrosilylation of 3-(Chlorodimethylsilyl)propyl 2-bromo-2-methylpropanoate (2)

3-(Chlorodimethylsilyl)propyl 2-bromo-2-methylpropanoate (2) can be synthesized via hydrosilylation of 2-bromo-2-methylpropionic acid allyl ester (1) by dimethylchlorosilane (Scheme 4.2). This reaction was carried out by refluxing in the presence of Pt/C catalyst for 24 h. The crude product was colorless oil and obtained in 95% yield. The mechanism of hydrosilylation is shown in Scheme 4.3. The ^{1}H-NMR (Figure A-2) of 3-(chlorodimethylsilyl)propyl 2-bromo-2-methylpropanoate (2) shows a triplet signal of methylene proton (C<u>H</u>$_2$O) at 4.0-4.2 ppm, singlet signals of methyl protons (CC<u>H</u>$_3$) at 1.9 ppm and (SiC<u>H</u>$_3$) at 0.1 ppm, multiplet signals of methylene proton (SiC<u>H</u>$_2$CH$_2$CH$_2$O) at 0.5 ppm and (SiCH$_2$C<u>H</u>$_2$CH$_2$O) at 1.8 ppm. The fact that a doublet of doublet signal and a multiplet signal of alkene protons, (C<u>H</u>$_2$=CH, b) at 5.2-5.4 ppm and (CH$_2$=C<u>H</u>, a) at 5.8-6.0 ppm, respectively from the starting reagent (1) disappeared after the reaction indicating the completion of the reaction.
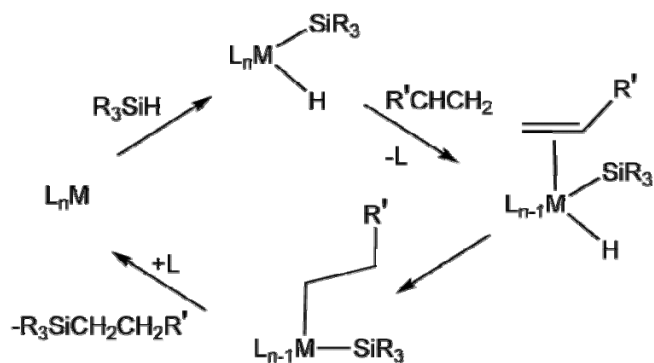
Scheme 4.3 Mechanism of hydrosilylation [88]

4.2 Synthesis of Tris (2-(dimethylamino)ethyl)amine [Me₆TREN]
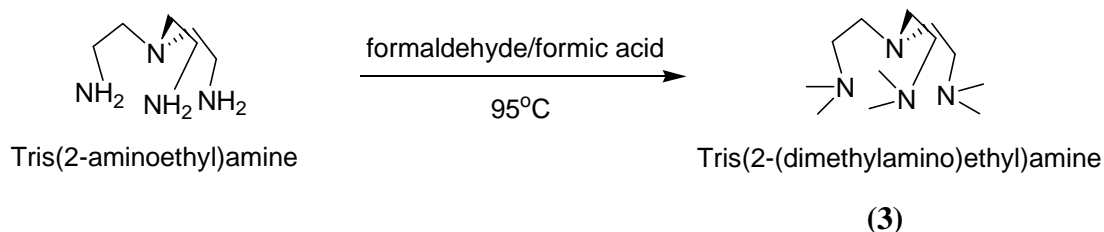
Scheme 4.4 Methylation of tris(2-aminoethyl)amine

Tris(2-(dimethylamino)ethyl)amine (Me$_6$TREN) (3) was synthesized by methylation, Eschweiler-Clarke reaction, of tris(2-aminoethyl)amine (TREN) (Scheme 4.4). The product was light yellow oil obtained in 88% yield. The product was sufficiently pure for complexing with copper(II) ion in polymerization reaction. The mechanism of Eschweiler-Clarke reaction is shown in Scheme 4.5. The ^{1}H-NMR (Figure A-3) of tris(2-(dimethylamino)ethyl)amine shows two doublet of doublet signals of methylene protons (NC$\underline{H}_2$CH$_2$N(CH$_3$)$_2$) and (NCH$_2$C$\underline{H}_2$N(CH$_3$)$_2$) at 2.6 ppm and 2.4 ppm, respectively. Moreover, a singlet signal of (N(C$\underline{H}_3$)$_2$) is shown at 2.2 ppm.
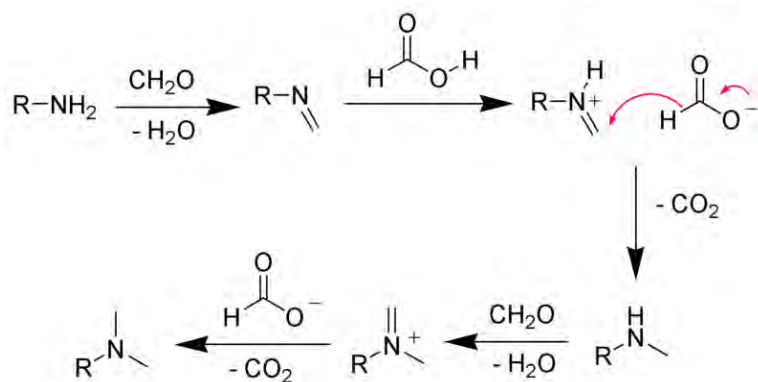
Scheme 4.5 Mechanism of Eschweiler-Clarke reaction [89]

4.3   Preparation of Poly(acrylic acid) (PAA) Brushes

4.3.1   Preparation of Surface-tethered Initiator
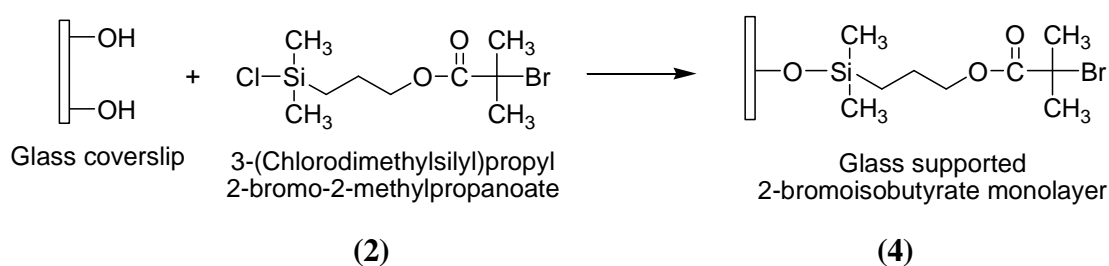
Scheme 4.6 Synthesis of surface-tethered 2-bromoisobutyrate monolayer

The water contact angle of a clean glass coverslip have increased from 22°/13° to 70°/60° after silanization with 3-(chlorodimethylsilyl)propyl 2-bromo-2-methylpropanoate **(2)** which acts as a surface initiator indicating that hydrophobic α-bromoisobutyrate monolayer was formed on the glass surface (Scheme 4.6).

4.3.2 Surface-initiated Polymerization of *tert*-Butyl Acrylate
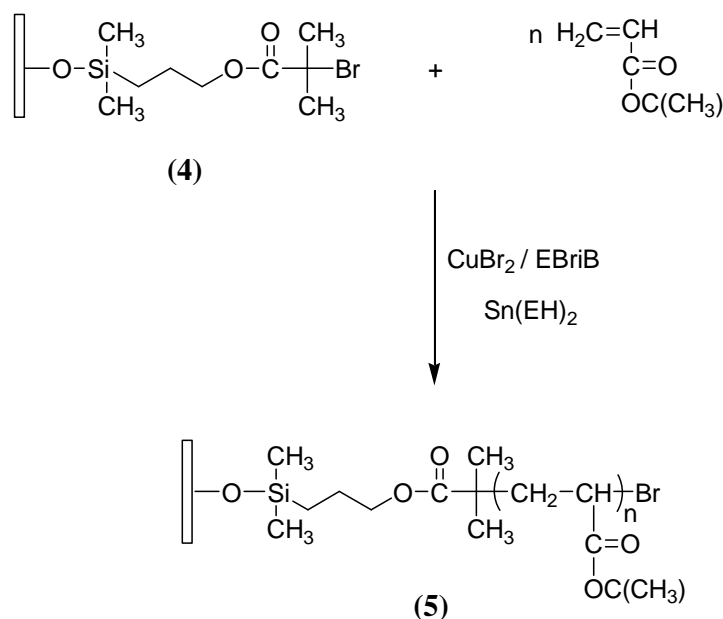
Scheme 4.7 Polymerization reaction of *tert*-butyl acrylate

It is rather difficult to obtain the molecular weight of the polymer brush directly since the amount of polymer on the substrate is too small to degraft and analyze. The polymer chains formed by the free initiator ("sacrificial" initiator) in solution were then used to monitor the surface-initiated polymerization process and molecular weight. It has been proven that the molecular weight and polydispersity of the graft polymer were nearly equal to those of the free polymer produced in the solution, meaning that the free polymer is a good measure of the characteristics of the graft polymer [90]. The free initiator plays a role not only as an indicator of the polymerization but also as a controller for the ARGET ATRP on the surface. The concentration of the Cu(II) complex produced from the reaction at the substrate surface is too low to reversibly deactivate polymer radicals with a sufficiently high rate. The addition of the free initiator creates the necessary concentration of the Cu(II) complex, which in turn controls polymerization from the substrate as well as in solution. Moreover, Cu(II) can be reduced to Cu(I) by reducing agent (Scheme 2.1).

To seek for an optimal condition that yields polymer with well-controlled molecular weight and molecular weight distribution, the effect of mole ratio of

Sn(EH)$_2$:Me$_6$TREN and polymerization time were investigated. Sn(EH)$_2$Br$_2$ as a product in reactivation process (Scheme 2.4) is a strong Lewis acid which can from complex with ligand. Therefore, the amount of ligand affected the reactivity of the catalyst in polymerization reaction.

According to the results shown in Figure 4.1, the molar ratio of Sn(EH)$_2$:Me$_6$TREN of 10:1 was considered as the optimal value because it gave reasonably high $\overline{M}_n$ with a narrow molecular weight distribution (close to 1). Further reduction of the amount of Me$_6$TREN by increasing the ratio to 15:1 led to a negative impact on the livingness of the polymerization. Reducing the ratio to 8:1 and 5:1, the molecular weight distribution was closer to 1 showing the narrow molecular weight distribution. It should be emphasized that ones try to consume the least amount of Me$_6$TREN in order to minimize the expense from the costly ligand.
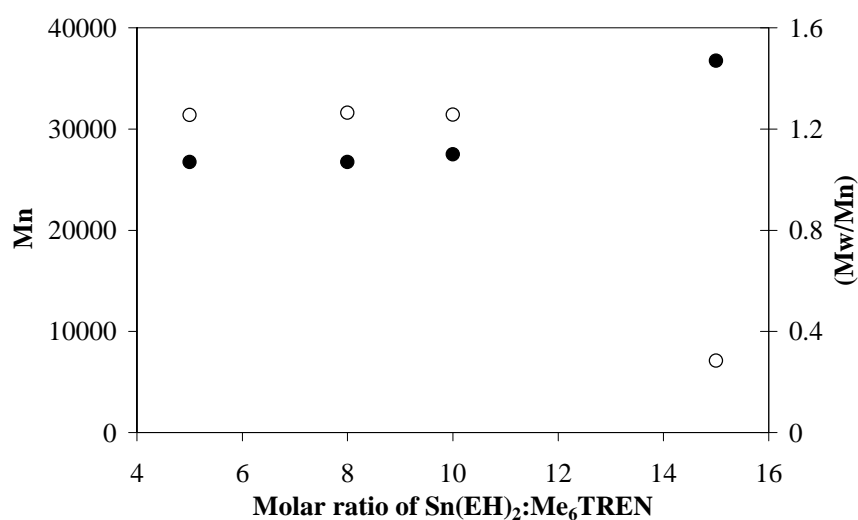
Figure 4.1 $\overline{M}_n$ (o) and $\overline{M}_w/\overline{M}_n$ (●) of Pt-BA as a function of Sn(EH)$_2$:Me$_6$TREN molar ratio for targeted DP = 200
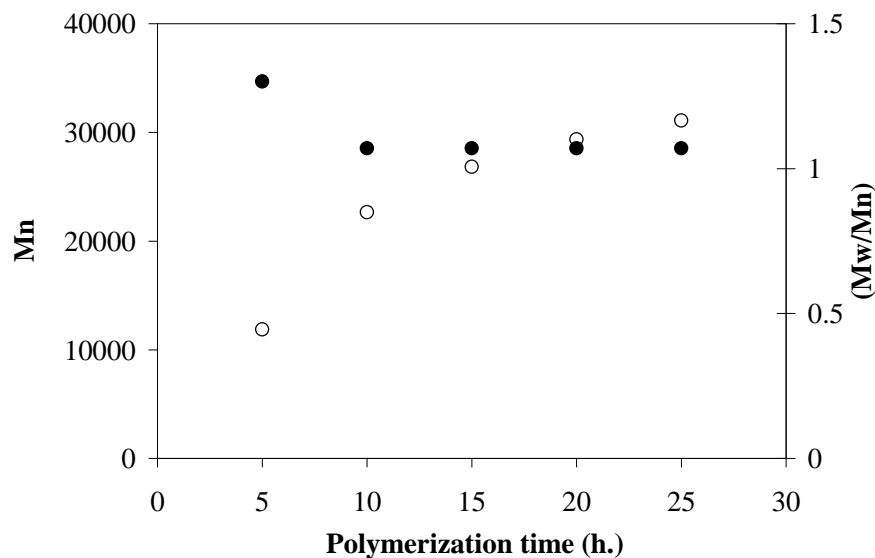
Figure 4.2 $\overline{M}_n$ (o) and $\overline{M}_w/\overline{M}_n$ (•) of P*t*-BA as a function of time for targeted DP = 200

Figure 4.2 shows the changing in the molecular weight ($\overline{M}_n$) and molecular weight distribution ($\overline{M}_w/\overline{M}_n$) of free P*t*-BA as a function of polymerization time at targeted degree of polymerization (DP) of 200. The monomer (*t*-BA) concentration of 4.8 M and the [I]/[CuBr$_2$]/[Sn(EH)$_2$]/[Me$_6$TREN] mole ratio of 1:0.01:1.6:0.16 were fixed in these experiments. The data suggested that 15-20 h is sufficiently long for the polymerization to reach the completion while the molecular weight distribution remained low, being close to 1.0, the ideal target of living polymerization. It should be noted at this point that the obtained $\overline{M}_n$ (~29,000) was somewhat higher than the target one ($\overline{M}_n$ = 25,634) of which the targeted degree of polymerization (DP) is 200. This characteristic seems to be typical and has been also observed by others [25]. From this result, polymerization time at 15 h gave a high molecular weight suitable for DP 200 and molecular weight distribution being close to 1.0 suggested that the polymerization mechanism is living.

Figure 4.3 shows the development of P*t*-BA brushes thickness as a function of polymerization time at target DP = 200. The thickness of dry polymer layer was obtained by measuring the surface profile after being scraped by AFM tip using AFM technique (Figure A-9). It was found that the thickness of P*t*-BA brushes linearly

increased as a function of polymerization time suggesting that the polymerization is living and can be well controlled.
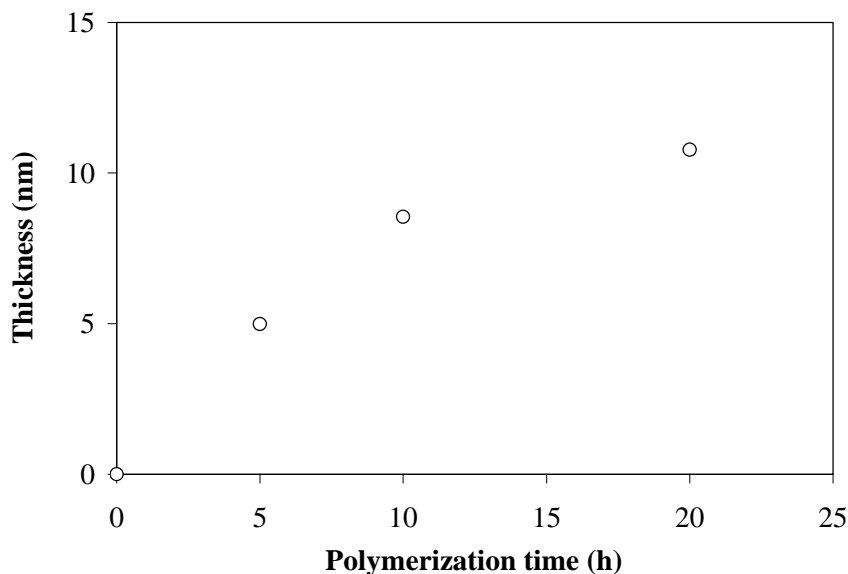
Figure 4.3 Thickness of Pt-BA brushes determined by AFM technique versus polymerization time for targeted DP = 200

The information related to molecular weight and thickness can be used to calculate a grafting density of polymer brushes. The grafting density (σ) which is a unit per cross-sectional area (A_x) per chain can be determined from the corresponding film thickness (t) and the molecular weight of the chain (M_n) from the following equation by

$$\sigma = \frac{t\rho N_A}{Mn} = \frac{1}{A_X} \tag{4.1}$$

Where ρ is the mass density (1.1 g/cm^3 for Pt-BA) and N_A is Avogadro's number. Using slopes obtained from the plot in Figures 4.4 which corresponds to t/M_n, the calculated grafting density is 0.33 chains/nm^2 for the targeted DP = 200. These results agree quite well with the data previously reported that the grafting densities for various polymers prepared by surface-initiated ATRP which are ranged from 0.1 to 0.6 chains/nm^2 [20] and by ARGET ATRP which is about 0.4 chains/nm^2 [25].
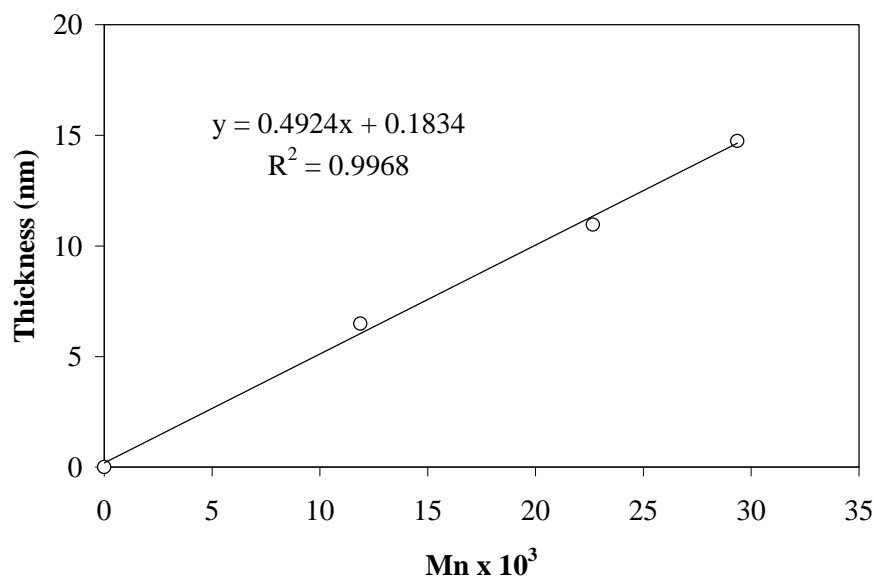
Figure 4.4 Relationship between the thickness of P*t*-BA brushes with molecular weight of free P*t*-BA for targeted DP = 200

The percent conversion of monomer (*t*-BA) can be calculated from peak integration from ^{1}H-NMR spectra of P*t*-BA. Figure 4.5 displays a ^{1}H-NMR spectra of P*t*-BA after polymerization for 15 h. The hydrogen atom bonded to carbon 2 in backbone of P*t*-BA is responsible for a set of signals at 2.2 ppm (b) while those signals observed at 6.0 ppm (a) are attributed to the hydrogen atoms of the methylene groups of *t*-BA. From the ratio between the area under the peak at 2.2 ppm (b) and that under the peak at 6.0 ppm (a), it is possible to determine the percent conversion of the P*t*-BA by using the following expression:

$$\% \ Conversion \ of \ t-BA \ = \ \left[\frac{\int CH_b}{\int CH_a + \int CH_b} \right] \times 100 \qquad (4.2)$$
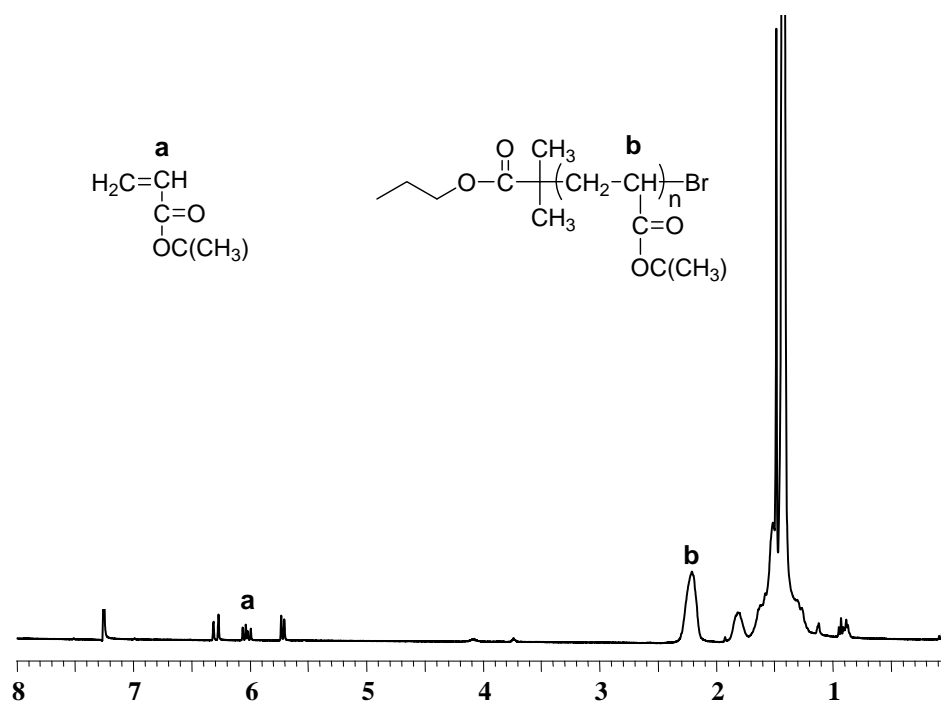
Figure 4.5 ^{1}H-NMR spectrum (400 MHz, CDCl$_3$) of Pt-BA after polymerization of t-BA for 15 h

According to Figure 4.6, %conversion of monomer, t-BA has reached ~99% after the molecular weight was above 25,000 (a target $\overline{M}_n$ for DP = 200) which can be achieved after the polymerization was carried out for 15 h. This indicated that most of the monomer was consumed and converted to Pt-BA at this particular time point.
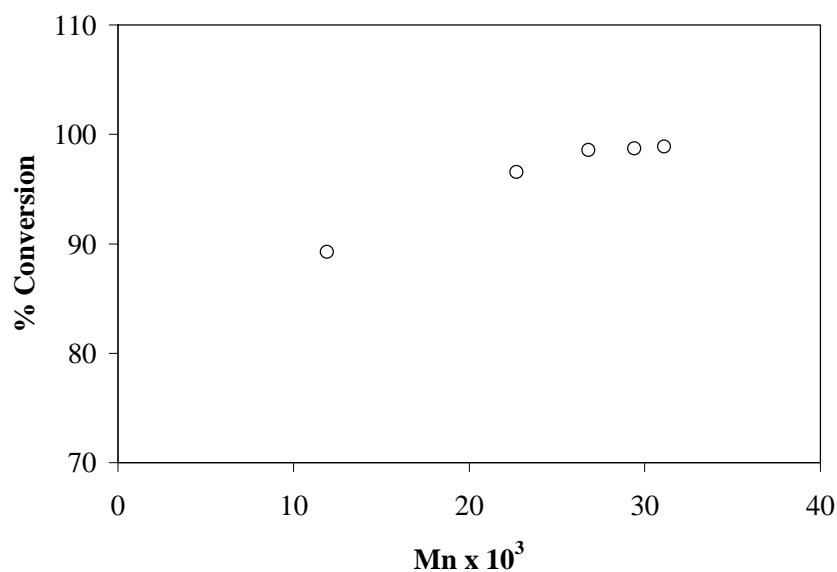
Figure 4.6 Relationship between % conversion of t-BA with molecular weight of Pt-BA for targeted DP = 200

Data shown in Table 4.1 suggests that the molecular weight of P*t*-BA can be varied as a function of targeted degree of polymerization (DP) which is determined by monomer to initiator ratio. Upon using polymerization time of 15 h, the $\overline{M}_n$ values obtained from GPC analysis at all targeted DPs are relatively close to the targeted ones. The molecular weight distribution or polydispersity index (PDI) are very close to 1 suggesting that the polymerization reaction is living and can be well controlled.

Table 4.1 Molecular weight and PDI of P*t*-BA having different DP

Degree of polymerization	Targeted MW	$\overline{M}_n$	PDI
50	6408	7490	1.13
100	12817	14229	1.1
200	25634	25576	1.07

The growth of P*t*-BA brushes can also be monitored by water contact angle analysis. Figure 4.7 illustrates advancing (θ_A) and receding (θ_R) water contact angles of glass-supported P*t*-BA brushes as a function of polymerization time. Both advancing (θ_A) and receding (θ_R) contact angles rapidly increased from $70^o/60^o$ of the glass-supported α-bromoisobutyrate monolayer to ~ $91^o/76^o$ for P*t*-BA. These results indicated that more hydrophobic surface has been obtained as a consequence of P*t*-BA brushes formation. The fact that the water contact has reached the highest value after the polymerization for 10 h suggests that the wettability of P*t*-BA brushes was no longer dependent on the thickness above 5 nm (See Figure 4.3). Moreover, the contact angle hysteresis (θ_A - θ_R) being less than 20° also implies that the surface bearing P*t*-BA brushes is quite homogeneous and smooth.
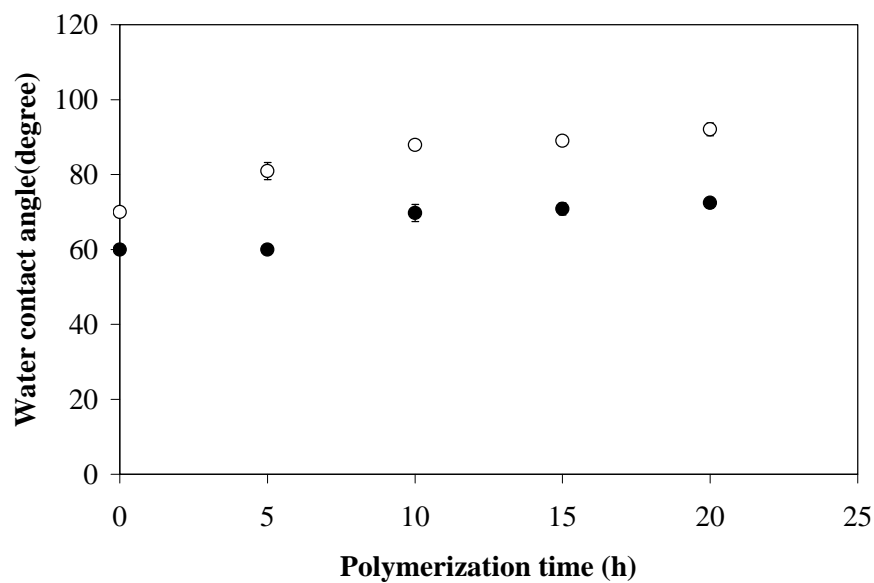
Figure 4.7 Water contact angle data of P*t*-BA brushes versus polymerization time for targeted DP = 200 (Θ_A (o), Θ_R (●))

Up to this point, it can be concluded that the polymerization of *t*-BA can be well controlled. The optimized condition includes [I]/[CuBr$_2$]/[Sn(EH)$_2$]/[Me$_6$TREN] mole ratio of 1:0.01:1.6:0.16, molar ratio of Sn(EH)$_2$: Me$_6$TREN of 10 : 1 molar ratio of Sn(EH)$_2$: initiator of 1:1, and polymerization time of 15 h.

4.3.3 Preparation of Surface-tethered Poly(acrylic acid) (PAA) Brushes
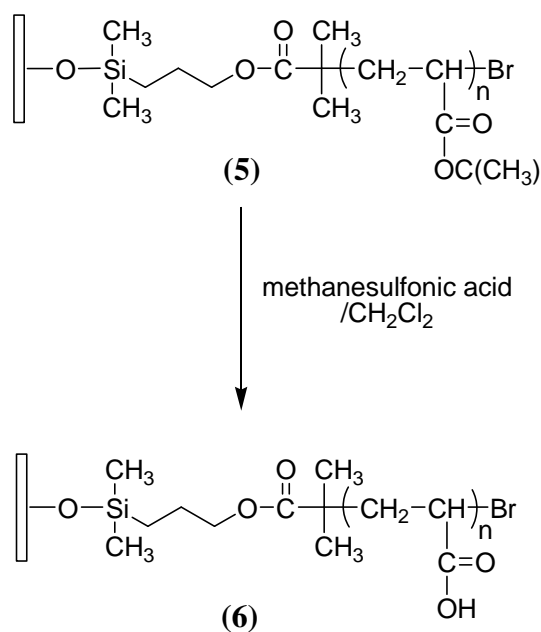
Scheme 4.8 Acid hydrolysis of poly(*tert*-butyl acrylate) (P*t*-BA) brushes

Poly(acrylic acid) (PAA) brushes can be prepared by acid hydrolysis of poly(*tert*-butyl acrylate) (P*t*-BA) brushes using optimal condition previously identified which is 0.1 mL of methanesulfonic acid (MeSO$_3$H) in 10 mL of dichloromethane at room temperature [45]. The success of PAA formation upon hydrolysis of P*t*-BA in solution was first demonstrated by ^{1}H NMR analysis. As shown in Figure 4.8, a signal of methyl proton (CH$_3$) belonging to the *t*-butyl groups at 1.4 ppm in spectrum B of P*t*-BA is absent in spectrum A of PAA indicating that the *t*-butyl groups were completely removed.
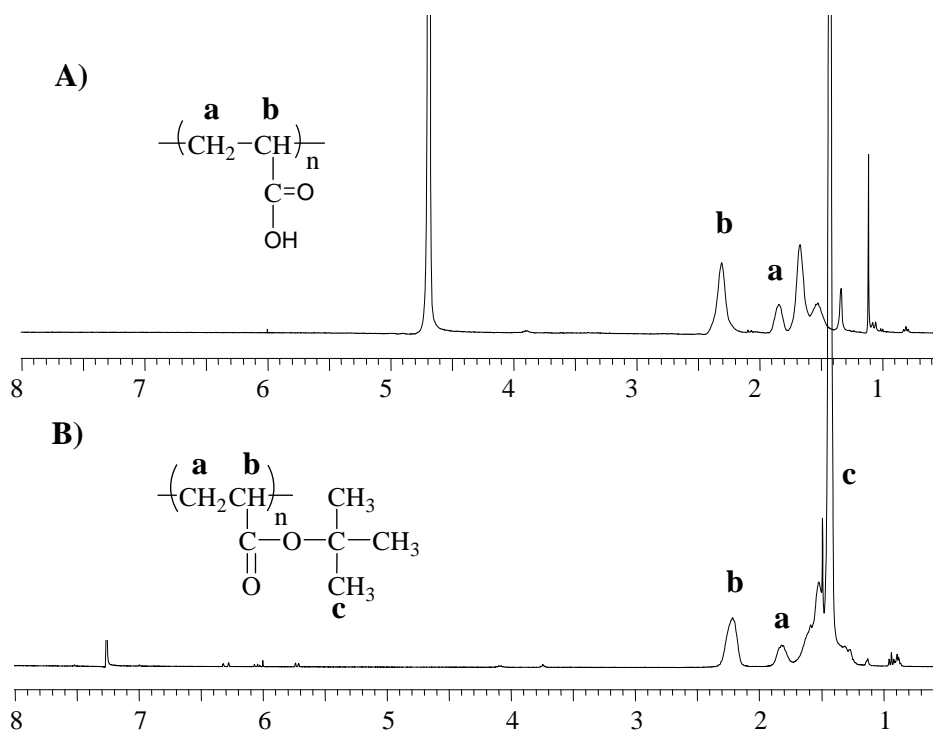
Figure 4.8 ^{1}H-NMR spectra of (A) PAA (400 MHz, D$_2$O) and (B) Pt-BA (400 MHz, CDCl$_3$) in solution

Evidence indicating the formation of PAA brushes was obtained from ATR-IR analysis of silica particles grafted with Pt-BA brushes before and after hydrolysis. As shown in Figure 4.9, a signal of C=O stretching of ester groups of Pt-BA brushes at 1725 cm^{-1} shifted slightly down to 1711 cm^{-1} of C=O stretching of carboxyl groups of PAA brushes upon hydrolysis indicating that Pt-BA brushes have been transformed to PAA brushes.
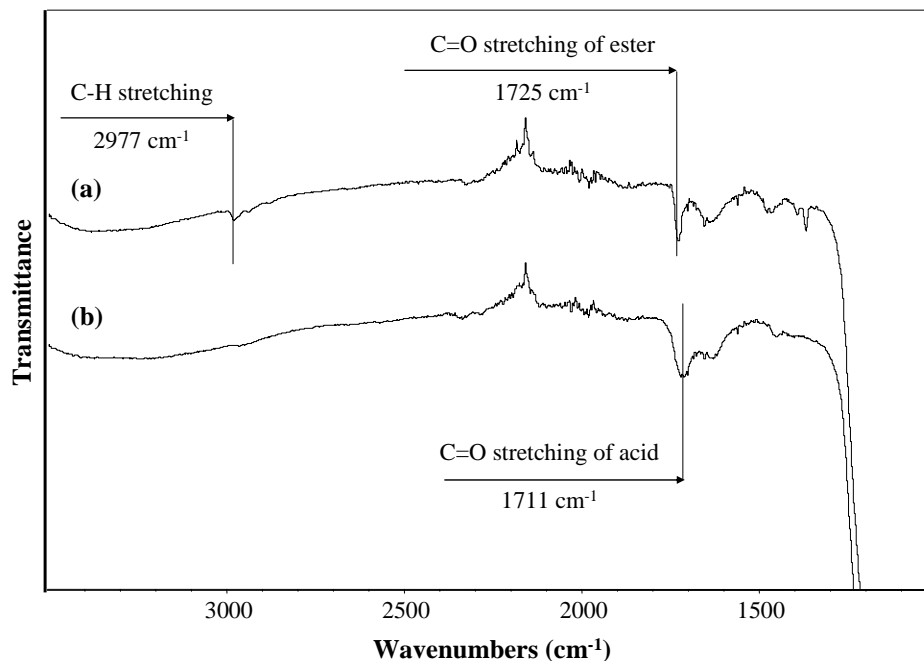
Figure 4.9 ATR-FTIR spectra of silica particles grafted with (a) P*t*-BA brushes and (b) PAA brushes

Carboxyl group density of PAA brushes versus polymerization time was investigated in order to identify the relationship between molecular weight and amount of carboxyl groups. The density of carboxyl group (COOH) on PAA brushes was quantitatively determined by using Toluidine blue O assay. The carboxyl groups of PAA brushes can form a complex with Toluidine blue O. The absorbance of the solution containing the desorbed complex was measured at 633 nm. The COOH content was obtained from a calibration plot of the optical density versus dye concentration which is displayed in Appendix C. From Figure 4.10, it was found that the density of carboxyl group increased as a function of molecular weight or chain length of PAA brushes. The density was ranged from 0.7×10^{-9} to 1.6×10^{-9} mol/cm^2) for the PAA brushes having $\overline{M}_n$ in the range of 11.8×10^3 to 29.3×10^3.
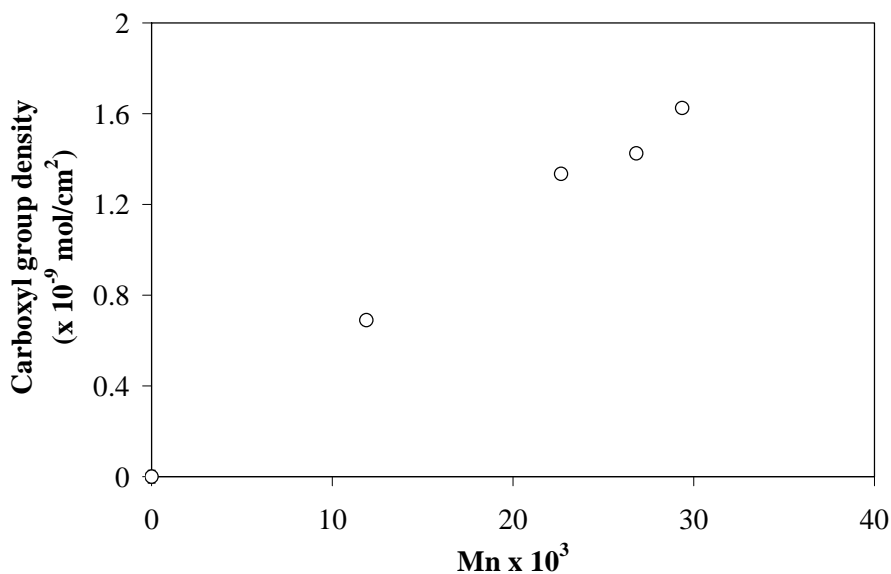
Figure 4.10 Carboxyl group density of PAA brushes as a function of molecular weight for target DP = 200

Figure 4.11 shows water contact angles of PAA brushes as a function of polymerization time. The lowering water contact angle from those of P*t*-BA brushes (Figure 4.7) to these of PAA brushes suggesting that the hydrophobic *tert*-butyl groups of P*t*-BA were converted to the hydrophilic carboxyl groups of PAA brushes. The molecular weight dependent water contact angle values are in good agreement with the carboxyl group density data. The higher the carboxyl group density is, the lower water contact angle and the more hydrophilic of surface becomes.
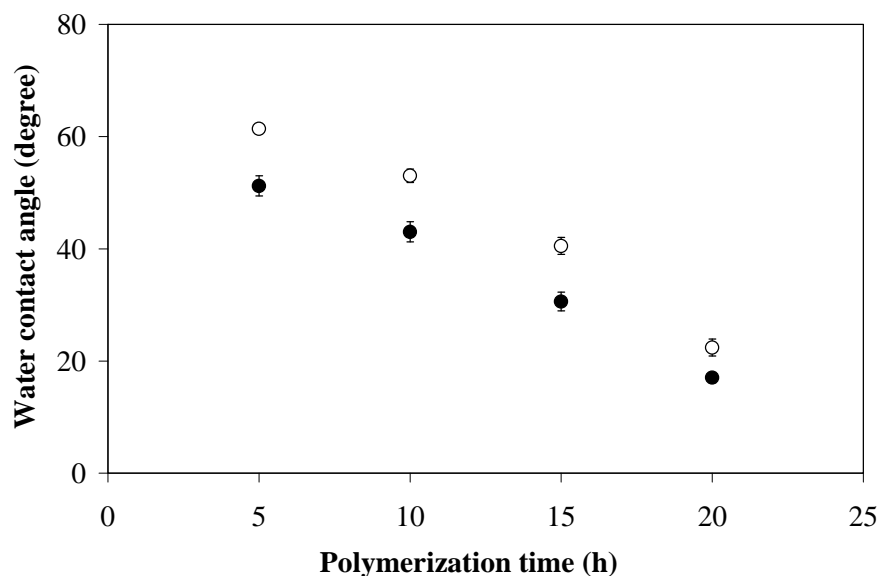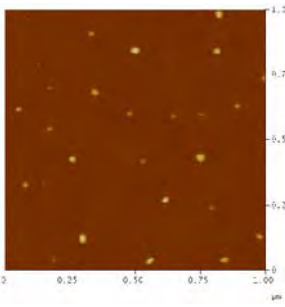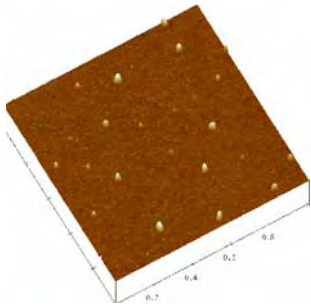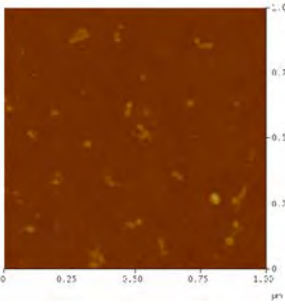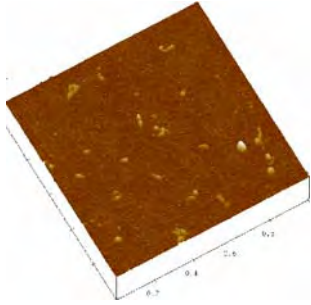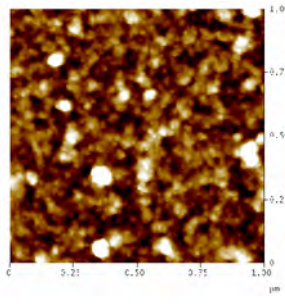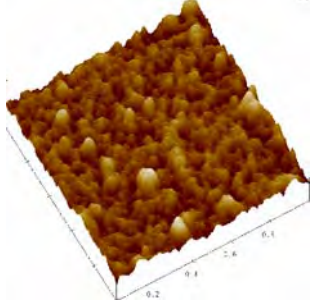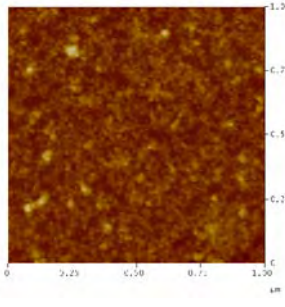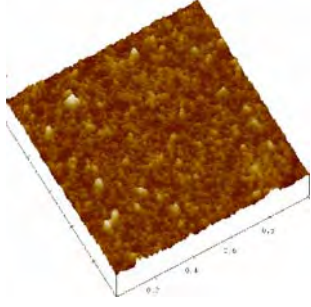
Figure 4.11 Water contact angle data of PAA brushes versus polymerization time for targeted DP = 200 (Θ_A (o), Θ_R (●))

Atomic force microscopy (AFM) was used as a tool to determine the surface topography and roughness of polymer brushes. As demonstrated in Table 4.2, the roughness and topography of a glass coverslip was not much changed after the immobilization of surface initiator. Both surfaces are featureless and extremely smooth with very low surface roughness. After being covered by P*t*-BA brushes, the surface of glass coverslip became rougher with a roughness of 6.337 nm. Nonetheless, the coverage of the grafted P*t*-BA brushes are relatively uniform. Evidently, the grafted PAA brushes are smoother than the grafted P*t*-BA brushes with uniform coverage on the surface.

Table 4.2 AFM images of surface-modified glass coverslips

Sample	Morphology in 2D	Morphology in 3D
Cleaned glass coverslip		
Rms Roughness (nm)	1.049 nm	
Glass coverslip-surface initiator		
Rms Roughness (nm)	0.764 nm	
Glass coverslip-Pt-BA		
Rms Roughness (nm)	6.337 nm	
Glass coverslip-PAA		
Rms Roughness (nm)	1.964 nm	

4.4 Immobilization of Protein/Peptide on Poly(acrylic acid) (PAA) Brushes
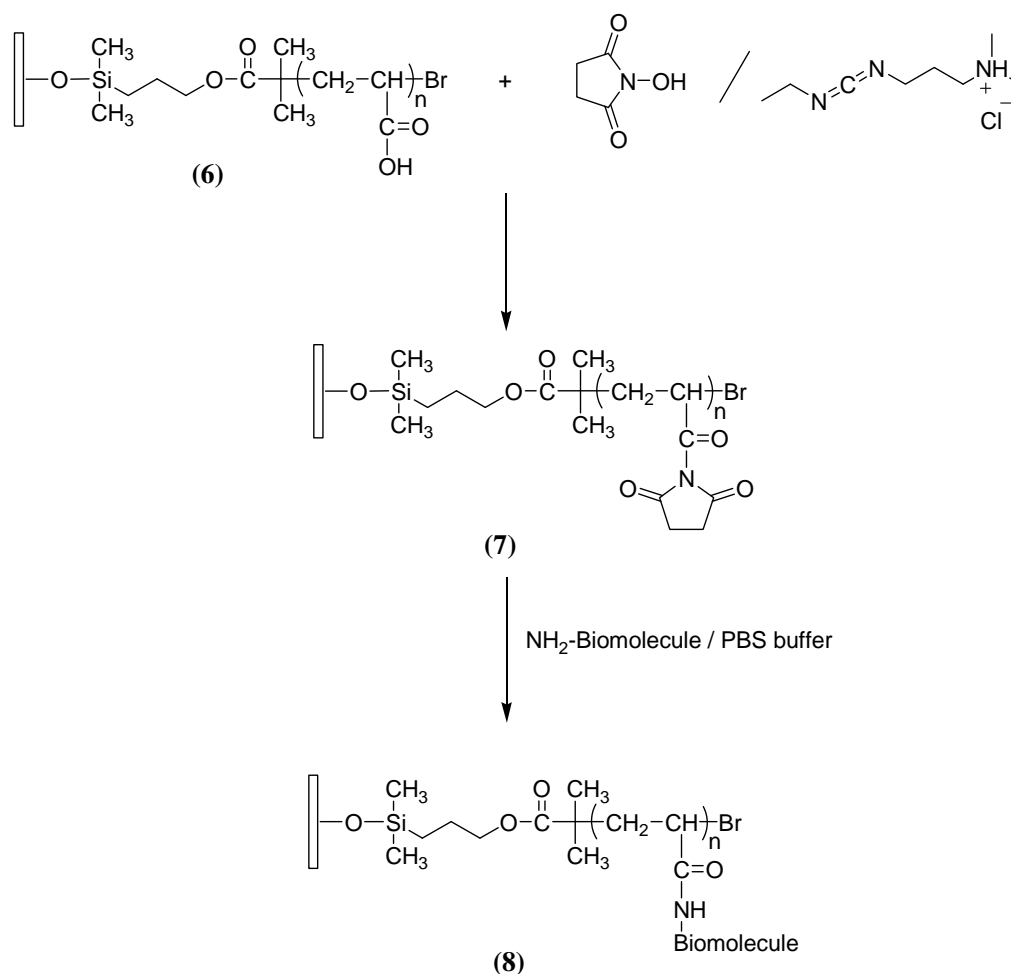
Scheme 4.9 Immobilization of protein/peptide on PAA brushes

4.4.1 Immobilization of BSA

In general, biomolecules are often immobilized on polymer surfaces via an amide bond formation between the carboxyl groups of polymer and the amine groups of biomolecule. Bovine serum albumin (BSA) was chosen as a model biomolecule. To achieve the covalent attachment of BSA to the carboxyl groups of PAA brushes, a method of introducing reactive intermediate, *N*-hydroxysuccinimidyl (NHS) ester was used. The carboxyl groups of PAA brushes were first activated by a water-soluble carbodiimide, 1-(3-dimethylaminopropyl)-3-ethylcarbodiimide hydrochloride (EDC) and *N*-hydroxysuccinimide (NHS) to form NHS group. The NHS group was then coupled with amine-terminated BSA leading to amide bond formation.

The success of activation and BSA immobilization on PAA brushes was first verified by FT-IR analysis in ATR mode. The shoulder peaks in spectrum (b) at 1736,

1781 and 1811cm^{-1} assigned to the carbonyl stretching of N-succinimidyl ester (NHS) of FT-IR spectrum shown in Figure 4.12 indicated that the carboxyl group was transformed to NHS group after activation by EDCI/NHS. The binding of NH$_2$-biotin can be verified by the presence of amide I band (C=O stretching) and amide II band (N-H bending) at 1648 and 1550 cm^{-1}, respectively together with the disappearance of signals of succinimidyl ester at 1736, 1781 and 1811 cm^{-1}.
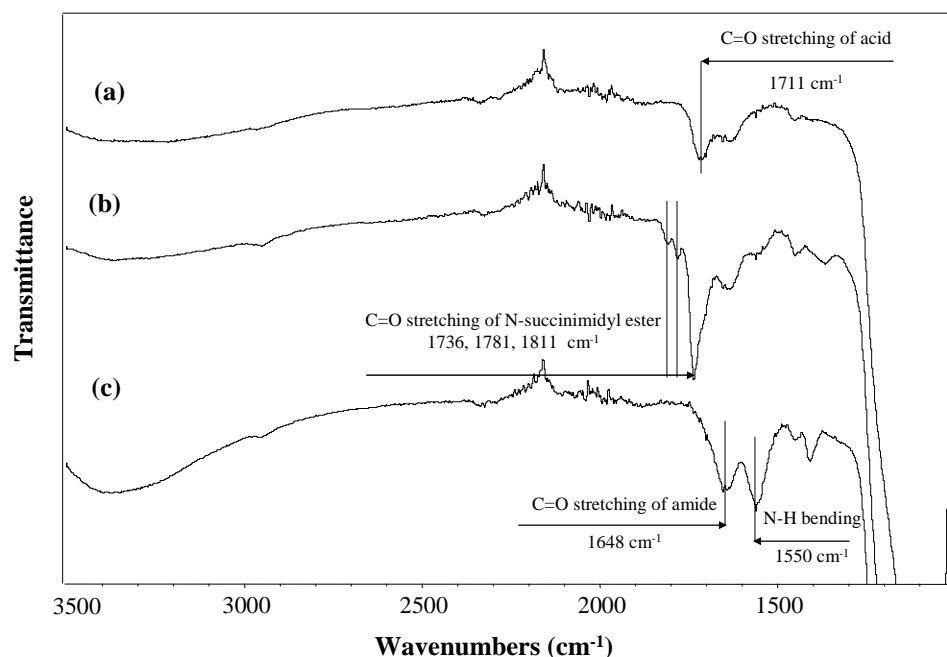
Figure 4.12 ATR-FTIR spectra of (a) PAA brushes (b) PAA brushes-NHS (c) PAA brushes-BSA

The carboxyl group activation and BSA immobilization were also determined by water contact angle measurements (Table 4.3). After the formation of P*t*-BA, the water contact angle was increased from 70.0°/60.2° of the surface immobilized initiator to 91.0°/75.6°. The water contact angle was then decreased after conversion of P*t*-BA brushes to PAA brushes. The increasing of water contact angle after the activation from 21.3°/10.2° to 76.9°/60.3° suggests that the hydrophilic carboxyl groups of PAA brushes have been replaced by hydrophobic *N*-succinimidyl groups. The contact angles were lower after BSA immobilization.

Table 4.3 Advancing (θ_A) and receding (θ_R) water contact angle of surface modified glass coverslips

Surface modified glass coverslip	Water contact angles (degree)	
	θ_A	θ_R
initiator	70.0 ± 0.9	60.2 ± 1.3
Pt-BA brushes	91.0 ± 2.9	75.6 ± 1.7
PAA brushes	21.3 ± 1.8	10.2 ± 1.8
PAA brushes-NHS	76.9 ± 2.5	60.3 ± 1.2
PAA brushes-BSA	68.3 ± 1.9	51.7 ± 1.1

4.4.2   Immobilization of N-cadherin Mimic Cyclic Peptide

N-cadherin mimic cyclic peptide was synthesized by iodine oxidation of linear peptide having a sequence of *N*-CHAVDINGHAVDIC-NH$_2$. As analyzed by mass spectrometry, a formation of disulfide bridge was evidenced from a reduction of the molecular weight from 1469 of the linear peptide to 1467 of the cyclized one. The mass spectra of the peptide both before and after cyclization are displayed in Appendix A.

Surface plasmon resonance (SPR) is a well-recognized optical-based method that relies on the measurement of changes in the refractive index, which is proportional to the mass of the bound or adsorbed species on its surface. It is commonly used for studying interactions between biomolecules that are attached to the substrates and those in solution. In our particular case, we chose to use SPR as a tool to determine an optimized condition in terms of time used for EDC/NHS activation and peptide immobilization as well as peptide concentration mainly because the activation and peptide immobilization can be monitored in real time. This helps minimize the use of the costly peptide. In this study, a gold-coated SPR disk grafted with PAA brushes having a target DP = 200 was used as a substrate. The measured SPR angle shifts during the activation and immobilization steps can be converted into mass uptakes, using a sensitivity factor of 120 mDegrees per 100 ng/cm^2 [91].

As shown in Table 4.4, there was no variation of SPR angle shift upon increasing the activation time from 15 to 30 min suggesting that the maximum degree of activation was achieved even after the activation for 15 min. In the peptide immobilization step, a similar observation was obtained (Table 4.5). Upon using a peptide concentration of 0.1 mg/mL, a period of 15 minute was sufficient to obtain the highest amount of immobilized N-cadherin mimic cyclic peptide. SPR signals as a function of time for all SPR analysis are shown in Appendix D.

Table 4.4 SPR angle shift and the corresponding amount of immobilized NHS on PAA brushes as a function of EDC/NHS activation time

Activation time (min)	SPR angle shift (m°)	Amount of immobilized NHS (ng/cm^2)
15	69.2 ± 6.2	57.5 ± 5.2
30	68.8 ± 4.2	57.3 ± 3.5

Table 4.5 SPR angle shift and the corresponding amount of immobilized N-cadherin mimic cyclic peptide on PAA brushes as a function of immobilization time

Immobilization time (min)	SPR angle shift (m°)	Amount of immobilized N-cadherin mimic cyclic peptide (ng/cm^2)
15	76.0 ± 0.8	63.3 ± 0.6
30	75.8 ± 2.9	63.2 ± 2.4

The results illustrated in Figure 4.13 indicated that the amount of immobilized N-cadherin mimic cyclic peptide can be controlled by varying N-cadherin mimic cyclic peptide concentration in solution. To minimize the amount of peptide used, the concentration of 0.1 mg/mL was chosen for immobilizing N-cadherin mimic cyclic peptide on the glass coverslip to be used for further studies. The time period of 15 min was used for both the step of activation and peptide immobilization.
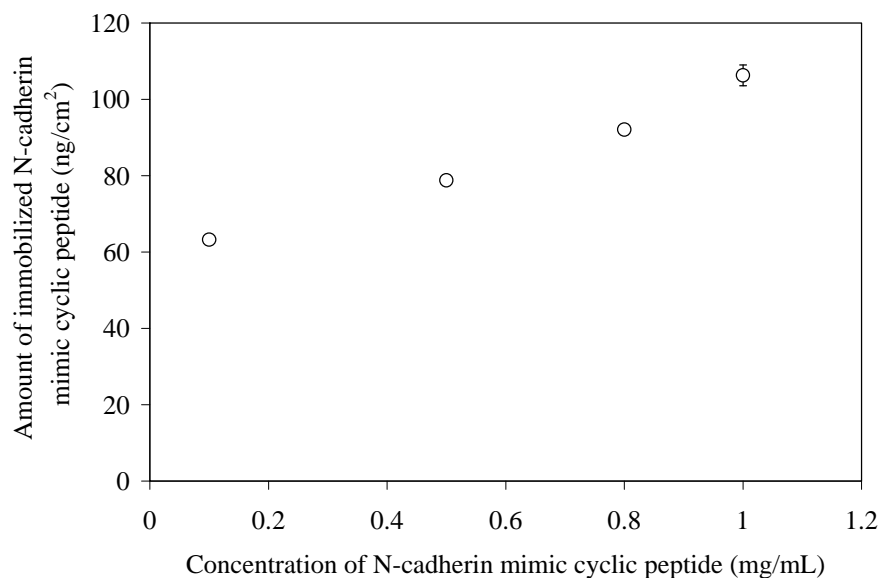
Figure 4.13 Amount of immobilized N-cadherin mimic cyclic peptide as a function of N-cadherin mimic cyclic peptide concentration

4.5 Cytotoxicity Test

Cytotoxicity test is a primary test for evaluating the applicability of materials for biomedical applications. The mouse neural progenitor cells (mNSC) were used for cytotoxicity test. The initial cell seeding density was 5×10^3 cells/well. The results are shown in Figure 4.14. As counted by Haemacytometer using trypan blue exclusion staining, it was found that after 4 days of incubation, the number of cells on glass coverslip immobilized with *N*-cadherin mimic cyclic peptide (3.03×10^6 cells/mL) was comparible to those on the glass coverslip coated with laminin (3.57×10^6 cells/mL), an adhesive protein commonly used in stem cell culture, and significantly higher than those on the glass coverslip (1.47×10^6 cells/mL) which acted as a control. Statistical significance was associated with the value of $p < 0.01$. These preliminary results indicated that the surface-immobilized N-cadherin mimic cyclic peptide was non toxic because cells can still adhere and proliferate.
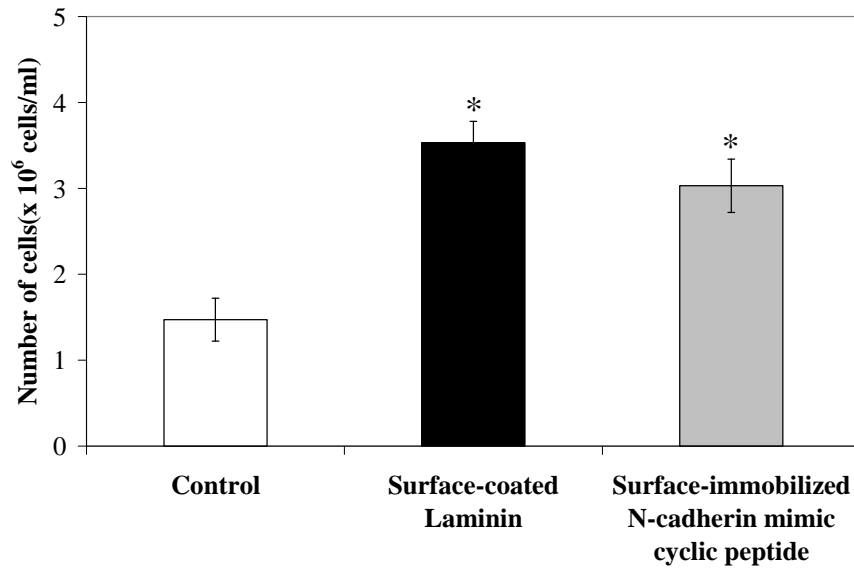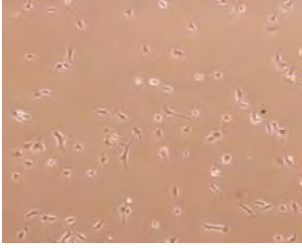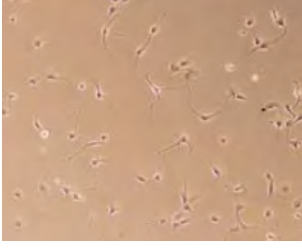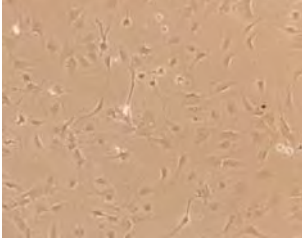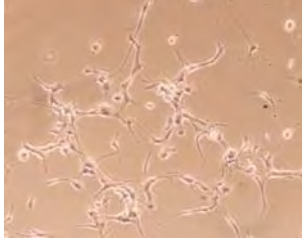
Figure 4.14 Number of mouse neural progenitor cells adhered on various substrates after 4 days incubation *$p < 0.01$ as compared with the control

As visualized under bright field microscope (Table 4.6), mNSC on the control substrate could not attach but remained rounded with little spreading after 1 day (d) and 4 days (g) of culturing. In contrast, mNSC on the surface coated with laminin and surface immobilized with N-cadherin mimic cyclic peptide exhibited a clear adhesive phenotype. At 6 hours after plating, cells on the surface coated with laminin (b) showed early increase in spreading as compared with the control substrate (a) but not quite obvious on the surface-immobilized with N-cadherin mimic cyclic peptide (c). After 1 day of culture, the cell body was mostly round on the substrate -immobilized with N-cadherin mimic cyclic peptide (f) whereas a small extent of exonal outgrowth was observed on the surface coated with laminin (e). At day 4 of culture, more cells proliferated from original cells and exhibited exonal outgrowth from cell body (i). The extent of exonal outgrowth seems to be greater than that appeared on the surface coated with laminin (h). However, the evidences from cell adhesion and proliferation as well as morphological appearance are not enough to guarantee that the cells still maintain their stem cell characteristics. Further investigation are necessary.

Table 4.6 Morphology of mouse neural progenitor cells on various substrates observed by bright field optical microscope

Time	Control	Surface-coated with laminin	Surface-immobilized with N-cadherin mimic cyclic peptide
6 h	(a)	(b)	(c)
1 day	(d)	(e)	(f)
4 days	(g)	(h)	(i)

CHAPTER V

CONCLUSION AND SUGGESTION

Poly(*tert*-butyl acrylate) (P*t*-BA) brushes can be prepared from the surfaces bearing α-bromoester groups by surface-initiated activators regenerated by electron transfer for atom transfer radical polymerization (ARGET ATRP) of *tert*-butyl acrylate (*t*-BA). The molecular weight and thickness of the P*t*-BA brushes can be controlled by polymerization time and monomer to initiator ratio. The optimized condition that was identified was $[I]/[CuBr_2]/[Sn(EH)_2]/[Me_6TREN]$ molar ratio of 1:0.01:1.6:0.16, molar ratio of $Sn(EH)_2:Me_6TREN$ of 10:1, molar ratio of $Sn(EH)_2$:initiator of 1:1, and polymerization time of 15 h. The P*t*-BA brushes were relatively dense with a graft density of approximately 0.33 chains/nm^2.

Poly(acrylic acid) (PAA) brushes were subsequently obtained after *tert*-butyl groups of P*t*-BA brushes were removed by acid hydrolysis. As determined by toluidine blue O assay, the carboxyl group density of the PAA brushes can be varied as a function of the chain length (MW). The density was ranged from 0.7×10^{-9} to 1.6×10^{-9} mol/cm^2 for the PAA brushes having $\overline{M}_n$ in the range of 11.8×10^3 to 29.3×10^3. It has been demonstrated that the carboxyl groups of PAA brushes are readily available for activation by EDC/NHS and subsequent attachment of BSA and N-cadherin mimic cyclic peptide. According to SPR analysis, the density of the immobilized N-cadherin mimic cyclic peptide relied on the concentration of the peptide. The successive surface modification via polymer brushes formation and protein/peptide immobilization were also verified by ATR-FTIR analysis and water contact angle measurements.

Results from cytotoxicity test against mouse neural progenitor cell suggested that the immobilized N-cadherin mimic cyclic peptide on PAA brushes was non toxic. The level of cell compatibility determined based on cell adhesion and proliferation as well as cell morphology was comparable to the surface coated with laminin, a commonly used adhesive protein for stem cell culture. To determine whether the proliferated cells maintain stem cell characteristics is a subject of future investigation. It

is also interesting to test the potential of the developed material for specific cell selection.

REFERENCES

[1]   Zhao, B.,and Brittain, W. J., Polymer brushes: Surface-immobilized
        macromolecules *Progress in Polymer Science 25* (5) (2000): 677-710.

[2]   Raphael, E.,and De Gennes, P. G., Rubber-rubber adhesion with connector
        molecules. *The Journal of Physical Chemistry 96* (10) (1992):
        4002-4007.

[3]   Ji, H., and Gennes, P. G. D., Adhesion via connector molecules : the many-
        stitch problem. *Macromolecules 26* (3) (1993): 520-525.

[4]   Mansoor, A.,and Kinam, P., Surface modification of polymeric biomaterials
        with poly(ethylene oxide), albumin, and heparin for reduced
        thrombogenicity *Journal of Biomaterials Science, Polymer Edition 4*
        (3) (1993): 217-234.

[5]   van Zanten , J. H., Terminally anchored chain interphases: Their
        chromatographic properties. *Macromolecules 27* (23) (1994):
        6797-6807.

[6]   Takei, Y. G.; Aoki, T.; Sanui, K.; Ogata, N.; Sakurai, Y.,and Okano, T.,
        Dynamic contact angle measurement of temperature-responsive
        surface properties for poly(*N*-isopropylacrylamide) grafted surfaces.
        Macromolecules 27 (21) (1994): 6163-6166.

[7]   Ito, Y.; Ochiai, Y.; Park, Y. S.,and Imanishi, Y., pH-sensitive gating by
        conformational change of a polypeptide brush grafted onto a porous
        polymer membrane. *Journal of the American Chemical Society 119* (7)
        (1997): 1619-1623.

[8]   Ito, Y.,and Park, Y. S.; Imanishi, Y., Visualization of critical pH-controlled
        gating of a porous membrane grafted with polyelectrolyte brushes.
        Journal of the American Chemical Society 119 (11) (1997):
        2739-2740.

[9]   Ito, Y.; Nishi, S.; Park, Y. S.,and Imanishi, Y., Oxidoreduction-sensitive control of water permeation through a polymer brushes-grafted porous membrane. *Macromolecules 30* (19) (1997): 5856-5859.

[10]   Velten, U.; Shelden, R. A.; Caseri, W. R.,and Suter, U. W., Polymerization of styrene with peroxide initiator ionically bound to high surface area mica. *Macromolecules 32* (11) (1999): 3590-3597.

[11]   Velten, U.; Tossati, S.; Shelden, R. A.; Caseri, W. R.,and Suter, U. W., Graft polymerization of styrene on mica: Formation and behavior of molecular droplets and thin films. *Langmuir 15* (20) (1999): 6940-6945.

[12]   Niu, Q. J.,and Fréchet, J. M. J., Polymers for 193-nm microlithography: regioregular 2-alkoxycarbonylnortricyclene polymers by controlled cyclopolymerization of bulky ester derivatives of norbornadiene. *Angewandte Chemie International Edition (English) 37* (5) (1998): 667-670.

[13]   Singhvi, R.; Kumar, A.,and Lopez, G. P.; Stephanopoulos, G. N.; Wang, D. I.; Whitesides, G. M.; Ingber, D. E., Engineering cell-shape and function. *Science 264* (5159) (1994): 696-698.

[14]   Aksay, I. A.; Trau, M.; Manne, S.; Honma, I.; Yao, N.; Zhou, L.; Fenter, P.; Eisenberger, P. M.; Gruner, S. M., Biomimetic pathways for assembling inorganic thin films. *Science 273* (5277) (1996): 892-898.

[15]   Balazs, A. C.; Singh, C.; Zhulina, E.; Gersappe, D.,and Pickett, G., Patterned polymer films. *MRS Bulletin 22* (1) (1996): 16-21.

[16]   Soga, K. G.; Zuckermann, M. J.,and Guo, H., Binary polymer brush in a solvent. *Macromolecules 29* (6) (1996): 1998-2005.

[17]   Mansky, P.; Liu, Y.; Huang, E.; Russell, T. P.,and Hawker, C., Controlling polymer-surface interactions with random copolymer brushes. *Science 275* (5305) (1997): 1458-1460.

[18]   Zhao, B.,and Brittain, W. J., Synthesis of tethered polystyrene-*block*-poly(methyl methacrylate) monolayer on a silicate substrate by sequential carbocationic polymerization and atom transfer radical polymerization. *Journal of the American Chemical Society 121* (14) (1999): 3557-3558.

[19]   Nakayama, Y.,and Matsuda, T., Surface macromolecular architectural designs using photo-graft copolymerization based on photochemistry of benzyl *N,N*-diethyldithiocarbamate. *Macromolecules 29* (27) (1996): 8622-8630.

[20]   Husseman, M.; Malmström, E. E.; McNamara, M.; Mate, M.; Mecerreyes, D.; Benoit, D. G.; Hedrick, J. L.; Mansky, P.; Huang, E.; Russell, T. P.; Hawker, C. J., Controlled synthesis of polymer brushes by "living" free radical polymerization techniques. *Macromolecules 32* (5) (1999): 1424-1431.

[21]   Jakubowski, W.,and Matyjaszewski, K., Activators regenerated by electron transfer for atom-transfer radical polymerization of (meth)acrylates and related block copolymers. *Angewandte Chemie International Edition 45* (27) (2006): 4482-4486.

[22]   Min, K.; Gao, H.,and Matyjaszewski, K., Use of ascorbic acid as reducing agent for synthesis of well-defined polymers by ARGET ATRP. *Macromolecules 40* (6) (2007): 1789-1791.

[23]   Bombalski, L.; Dong, H.; Listak, J.; Matyjaszewsk, K.,and Bockstaller, M. R., Null-scattering hybrid particles using controlled radical polymerization. *Advanced Materials 19* (24) (2007): 4486-4490.

[24]   Braunecker, W. A.,and Matyjaszewski, K., Controlled/living radical polymerization: Features, developments, and perspectives. *Progress in Polymer Science 32* (1) (2007): 93-146.

[25]   Matyjaszewski, K.; Dong, H.; Jakubowski, W.; Pietrasik, J.,and Kusumo, A., Grafting from surfaces for "everyone": ARGET ATRP in the presence of air. *Langmuir 23* (8) (2007): 4528-4531.

[26]   Cao, L.,and Kruk, M., Grafting of polymer brushes from nano pore surface via atom transfer radical polymerization with activators regenerated by electron transfer. *Polymer Chemistry 1* (1) (2010): 97-101.

[27]   Szwarc, M.; Levy, M.,and Milkovich, R., Polymerization initiated by electron transfer to monomer a new method of formation of block polymers. *Journal of the American Chemical Society 78* (11) (1956): 2656-2657.

[28]   Flory, P. J., Principles of polymer chemistry. 1 ed. Cornell Uni. Press: Ithaca, New York, 1978.

[29]   Webster, O. W., Living polymerization methods. *Science 251* (4996) (1991):
            887-893.

[30]   Moad, G.; Rizzardo, E.,and Solomon, D. H., Selectivity of the reaction of free
            radicals with styrene. *Macromolecules 15* (3) (1982): 909-914.

[31]   Georges, M. K.; Veregin, R. P. N.; Kazmaier, P. M.,and Hamer, G. K.,
            Narrow molecular weight resins by a free-radical polymerization
            process. *Macromolecules 26* (11) (1993): 2987-2988.

[32]   Kato, M.; Kamigaito, M.; Sawamoto, M.,and Higashimura, T., Polymerization
            of methyl methacrylate with the carbon tetrachloride/ dichlorotris-
            (triphenylphosphine) ruthenium (II) / methylaluminum bis(2,6-di-*tert*-
            butylphenoxide) initiating system: possibility of living radical
            polymerization. *Macromolecules 28* (5) (1995): 1727-1723.

[33]   Wang, J.-S.,and Matyjaszewski, K., Controlled/"living" radical
            polymerization atom transfer radical polymerization in the presence of
            transition-metal complexs. *Journal of the American Chemical Society
            117* (20) (1995): 5614-5615.

[34]   Percec, V.,and Barboiu, B., "Living" radical polymerization of styrene
            initiated by arenesulfonyl chlorides and Cu(I)(bpy)$_n$Cl.
            Macromolecules 28 (23) (1995): 7970-7972.

[35]   Wayland, B. B.; Poszmik, G.; Mukerjee, S. L.,and Fryd, M., Living radical
            polymerization of acrylates by organocobalt porphyrin complexes.
            Journal of the American Chemical Society 116 (17) (1994):
            7943-7944.

[36]   Jakubowski, W.; Min, K.,and Matyjaszewski, K., Activators regenerated by
            electron transfer for atom transfer radical polymerization of styrene.
            Macromolecules 39 (1) (2006): 39-45.

[37]   Matyjaszewski, K., Controlled radical polymerization. ACS Symposium
            Series, American Chemical Society: Washington, DC, 1998.

[38]   Matyjaszewski, K., Mechanistic and synthetic aspects of atom transfer radical
            polymerization. *Journal of Macromolecular Science: Pure and Applied
            Chemistry 34A* (10) (1997): 1785-1801.

[39]   Chambard, G.; Klumperman, B.,and German, A. L., Effect of solvent on the
            activation rate parameters for polystyrene and poly(butyl acrylate)

macroinitiators in atom transfer radical polymerization. *Macromolecules 33* (12) (2000): 4417-4421.

[40] Matyjaszewski, K.,and Xia, J., Atom transfer radical polymerization. *Chemical Reviews 101* (9) (2001): 2921-2990.

[41] Boer, B. d.; Simon, H. K.; Werts, M. P. L.; Vegte, E. W. v. d.,and Hadziioannou, G., "Living" free radical photopolymerization initiated from surface-grafted iniferter monolayers. *Macromolecules 33* (2) (2000): 349-356.

[42] Xia, J.,and Matyjaszewski, K., Controlled/"living" radical polymerization atom transfer radical polymerization using multidentate amine ligands. *Macromolecules 30* (25) (1997): 7697-7700.

[43] Xia, J.,and Matyjaszewski, K., Controlled/"living" radical polymerization atom transfer radical polymerization of acrylates at ambient temperature. *Macromolecules 31* (17) (1998): 5958-5959.

[44] Hollmann, O.,and Czeslik, C., Characterization of a planar poly (acrylicacid) brush as a materials coating for controlled protein immobilization. *Langmuir 22* (7) (2006): 3300-3305.

[45] Dai, J.; Bao, Z.; Sun, L.; Hong, S. U.; L.Baker, G.,and Merlin, L.Bruening, High-capacity binding of proteins by poly (acrylic acid) brushes and their derivatives. *Langmuir 22* (9) (2006): 4274-4281.

[46] Cullen, S. P.; Liu, X.; Mandel, I. C.; Himpsel, F. J.,and Gopalan, P., Polymeric brushes as functional templates for immobilizing ribonuclease A: Study of binding kinetics and activity. *Langmuir 24* (3) (2008) 913-920.

[47] Peez, R. F.; Dermody, D. L.; Franchina, J. G.; Jones, S. J.; Bruening, M. L.; Bergbreiter, D. E.; Crooks, R. M., Aqueous solvation and functionalization of weak-acid polyelectrolyte thin films. *Langmuir 14* (15) (1998): 4232-4237.

[48] Ghosh, P.; Amirpour, M. L.; Lackowski, W. M.; Pishko, M. V.,and Crooks, R. M., A simple lithographic approach for preparing patterned, micron-scale corrals for controlling cell growth. *Angewandte Chemie International Edition 38* (11) (1999): 1592-1595.

[49]   Mori, H.,and Müller, A. H. E., New polymeric architectures with
          (meth)acrylic acid segments *Progress in Polymer Science 28* (10)
          (2003): 1403-1439.

[50]   Matyjaszewski, K.; Miller, P. J.; Shukla, N.; Immaraporn, B.; Gelman, A.;
          Luokala, B. B.; Siclovan, T. M.; Kickelbick, G.; Vallant, T.;
          Hoffmann, H.; Pakula, T., Polymers at Interfaces: Using atom transfer
          radical polymerization in the controlled growth of homopolymers and
          block copolymers from silicon surfaces in the absence of untethered
          sacrificial initiator. *Macromolecules 32* (26) (1999): 8716-8724.

[51]   Davis, K. A.,and Matyjaszewski, K., Atom transfer radical polymerization of
          tert-butyl acrylate and preparation of block copolymers.
          Macromolecules 33 (11) (2000): 4039-4047.

[52]   Davis, K. A.; Charleux, B.,and Matyjaszewski, K., Preparation of block
          copolymers of polystyrene and poly(t-butyl acrylate) of various
          molecular weights and architectures by atom transfer radical
          polymerization. *Journal of Polymer Science Part A: Polymer
          Chemistry 38* (12) (2000): 2274-2283.

[53]   Mori, H.; Böker, A.; Krausch, G.,and Müller, A. H. E., Surface-grafted
          hyperbranched polymers via self-condensing atom transfer radical
          polymerization from silicon surfaces. *Macromolecules 34* (20) (2001):
          6871-6882.

[54]   Boyes, S. G.; Akgun, B.; Brittain, W. J.,and Foster, M. D., Synthesis,
          characterization, and properties of polyelectrolyte block copolymer
          brushes prepared by atom transfer radical polymerization and their use
          in the synthesis of metal nanoparticles. *Macromolecules 36* (25)
          (2003): 9539-9548.

[55]   Kong, H.; Gao, C.,and Yan, D., Constructing amphiphilic polymer brushes on
          the convex surfaces of multi-walled carbon nanotubes by in situ atom
          transfer radical polymerization. *Journal of Materials Chemistry 14*
          (2004): 1401-1405.

[56]   Mao, C.; Qiu, Y.; Sang, H.; Mei, H.; Zhu, A.; Jian Shen,and Lin[a] S., Various
          approaches to modify biomaterial surfaces for improving
          hemocompatibility. *Advances in Colloid and Interface Science 110* (1-
          2) (2004): 5-17.

[57]   Norde, W.,and Gage, D., Interaction of bovine serum albumin and human blood plasma with PEO-tethered surfaces: Influence of PEO chain length, grafting density, and temperature. *Langmuir 20* (10) (2004): 4162-4167.

[58]   Ostuni, E.; Chapman, R. G.; Liang, M. N.; Meluleni, G.; Pier, G.; Ingber, D. E.; Whitesides, G. M., Self-assembled monolayers that resist the adsorption of proteins and the adhesion of bacterial and mammalian cells. *Langmuir 17* (20) (2001): 6336-6343.

[59]   Ngankam, A. P.; Mao, G.,and Tassel, P. R. V., Fibronectin adsorption onto polyelectrolyte multilayer films. *Langmuir 20* (8) (2004): 3362-3370.

[60]   Bission, I.; Kosinski, M.; Ruault, S.; Gupta, B.; Hilbron, J.; Wurm, F.; Frey, P., Acrylic acid grafting and collagen immobilization on poly(ethylene terephthalate) surfaces for adherence and growth of human bladder smooth muscle cells. *Biomaterials 23* (2002): 3149-3158.

[61]   Dong, R.; Krishnan, S.; Baird, B. A.; Lindau, M.,and Ober, C. K., Patterned biofunctional poly (acrylic acid) brushes on silicon surfaces. *Biomacromolecules 8* (10) (2007): 3082-3092.

[62]   Sigurjonsson, Q. E. The differentiation potential of human somatic stem cells. University of Oslo: Oslo, 2005.

[63]   Hayes, R.,and Darnovsky, M. Stem cell and public policy. Civil Society: New York, 2006; p 88.

[64]   Bethesda, M. *Stem cell basics: What are adult stem cells?. In stem cell information* [online]. 2009. Available from http://stemcells.nih.gov/info/basics/basics4 [2010, April 14].

[65]   Mimeault, M.,and K.Batra, S., Concise review: recent advances on the significance of stem cells in tissue regeneration and cancer therapies. *Stem Cells 24* (11) (2006): 2319-2345.

[66]   Evans, N. D.; Gentleman, E.,and Polak, J. M., Scaffolds for stem cells *Materialstoday 9* (12) (2006): 26-33.

[67]   Mitjavila-Garcia, M. T.; Simonin, C.,and Peschanski, M., Embryonic stem cells: Meeting the needs for cell therapy. *Advanced Drug Delivery Reviews 57* (13) (2005):1935-1943.

[68]   Garreta, E.; Genové, E.; Borrós, S.,and Semino, C. E., Osteogenic differentiation of mouse embryonic stem cells and mouse embryonic

fibroblasts in a three-dimensional self-assembling peptide scaffold. *Tissue Engineering 12* (8) (2006): 2215-2227.

[69]   Liu, H.,and Roy, K., Biomimetic three-dimensional cultures significantly increase hematopoietic differentiation efficacy of embryonic stem cells. *Tissue Engineering 11* (1-2) (2005): 319-330.

[70]   Willerth, S. M.; Arendas, K. J.; Gottlieb, D. I.,and Sakiyama-Elbert, S. E., Optimization of fibrin scaffolds for differentiation of murine embryonic stem cells into neural lineage cells *Biomaterials 27* (36) (2006): 5990-6003.

[71]   Hwang, N. S.; Kim, M. S.; Vanich, S. S.; Baek, J. H.; Zhang, Z.,and Elisseeff, J., Effects of three-dimensional culture and growth factors on the chondrogenic differentiation of murine embryonic stem cells. *Stem Cells 24* (2) (2006): 284-291.

[72]   Bissell, D. M.; Arenson, D. M.; Maher, J. J.,and Roll, F. J., Support of cultured hepatocytes by a laminin-rich gel. Evidence for a functionally significant subendothelial matrix in normal rat liver. *The Journal of Clinical Investigation 79* (3) (1987): 801-812.

[73]   Im, G.-I., Chondrogenesis from mesenchymal stem cells derived from adipose tissue on the fibrin scaffold *Current Applied Physics 5* (5) (2005): 438-443.

[74]   Mondrinos, M. J.; Koutzaki, S.; Jiwanmall, E.; Li, M.; Dechadarevian, J.-P.; Lelkes, P. I.,and Finck, C. M., Engineering three-dimensional pulmonary tissue constructs. *Tissue Engineering 12* (4) (2006): 717-728.

[75]   Maeda, M.; Hirose, M.; Ohgushi, H.,and Kirita, T., *In vitro* mineralization by mesenchymal stem cells cultured on titanium scaffolds. *Journal of Biochemistry 141* (5) (2007): 729-736.

[76]   Shin, H.; Zygourakis, K.; Farach-Carson, M. C.; Yaszemski, M. J.,and Mikos, A. G., Attachment, proliferation, and migration of marrow stromal osteoblasts cultured on biomimetic hydrogels modified with an osteopontin-derived peptide *Biomaterials 25* (5) (2004): 895-906.

[77]   Higuchi, A.; Aoki, N.; Yamamoto, T.; Gomei, Y.; Egashira, S.; Matsuoka, Y.; Miyazaki, T.; Fukushima, H.; Jyujyoji, S.; Natori, S. H., Bioinert

surface of pluronic-immobilized flask for preservation of hematopoietic stem cells. *Biomacromolecules 7* (4) (2006): 1083-1089.

[78] Dey, S.; Alexander, M.; Kellam, B.; Alexander, C.,and Rose, F. R., Biocompatible responsive surfaces for embryonic stem cell culture. *European Cells and Materials 16* (3) (2008): 47.

[79] O'Day, P. *Human cell biology*. [online]. 1998. Available from http://www.utm.utoronto.ca/~w3bio315/index.html [2010, April 14].

[80] Wickenhauser, C.; Schmitz, B.; ErnstBaldus, S.; Henze, F.; Farahmand, P.,and Frimpong, S.; Thiele, J.; Fischer, R., Selectins (CD62L, CD62P) and megakaryocytic glycoproteins (CD41a, CD42b) mediate megakaryocyte–fibroblast interactions in human bone marrow *Leukemia Research 24* (12) (2000): 1013-1021.

[81] Tsuchiya, K.; Chen, G.; Ushida, T.; Matsuno, T.,and Tateishi, T., Effects of cell adhesion molecules on adhesion of chondrocytes, ligament cells and mesenchymal stem cells *Materials Science and Engineering: C 17* (1-2) (2001): 79-82.

[82] Lu, Z. F.; Doulabi, B. Z.; Huang, C. L.; Bank, R. A.,and Helder, M. N., β1 integrins regulate chondrogenesis and rock signaling in adipose stem cells *Biochemical and Biophysical Research Communications 372* (4) (2008): 547-552.

[83] Williams, E.; Williams, G.; Gour, B. J.; Blaschuk, O. W.,and Doherty, P., A novel family of cyclic peptide antagonists suggests that N-cadherin specificityIs determined by amino acids that flank the HAV motif. *The Journal of Biological Chemistry 275* (6) (2000): 4007-4012.

[84] Williams, G.; Williams, E.-J.,and Doherty, P., Dimeric versions of two short N-cadherin binding motifs (HAVDI and INPISG) functionas N-cadherin agonists. *The Journal of Biological Chemistry 277* (8) (2002): 4361-4367.

[85] Honda, M.; Kurisaki, A.; Ohnuma, K.; Okochi, H.; Hamazaki, T. S.,and Asashima, M., *N*-cadherin is a useful marker for the progenitor of cardiomyocytes dierentiated from mouse ES cells in serum-free condition. *Biochemical and Biophysical Research Communications 351* (4) (2006): 877-882.

[86]   Haug, J. S.; He, X. C.; Grindley, J. C.; Wunderlich, J. P.; Gaudenz, K.; Ross, J. T.; Paulson, A.; Wagner, K. P.; Xie, Y.; Zhu, R.; Yin, T.; Perry, J. M.; Hembree, M. J.; Redenbaugh, E. P.; Radice, G. L.; Seidel, C.; Li, L., *N*-cadherin expression level distinguishes reserved versus primed states of hematopoietic stem cells. *Cell Stem Cell 2* (4) (2008): 367-379.

[87]   Queffelec, J.; Gaynor, S. G.,and Matyjaszewski, K., Optimization of atom transfer radical polymerization using Cu(I)/ tris(2-(dimethylamino)ethyl)amine as a catalyst. *Macromolecules 33* (23) (2000): 8629-8639.

[88]   *Hydrosilylation*. [online]. 2010. Available from http://en.wikipedia.org/wiki/Hydrosilylation. [2010].

[89]   *Eschweiler-Clarke reaction*. [online]. 2009. Available from http://en.wikipedia.org/wiki/Eschweiler-Clarke_reaction. [2010].

[90]   Marutani, E.; Yamamoto, S.; Ninjbadgar, T.; Tsujii, Y.; Fukuda, T.,and Takano, M., Surface-initiated atom transfer radical polymerization of methyl methacrylate on magnetite nanoparticles. *Polymer 45* (7) (2004): 2231-2235.

[91]   Su, X.; Wu, Y.-J.; Robelek, R.,and Knoll, W., Surface plasmon resonance spectroscopy and quartz crystal microbalance study of streptavidin film structure effects on biotinylated DNA assembly and target DNA hybridization. *Langmuir 21* (1) (2005): 348-353.

APPENDICES

APPENDIX A
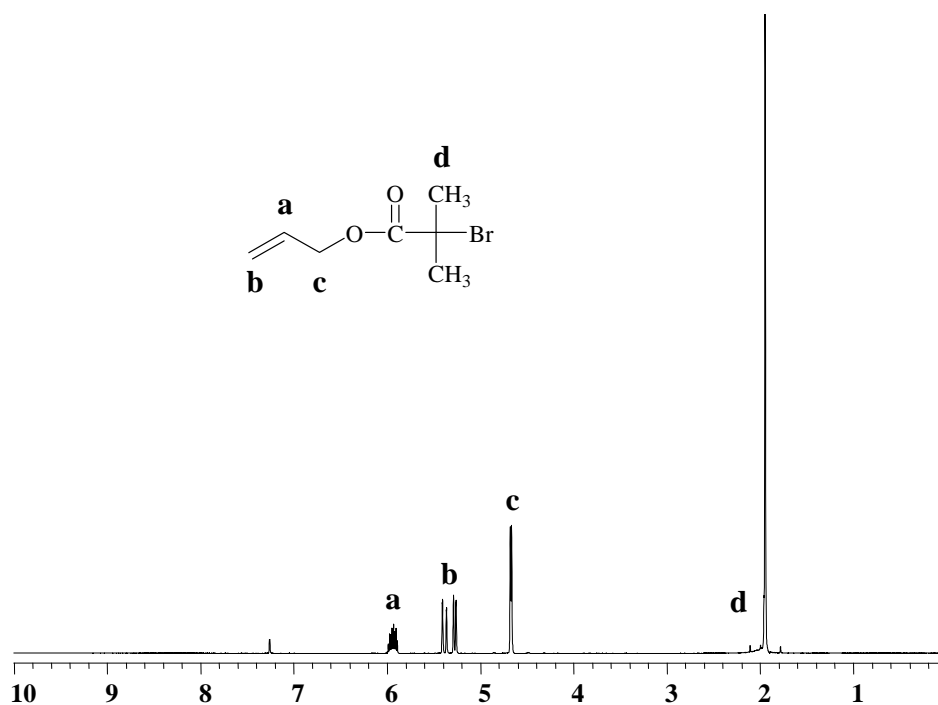
Figure A.1 ^{1}H-NMR spectrum (400 MHz, CDCl$_3$) of 2-bromo-2-methylpropionic acid allyl ester (1)
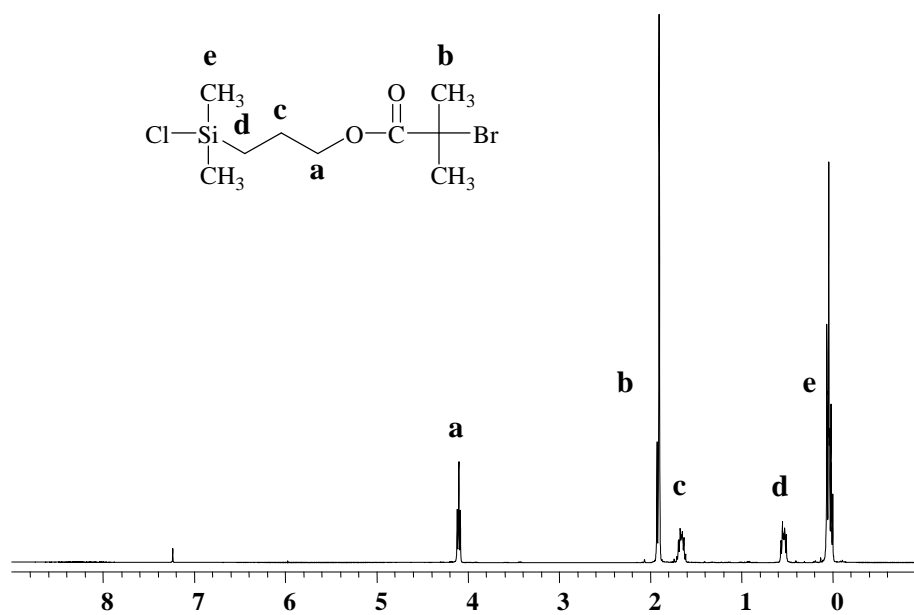
Figure A.2 ^{1}H-NMR spectrum (400 MHz, CDCl$_3$) of 3-(chlorodimethylsilyl)propyl 2-bromo-2-methylpropanoate (2)
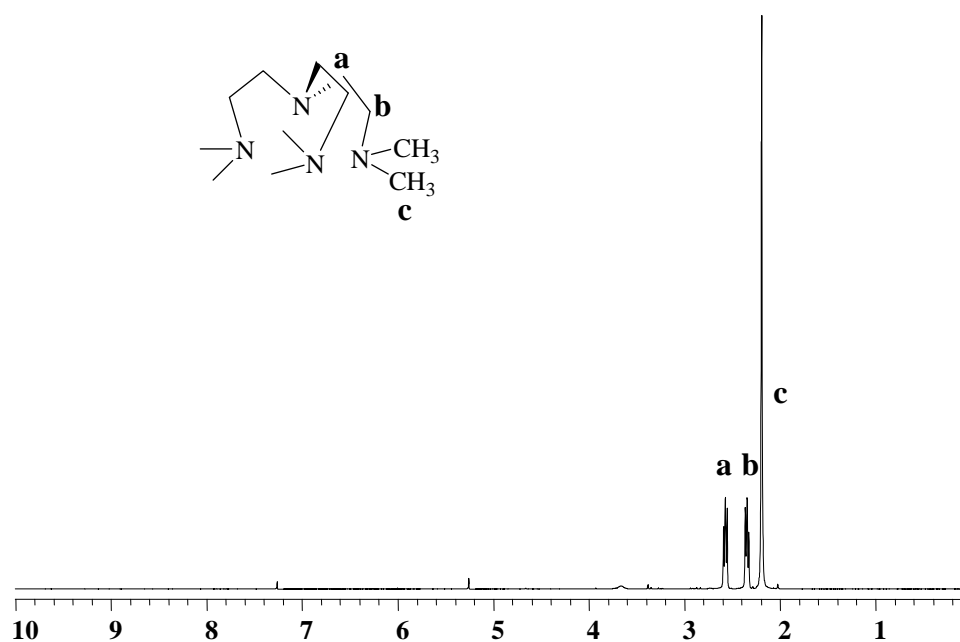
Figure A.3 ^{1}H-NMR spectrum (400 MHz, CDCl$_3$) of tris (2-(dimethylamino) ethyl)amine [Me$_6$TREN] (3)
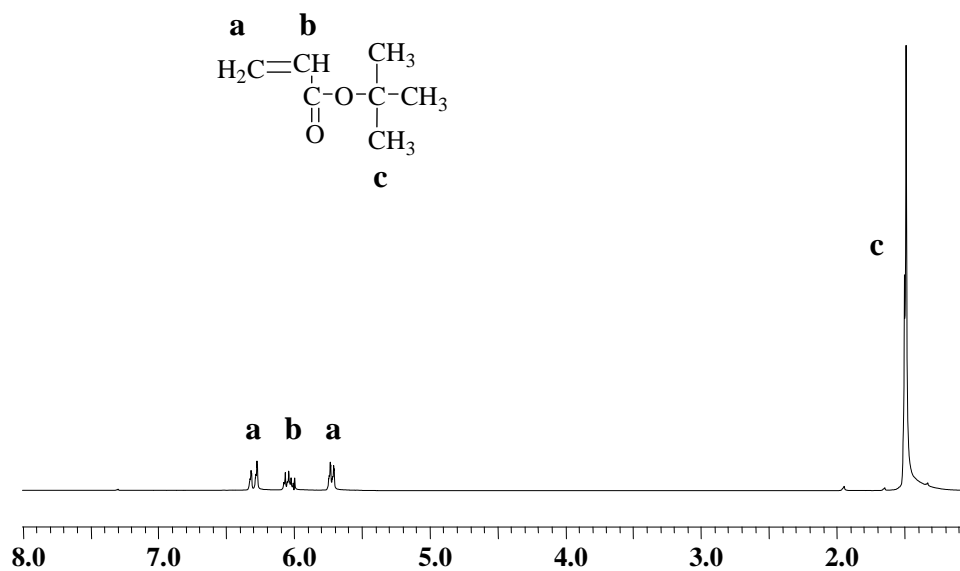
Figure A.4 The ^{1}H-NMR (400 MHz, CDCl$_3$) of *t*-BA
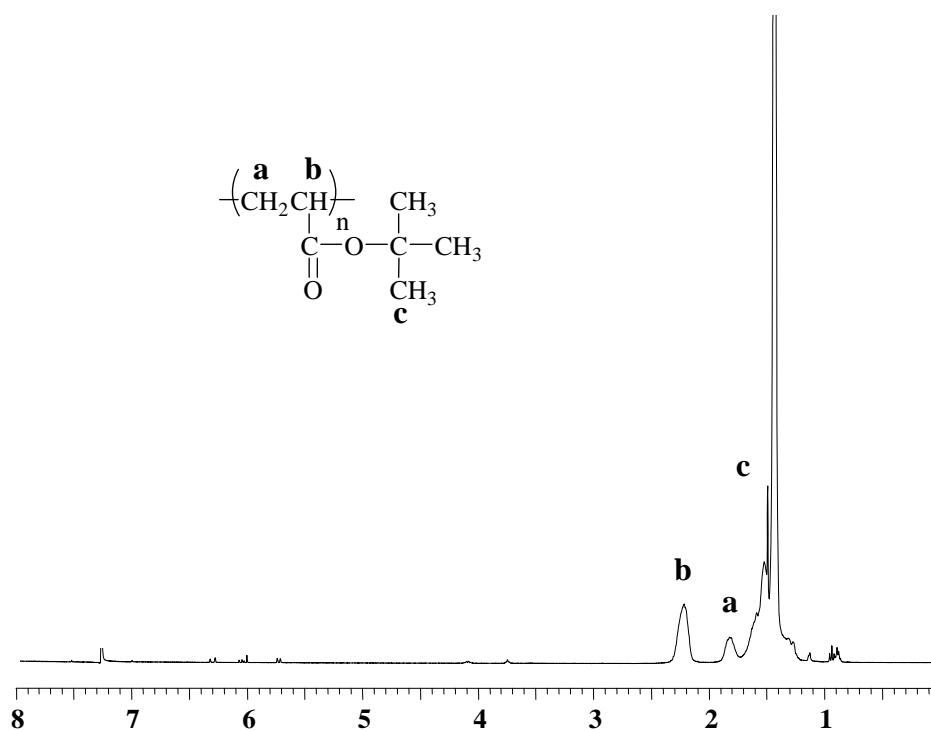
Figure A.5 The ^{1}H-NMR (400 MHz, CDCl$_3$) of Pt-BA
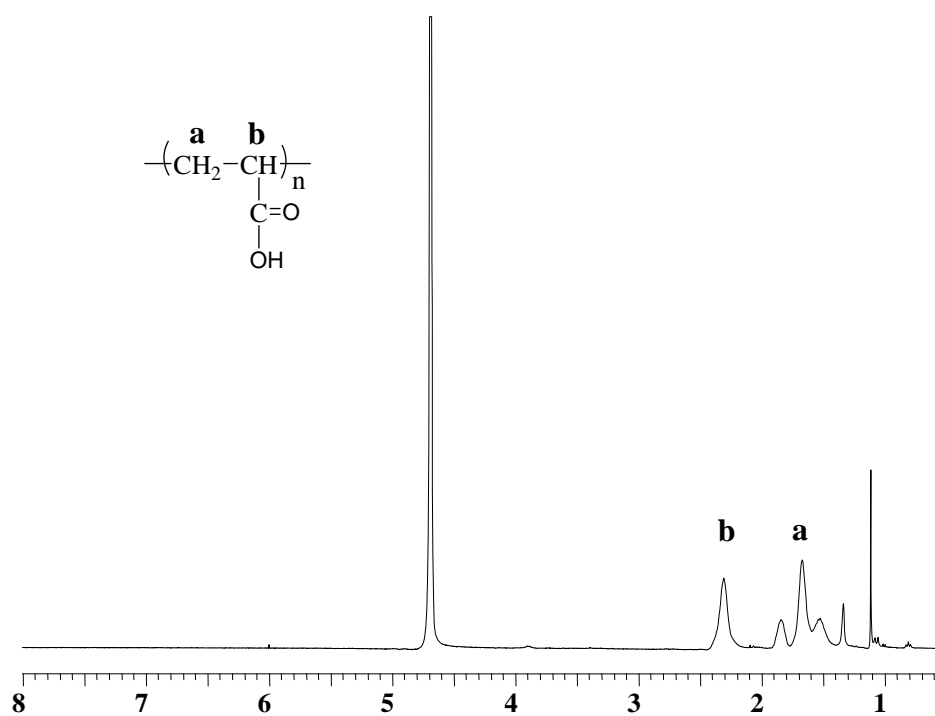
Figure A.6 The ^{1}H-NMR (400 MHz, CDCl$_3$) of PAA
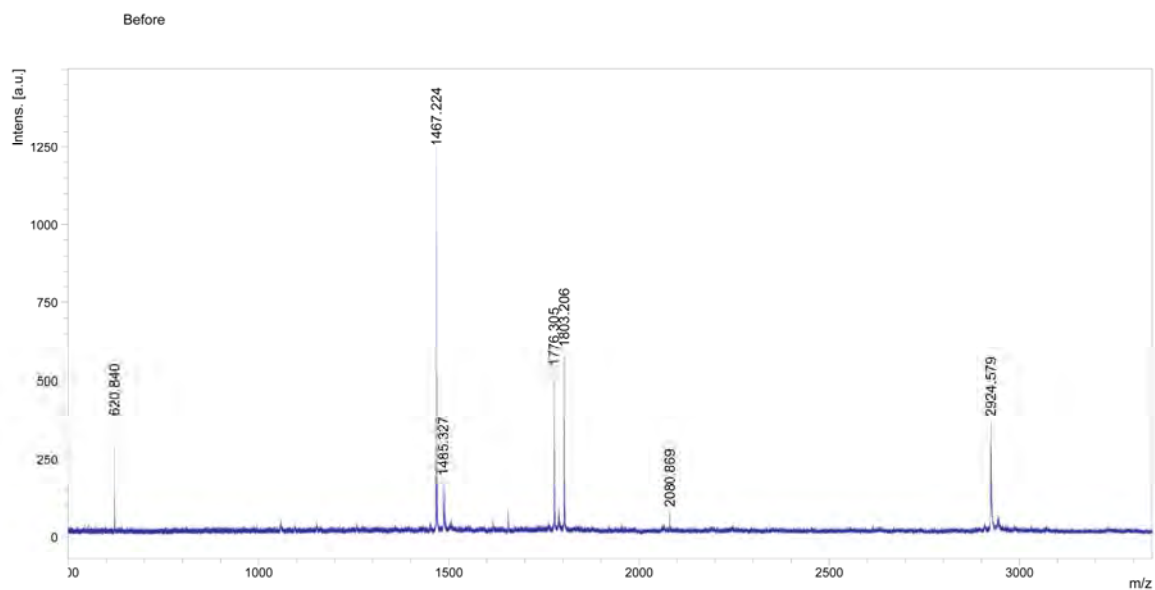
Figure A.7 Mass spectrum of N-cadherin mimic peptide before cyclization
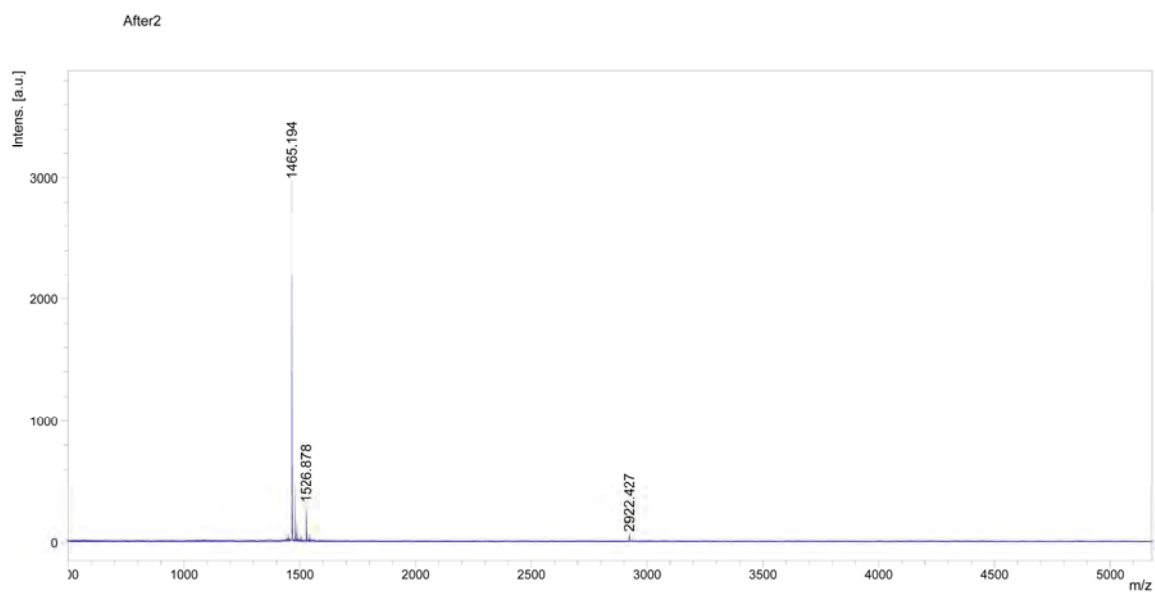
Figure A.8 Mass spectrum of N-cadherin mimic cyclic peptide after cyclization

APPENDIX B

Data corresponding to the plots in Chapter IV

Table B.1 Average molecular weight and molecular weight distribution of Pt-BA brushes analyzed by GPC as a function of Sn(EH)$_2$:Me$_6$TREN molar ratio for targeted DP = 200

Sn(EH)$_2$:Me$_6$TREN molar ratio	GPC data		
	$\overline{M}_n$	$\overline{M}_w$	$\overline{M}_w/\overline{M}_n$
5:1	31375	33571	1.07
8:1	31590	33801	1.07
10:1	31418	34559	1.1
15:1	7118	10463	1.47

Table B.2 Average molecular weight and molecular weight distribution of Pt-BA brushes analyzed by GPC, the thickness of Pt-BA brushes calculated from AFM data and % conversion of Pt-BA brushes calculated from ^{1}H-NMR spectrum as a function of time (targeted DP =200)

Polymerization time (h)	Thickness (nm)	% Conversion	GPC data		
			$\overline{M}_n$	$\overline{M}_w$	$\overline{M}_w/\overline{M}_n$
5	6.48	89.3	11886	15451	1.3
10	10.97	96.6	22660	24246	1.07
15	N/A	98.6	26826	28703	1.07
20	14.75	98.7	29359	31414	1.07
25	N/A	98.9	31084	33259	1.07

Table B.3 Thickness of P*t*-BA brushes after being scraped by AFM for target DP= 200
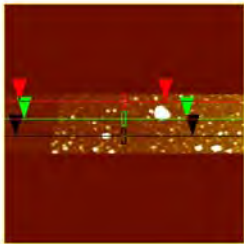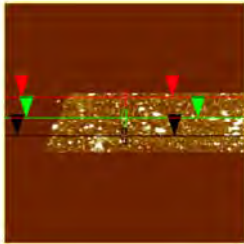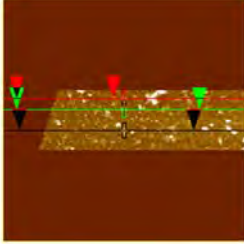
Time (h)	$\overline{M}_n$	AFM image	Thickness (nm)	Average thickness (nm)
5	11886		6.53	6.48 ± 0.05
			6.43	
			6.47	
10	22660		11.07	10.97 ± 0.10
			10.95	
			10.88	
20	29359		14.82	14.75 ± 0.07
			14.73	
			14.69	

Table B.4 Advancing (Θ_A) and receding (Θ_R) water contact angles of P*t*-BA brushes versus polymerization time for targeted DP = 200

Time (h)	Water contact angle (degree)	
	Θ_A	Θ_R
0	70.0 ± 0.9	60.0 ± 1.3
5	80.9 ± 2.3	60.0 ± 1.2
10	87.9 ± 1.2	69.7 ± 2.3
15	89.0 ± 1.2	70.8 ± 1.6
20	92.1 ± 1.7	72.4 ± 1.3

Table B.5 Amount of COOH group on linear PAA brushes as a function of molecular weight for targeted DP = 200

Time (h)	$\overline{M}_n$	Amount of COOH x 10^{-9} (mol/cm^2)
5	11,886	0.69 ± 0.03
10	22,660	1.34 ± 0.02
15	26,826	1.43 ± 0.02
20	29,359	1.63 ± 0.01

Table B.6 Advancing (Θ_A) and receding (Θ_R) water contact angles of PAA brushes versus polymerization time for targeted DP = 200

Time (h)	Water contact angle (degree)	
	Θ_A	Θ_R
0	92.1 ± 1.7	72.4 ± 1.3
5	61.4 ± 0.5	51.2 ± 1.8
10	53.0 ± 1.2	43.0 ± 1.8
15	40.5 ± 1.5	30.6 ± 1.7
20	22.4 ± 1.5	17.0 ± 0.9

Table B.7 Amount of N-cadherin mimic cyclic peptide immobilized on PAA brushes containing substrates determined by SPR as a function of N-cadherin mimic cyclic peptide concentration

N-cadherin mimic cyclic peptide concentration (mg/ml)	Amount of *N*-cadherin mimic cyclic peptide (ng/cm^2)
0.1	63.3 ± 0.5
0.5	78.8 ± 1.2
0.8	92.1 ± 1.0
1.0	106.3 ± 2.7

Table B.8 Advancing (θ_A) and receding (θ_R) water contact angles of surface modified glass coverslips

Silica surface-tethered sample	Water contact angles (degree)	
	θ_A	θ_R
initiator	70.0 ± 0.9	60.2 ± 1.3
Pt-BA	91.0 ± 2.9	75.6 ± 1.7
PAA	21.3 ± 1.8	10.2 ± 1.8
PAA-NHS	76.9 ± 2.5	60.3 ± 1.2
PAA-BSA	68.3 ± 1.9	51.7 ± 1.1
PAA-(N-cadherin)	62.4 ± 1.0	52.8 ± 1.3

Table B.9 Number of mouse neural progenitor cells on substrates determined by hemacytometer after incubation for 4 days in at 37 °C

Sample	Number of cells ($\times 10^6$ cells/mL)
Glass coverslips (control)	1.47 ± 0.25
Glass coverslips coated with laminin	3.57 ± 0.25
Glass coverslips-PAA brushes-immobilized with N-cadherin mimic cyclic peptide	3.03 ± 0.31

APPENDIX C

Toluidine blue O assay

Toluidine blue O assay is a method used for determination of the amount of carboxyl groups. The carboxyl groups of PAA brushes can form a complex with toluidine blue o. The absorbance of the solution containing the desorbed complex was measured at 633 nm. The COOH content was obtained from a calibration plot of the optical density versus dye concentration which is displayed in Figure C-2.
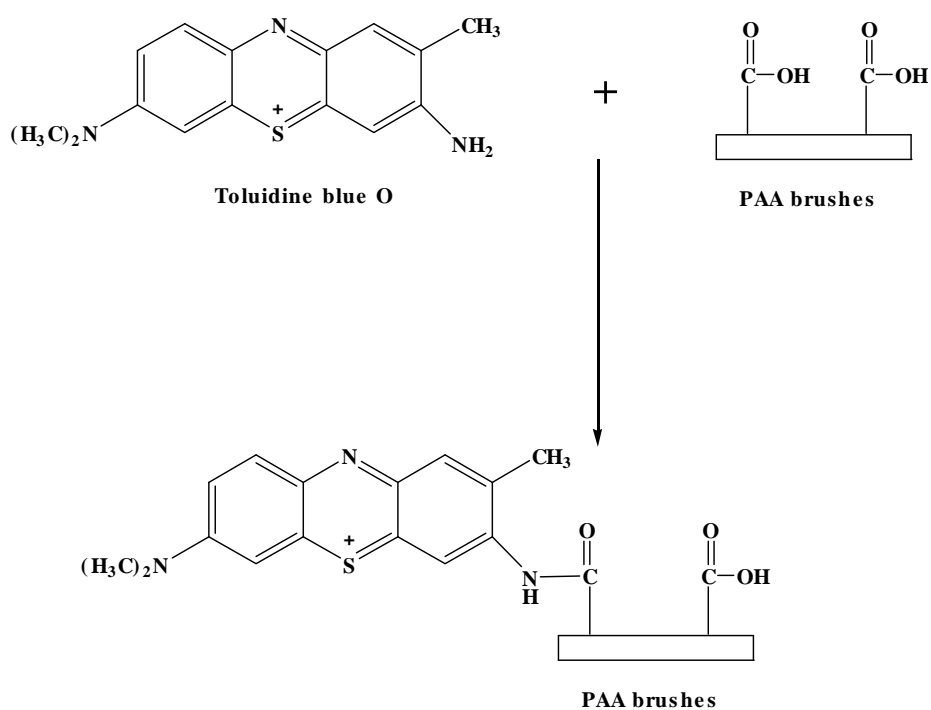
Figure C.1 Formation of toluidine blue O complex with carboxyl group.
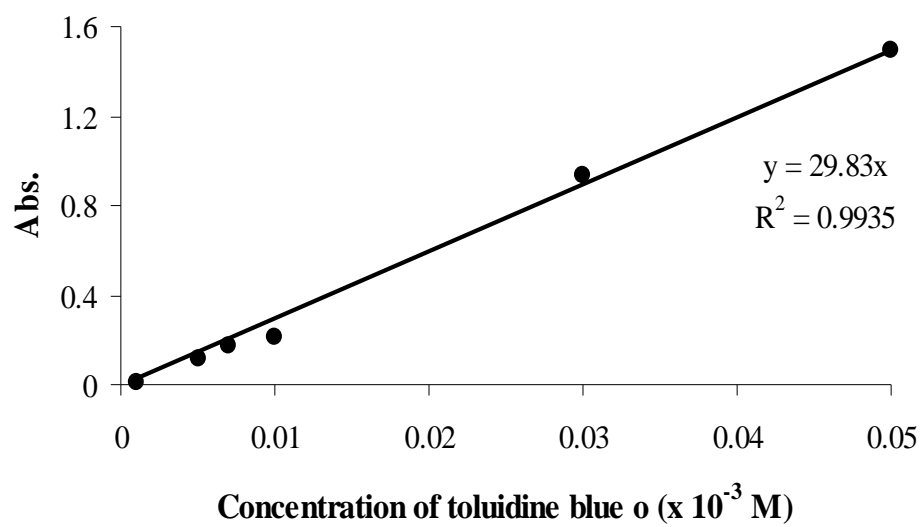
Figure C.2 Calibration curve of UV absorbance as a function of toluidine blue o concentration.

APPENDIX D
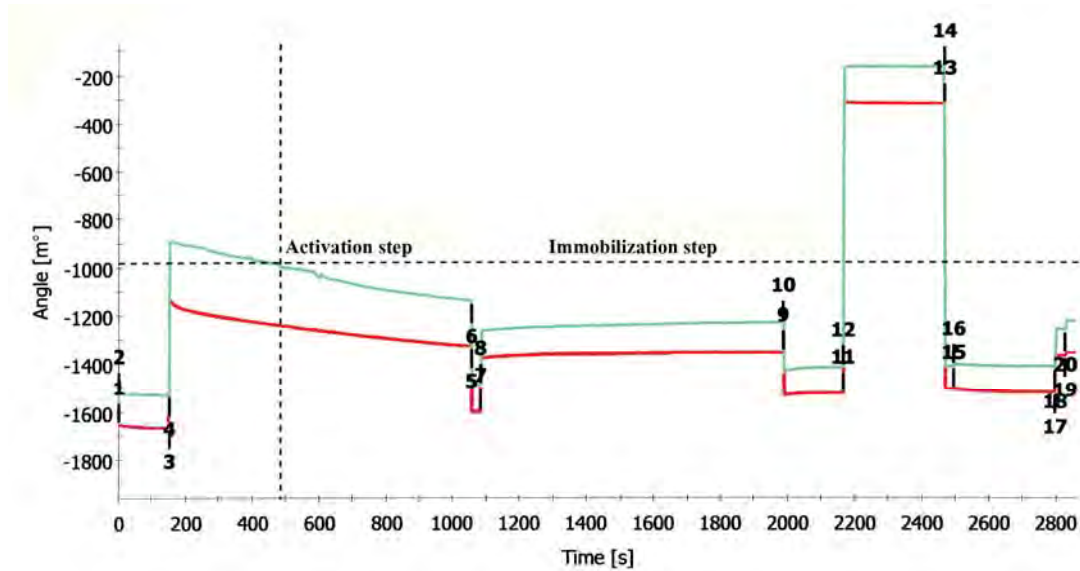
Figure D.1 SPR response of PAA brushes after EDC/NHS activated and immobilization of N-cadherin mimic cyclic peptide

The measured SPR angle shifts during the activation and immobilization steps can be converted into mass uptakes, using following equation D.1.

$$Amount\ of\ mass\ uptake\ (ng/cm^2) = \frac{SPR\ angle\ shift\ (m°) \times 100\ (ng/cm^2)}{120\ (m°)} \qquad (D.1)$$

Table D.1 SPR angle shift and amount of immobilized NHS on PAA brushes as a function of EDC/NHS activation time
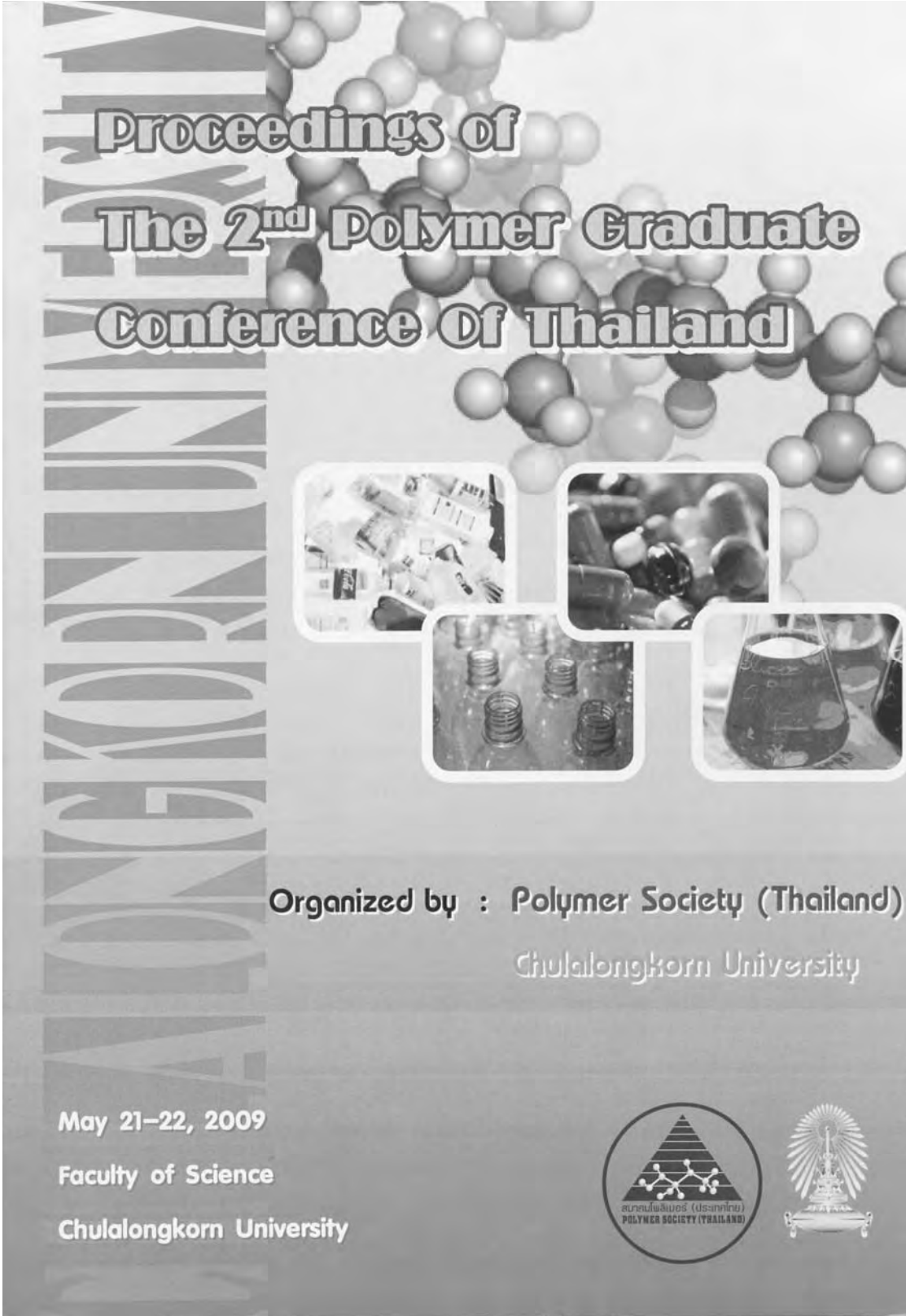
Activation time (min)	SPR angle shift (m°)	Amount of immobilized NHS (ng/cm^2)
15	64.1	53.4
	76.0	63.3
	66.9	55.7
30	72.5	60.4
	64.3	53.6
	69.5	57.9

Table D.2 SPR angle shift and amount of immobilized N-cadherin mimic cyclic peptide on PAA brushes as a function of immobilization time

Immobilization time (min)	SPR angle shift (m°)	Amount of N-cadherin mimic cyclic peptide (ng/cm^2)
15	75.9	63.3
	75.3	62.8
	76.8	64.0
30	74.0	61.7
	79.2	66.0
	74.3	61.9

Table D.3 Amount of N-cadherin mimic cyclic peptide immobilized on PAA brushes containing substrates determined by SPR as a function of N-cadherin mimic cyclic peptide concentration

N-cadherin mimic cyclic peptide concentration (mg/ml)	SPR angle shift (m°)	Amount of N-cadherin mimic cyclic peptide (ng/cm^2)
0.1	75.9	63.3
	75.3	62.8
	76.6	63.8
0.5	93.4	77.8
	91.6	76.3
	95.3	79.4
0.8	110.5	92.1
	111.8	93.2
	109.7	91.4
1.0	123.9	103.3
	127.6	106.3
	121.1	100.9

APPENDIX E

Poly(acrylic acid) Brushes: Synthesis via ARGET ATRP and Biomolecule Immobilization

Sasithon Rodtamai and Voravee P. Hoven*

Organic Synthesis Research Unit, Department of Chemistry, Faculty of Science,

Chulalongkorn University, Bangkok, 10330 Thailand

*Tel: +66-22-187627 ext 102, Fax: +66-2218-7598, E-mail: vipavee.p@chula.ac.th

Abstract

Surface-tethered poly(acrylic acid) (PAA) brushes were synthesized by surface-initiated polymerization of *tert*-butyl acrylate from silica surface via activator regenerated by electron transfer – atom transfer radical polymerization (ARGET ATRP) process followed by hydrolysis using methanesulfonic acid. The success of polymer brushes formation was monitored by gel permeation chromatography, water contact angle measurements, and ATR-FTIR. The covalent immobilization of BSA, a model biomolecule, to the carboxyl groups of PAA brushes was subsequently performed in order to determine the applicability of the surface-functionalized PAA brushes towards bio-related applications.

Keywords: PAA, Polymer brushes, ARGET ATRP, Biomolecule, Surface modification

1. Introduction

Surface-initiated polymerization (SIP) in combination with controlled radical polymerization (CRP) has been recently recognized as an efficient and powerful tool for generating surface-tethered polymer brushes that are potentially useful for a number of high-value technologies, ranging from biotechnology to advanced microelectronics. Due to the versatility of the process towards a wide range of readily available monomers, both chemical and physical properties of surface-tethered polymer brushes can be broadly tailored, in particular, the functional group density of the surface which can be varied as a function of the chain length and molecular weight.[1]

Atom transfer radical polymerization (ATRP) has been regarded as one of the most successful CRP process. Despite its great potential, conventional ATRP still suffers from the demand for rigorously deoxygenated condition as well as the catalyst removal. Such limitation has been recently overcome by an addition of minute quantity of an active copper catalyst with an excess amount of appropriate reducing agent [2-3]. Since the activators (Cu (I) species) can be continuously regenerated by electron transfer, this approach is thus named ARGET ATRP. This process is highly desirable for large-scale production because the reaction can be carried out in the presence of limited amount of air so the stringent deoxygenation is no longer necessary. The fact that only small amount of catalyst (at the level of ppm) is required apparently satisfies the bio-related applications of which the trace amount of catalyst may be detrimental.

Herein, we report, for the first time, the synthesis of poly(*t*-butyl acrylate) (P*t*-BA) brushes

and its subsequent hydrolyzed form, poly(acrylic acid) (PAA) brushes using the ARGET ATRP. Unlike the previous work reported on the systems of polystyrene [2] and poly (n-butyl acylate) [3], Me$_6$TREN, a more reactive ligand for copper catalyst was used. Since our ultimate goal is to employ this surface-functionalized poly(acrylic acid) brushes as substrates for cell culturing and tissue engineering applications, the reactivity of the carboxyl moieties along the chains of the PAA brushes were tested against immobilization of bovine serum albumin (BSA), a model representing biomolecules.

2. Experimental

2.1 Materials

t-BA (98%, Aldrich) was extracted tree times with 5% aqueous NaOH and then washed with distilled water before being dried over Na(SO$_4$)$_2$. 3-(Chlorodimethylsilyl) propyl 2-bromo-2-methylpropanoate (I) was synthesized as previously described [4]. The synthetic method of tris (2-(dimethylamino) ethyl) amine (Me$_6$TREN) was modified from that was reported by Queffelec et.al [5]. CuBr$_2$ (Fluka), ethyl α-bromoisobutyrate (EBiB, 97%, Fluka), tin(II) 2-ethylhexanoate (Sn(EH)$_2$, 95%, Sigma aldrich), 1-(3-dimethylaminopropyl)-3-ethylcarbodiimide hydrochloride (EDCl, Fluka), N-hydroxysuccinamide (NHS, Fluka) were used as received.

2.2 Preparation of poly(acrylic acid) brushes

The silica substrates, freshly cleaned with Piranya solution (conc.H$_2$SO$_4$: 30%H$_2$O$_2$ = 7:3 (v/v)) at room temperature, were tethered with surface-grafted initiator (I) under nitrogen atmosphere (Scheme 1). CuBr$_2$, acetone,

Me$_6$TREN and t-BA were added to a vial with a magnetic stirring bar. The mixture was then stirred at ambient temperature until it became homogeneous (approximately 10 min) followed by an addition of EBiB, the "sacrificial" initiator. The silica-tethered initiator (II) held in a slotted hollow glass cylinder was immersed in the vial that was later sealed with a rubber septum. The well-mixed solution of Sn(EH)$_2$, acetone and Me$_6$TREN in a separated vial was then added via syringe to the reaction vial carrying the silica substrates. The volume of air in the reaction vial above the solution was fixed at 10.8 mL. The polymerization was allowed to proceed at ambient temperature. After a set reaction time, the silica substrates were removed and rinsed with THF. To remove the untethered P(t-BA), the silica substrates were placed in a soxhlet extractor and extracted with THF for 24 h and dried in vacuo. To remove the t-butyl groups by hydrolysis, the substrates tethered Pt-BA brushes (III) were treated with a mixture of methanesulfonic acid in dichloromethane at ambient temperature for 30 min to prepare surface-tethered PAA brushes (IV). The substrates were removed, rinsed with dichloromethane, and then dried in vacuo.

2.3 Immobilization of biomolecules to carboxyl groups of poly(acrylic acid) brushes

Silica substrate bearing PAA brushes (IV) were immersed in an aqueous solution of EDCl (0.05 M) and NHS (0.1 M) and then stirred for 30 min. The substrate were removed from the solution and rinsed with deionized water. Then, the substrates (V) were immersed in a solution of BSA (1mg/mL) in phosphate-buffered saline (PBS, pH 7.4). After 1 h. the substrates(VI) were thoroughly rinsed with PBS solution.
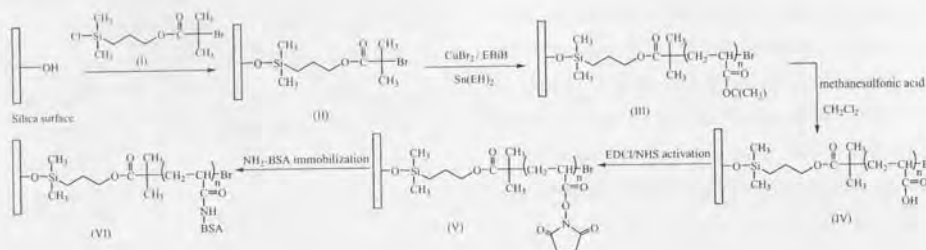
Scheme 1. Stepwise synthetic route for preparation of polymer brushes and biomolecule immobilization.

2.4. Characterization

Dynamic advancing (θ_A) and receding (θ_R) contact angles of the functionalized silica were measured using a contact angle goniometer model 100-00 and a Gilmont syringe with a 24-gauge flat-tipped needle (Ramé-Hart, Inc.). ATR-FTIR spectra of the surface-modified silica particles were recorded with a FT-IR spectrometer (Nicolet), model system 6700 with using DLa TGS detector. The spectra were collected at a resolution of 4 cm^{-1} and 16 scans.using diamond ATR IR accessory.

Molecular weight and molecular weight distribution (Mw/Mn) of the Pt-BA in solution were determined by gel permeation chromatography (GPC) having Water E600 column connected to the RI detector, using THF as eluent. The flow rate was set at 1 mL/min. Narrow PS standards were used for creating a calibration curve.

3. Results and discussion

The growth of polymer chains formed by the free initiator in solution can be used to monitor the surface-initiated polymerization process. To seek for the optimal condition that yields polymer with well-controlled molecular weight and molecular weight distribution, the

effect of mole ratio of Sn(EH)$_2$:Me$_6$TREN and reaction time were investigated. According to the results shown in Figure 1, the molar ratio of Sn(EH)$_2$:Me$_6$TREN of 10:1 was considered as the optimal value because it gave reasonably high Mn with narrow molecular weight distribution (close to 1). Further reduction of the amount of Me$_6$TREN by increasing the ratio to 15:1 led to a negative impact on the livingness of the polymerization. It should be emphasized that ones try to consume the least amount of Me$_6$TREN in order to minimize the expense from the costly ligand.
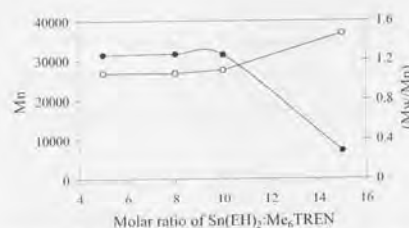
Figure 1. Mn ($\bullet$) and Mw/Mn (o) of Pt-BA as a function of Sn(EH)$_2$:Me$_6$TREN molar ratio.

The data shown in Figure 2 suggested that 15-20 h is sufficiently long for the polymerization to reach the completion while the molecular weight distribution remained low, being

close to 1.0, the ideal target of living polymerization. It should be noted at this point that the obtained Mn (~31,000) was somewhat higher than the target one (Mn = 25,634) of which the targeted degree of polymerization (DP) is 200. This characteristic seems to be typical and has been also observed by others [3].
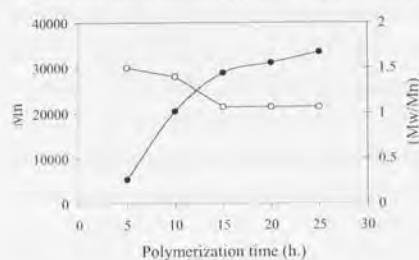

Figure 2. Mn (•) and Mw/Mn (o) of P*t*-BA as a function of time.

Table 1 outlines the water contact angles (θ_A/θ_R) of functionalized silica surface. The surface became hydrophobic after the attachment of intiator as opposed to the cleaned silica surface (θ_A/θ_R = 21.1/8.5). Upon the formation of P*t*-BA brushes, the water contact angle increased even further. The decreasing of θ_A/θ_R after the hydrolysis step was attributed to the hydrophobic *tert*-butyl groups of P*t*-BA being converted to the hydrophilic carboxyl groups of PAA brushes.

Table 1. Advancing (θ_A) and Receding (θ_R) water contact angles of functionalized silica surfaces

Silica surface-tethered sample	Water contact angles (degree)	
	θ_A	θ_R
initiator	61.38 ± 1.7	44.75 ± 2.6
P*t*-BA	91.02 ± 2.9	54.26 ± 1.6
PAA	21.3 ± 1.8	10.2 ± 1.7

Figure 3. ATR-FTIR spectra of surface-functionalized silica particles: (a) P*t*-BA brushes, (b) PAA brushes, (c) activated PAA brushes, and (d) activated PAA brushes-BSA.

ATR-FTIR spectra of the surface-functionalized silica particles are displayed in Figure 3. The carbonyl stretching at 1728 cm⁻¹ shifted slightly to 1718 cm⁻¹ after P*t*-BA brushes were transformed to PAA brushes. The shoulder peaks at 1736 cm⁻¹ and 1811 cm⁻¹ assigned to the carbonyl stretching of succinimidyl ester in Fig 3c. indicated the successful activation of carboxyl groups by EDCI/NHS. The immobilization of BSA to the activated PAA brushes can be verified by the appearance of N-H bending (Amide II) at 1550 cm⁻¹ in Fig. 3d.

4. Conclusion

Poly(acrylic acid) (PAA) brushes were successfully grafted onto silica surface by ARGET-ATRP of *t*-BA followed by hydrolysis. The molecular weight and molecular distribution could be regulated by the controlling of the preparation condition, e.g. polymerization time and molar ratio of Sn(EH)₂: Me₆TREN. Moreover, the BSA, a selected model for biomolecule can be further immobilized on the grafted PAA brushes via the activation by EDCI/NHS demonstrating the desirable reactivity of the carboxyl groups along the the chains of PAA brushes towards chemical functionalization.

References

[1] Akkahat, P. Attachment of biotin on silicon surface-tethered poly (acrylic acid) brushes), Master's thesis, Petrochemistry and Polymer Science, Faculty of Science, Chulalongkorn University., **2005.**

[2] Jukubowski, W., Min, K., Matyjaszewski, K. Macromolecules, **39**, 39-45 (2006).

[3] Matyjaszewski, K., Dong, H., Jukubowski, W., Pietrasik, J., Kusumo, A. Langmuir, **23**, 4528-4531 (2007).

[4] Ramakrishnan, A., Dhamodharan, R., Ruhe, J. Macromol. Rapid Commun., **23**, 612-616 (2002).

[5] Queffelec, J., Gaynor, G. S., Matyjaszewski, K. Macromolecule, **33**, 8629-8639 (2000).

PROGRAM

Organic and Polymer Solar Cells
(satellite meeting sponsored by DIISR ISL International Consortium on Organic Solar Cells)

Inaugural Australian Microplasma Workshop
(satellite meeting sponsored by DIISR)

2nd International Symposium on Ultimate Stability
of Nanostructured Polymers and Composites

PPC11 6 – 10 DECEMBER
CAIRNS CONVENTION CENTRE,
CAIRNS, AUSTRALIA
www.ppc11.org

POSTER SESSION 2

TUESDAY 6.00 - 8.00 PM TRADE EXHIBITION AREA CONT.

P325   Effect of cross-linker concentration on porosity, surface morphology and thermal behavior of calcium alginates prepared from algae (Undaria pinnatifida)
Tara Sankar Pathak, Jung-Ho Yun, *Se-Jong Lee*, Ki-Jung Paeng

P326   In situ crosslinkable hydrogels for tissue engineering and drug delivery
Kyung Min Park, Young Min Shin, Yoon Ki Joung, Heung Soo Shin, Seung Jin Lee, Ki Dong Park

P327   Inorganic salts effect on the poly(vinyl alcohol) cryogels properties
Silvia Patachia, Claudia Florea, Christian Friedrich, Yi Thomann, Camelia Scarneciu

P328   ARGET ATRP of 2-hydroxyethyl methacrylate using ascorbic acid as a reducing agent
Stefan Paterson, Murray Baker, Traian Chirila, Imelda Keen, David Brown, Andrew Whittaker

P329   Biologically functional scaffolds for treating spinal cord injury
Jerani Pettikiriarachchi, Clare Parish, John Forsythe, David Nisbet

P330   Thickness Effects of Switchable pNIPAAm Coatings on Cell Detachment
Ana Phan, David Haylock, John Forsythe, Helmut Thissen

P331   Supramolecular Networks Composed of Polymer Chains and Wormlike Micelles
Olga Philippova, V.S. Molchanov

P332   Poly(acrylic acid) Brushes: Synthesis via ARGET ATRP and Biomolecule Immobilization for Their Application in Cell Culture
Sasithon Rodtamai, Nipan Israsena Na Ayudhaya, Voravee Hoven

P333   Preparation of branched methacrylic copolymers: comparison between RAFT and ATRP and effect of varying the monomer concentration
Julien Rosselgong, Steven P Armes, William Barton, David Price

P334   The Australian National Deuteration Facility
Peter Holden, *Rob Russell*, Paramjit Bansal, Tamim Darwish, Anthony Duff, Christopher Garvey, Marie Gillon, Vanessa Lake, Emily Luks, Greta Moraes, Agata Rekas, Karyn Wilde

P335   ESR study of carboxymethyl cellulose radicalformed by OH radical attack
Seiichi Saiki, Naotsugu Nagasawa, Akihiro Hiroki, Norio Morishita, Masao Tamada, Hisaaki Kudo, Yosuke Katsumura

P336   Synthesis of heterotactic poly(methyl methacrylate) by free radical polymerization of catechol dimethacrylate
Yoichi Saito, Reiko Saito

P337   Polymerization behavior of methacrylic group on template polymerization with waterwheel-like cyclic novolac as a template
Yoichi Saito, Reiko Saito

P338   Application of hydrogen gas sensor using gel containing ionic liquid as solvent
Miki Saito, Hideki Myobudani, Takeshi Yamauchi, Norio Tsubokawa, Shuji Harada

P339   DSC Investigations of Absorbed Water for Evaluating the Microstructure of Elongated Polyamide 6
Eiichi Sakai, Makoto Kawagoe

P340   Nanoscale Surface Structures of Slide-Ring Gels Investigated by Atomic Force Microscopy
Yasuhiro Sakai, Yasushi Okumura, Kohzo Ito

P341   Synthesis of Substituted Polyacetylenes with Terphenyl Moieties in the Side Chain
Hideaki Sasaki, Hiroaki Kouzai

P342   Permeability and selectivity of benzene vapor and water vapor in silicon- or fluorine-containing polymer membranes
Shuichi Sato, Maiko Suzuki, Shinji Kanehashi, Kazukiyo Nagai

P343   Polymer nanocapsules for antibacterial material properties
Véronique Schwartz, Peter Cerniak, Katja Bender, Toby Jenkins, Renate Förch, Katharina Landfester

P344   Water-compatible molecularly imprinted polymer for solid phase extraction of 1-methyladenosine as biochemical marker
Giuseppe Vasapollo, Sonia Scorrano, *Roberta Del Sole*

P345   Energy Dissipating Behavior under Large Amplitude Shear Stress of Polyborosiloxane Composite
Nispa Seetapan, Asira Fuongfuchat, Doungporn Sirikittikul

P346   Hybrid Hydrogels with Nanogel-coated Liposomes as Cross-linking domain
Yurina Sekine, Yuki Moritani, Nobuyuki Morimoto, Kazunari Akiyoshi

P347   Coaxial Electrospinning of Regenerated Silk Fibroin/Sericin Aqueous Solutions
Yichun Hang, Yaopeng Zhang, Huili Shao, Xuechao Hu

P348   The Electrospinnability of Regenerated Silk Fibroin/Sericin Aqueous Solutions and the Structures of Resultant Fibers
Yichun Hang, Yaopeng Zhang, Huili Shao, Xuechao Hu

Poly(acrylic acid) Brushes: Synthesis via ARGET ATRP and

Biomolecule Immobilization for Their Application in Cell Culture

Sasithon Rodtamai[1,2], Nipan Israsena Na Ayudhaya[3] and Voravee P. Hoven[1]*

[1]Organic Synthesis Research Unit, Department of Chemistry, Faculty of Science
[2]Center for Petroleum, Petrochemicals, and Advanced Materials
[3]Stem Cells and Cell Therapy Research Unit, Department of Pharmacology,
Faculty of Medicine
Chulalongkorn University, Phayathai Road, Pathumwan, Bangkok 10330, Thailand
E-mail: poadea@hotmail.com, vipavee.p@chula.ac.th*

Atom transfer radical polymerization (ATRP) has been regarded as one of the most successful controlled living polymerization. Despite its great potential, the conventional ATRP still suffers from the demand for rigorously deoxygenated condition as well as the catalyst removal. Such limitation has been recently overcome by an addition of minute quantity of an active copper catalyst with an excess amount of appropriate reducing agent.[1,2] Since the activators (Cu (I) species) can be continuously regenerated by electron transfer, this approach is thus named ARGET ATRP. Herein, we report, the synthesis of poly(t-butyl acrylate) (Pt-BA) brushes and its subsequent hydrolyzed form, poly(acrylic acid) (PAA) brushes using the ARGET ATRP (Figure 1). Since our ultimate goal is to employ this surface-functionalized PAA brushes as substrates for cell culturing and tissue engineering applications, the reactivity of the carboxyl moieties along the chains of the PAA brushes were tested against immobilization of selected biomolecules.
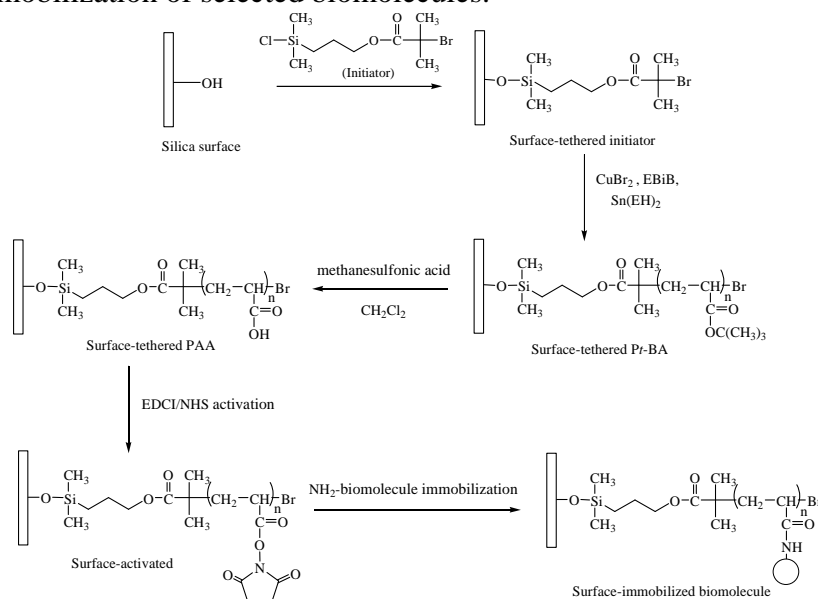
Figure 1: Stepwise synthetic route for preparation of PAA brushes and biomolecule immobilization

Upon using the optimized condition (Sn(EH)$_2$:Me$_6$TREN = 10:1, time = 15 h) and the monomer:initiator of 200:1, the Pt-BA having Mn of~31,000 (target Mn = 25,634) was obtained with polydispersity close to 1 suggesting that the reaction is living. Table 1 lists the water contact angles (θ_A/θ_R) of functionalized silica surface. The surface became hydrophobic after the attachment of initiator as opposed to the cleaned silica surface (θ_A/θ_R ~0). Upon the formation of Pt-BA brushes, the θ_A/θ_R increased even further. The decreasing of θ_A/θ_R after the hydrolysis step was

attributed to the hydrophobic *tert*-butyl groups of P*t*-BA being converted to the hydrophilic carboxyl groups of PAA brushes.

Table 1. *Advancing (θ_A) and receding (θ_R) water contact angles of functionalized silica surfaces*

Silica surface-tethered sample	Water contact angles (degree)	
	θ_A	θ_R
initiator	61.38 ± 1.7	44.75 ± 2.6
P*t*-BA	91.02 ± 2.9	54.26 ± 1.6
PAA	21.3 ± 1.8	10.2 ± 1.7

ATR-FTIR spectra of the surface-functionalized silica particles are displayed in Figure 2. The carbonyl stretching at 1728 cm^{-1} shifted slightly to 1718 cm^{-1} after P*t*-BA brushes were transformed to PAA brushes. The shoulder peaks at 1736 cm^{-1} and 1811 cm^{-1} assigned to the carbonyl stretching of succinimidyl ester in Figure 2(c) indicated the successful activation of carboxyl groups by EDCI/NHS. The immobilization of BSA to the activated PAA brushes can be verified by the appearance of N-H bending (Amide II) at 1550 cm^{-1} in Figure 2(d).
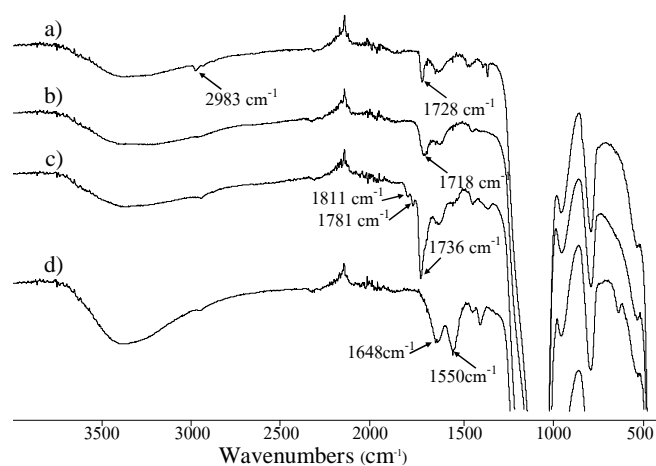

Figure 2: ATR-FTIR spectra of surface-functionalized silica particles: (a) Pt-BA brushes, (b) PAA brushes, (c) activated PAA brushes, and (d) activated PAA brushes-BSA

The ability of the surface-tethered PAA brushes to bind with a specific biomolecule, a cyclic peptide having sequence mimicking binding motives of *N*-cadherin,[3] a protein that was found to promote axonal outgrowth of nerve cells was also tested. The investigation based on surface plasmon resonance technique suggested that 0.26 ± 0.04 nmol/cm^2 can be bound to the activated carboxyl groups of PAA brushes.

References
[1] Jukubowski, W.; Min, K.; Matyjaszewski, K. *Macromolecules* **2006**, 39, 39-45.
[2] Matyjaszewski, K.; Dong, H.; Jukubowski, W.; Pietrasik, J.; Kusumo, A. *Langmuir* **2007**, 23, 4528-4531.
[3] Wiliams, G.; William, J. E.; Doherty, P. *Biol. Chem.* **2002**, *277*, 4361-4367.

การประชุมวิชาการ

คณะวิทยาศาสตร์ จุฬาลงกรณ์มหาวิทยาลัย
ครั้งที่ 18 ประจำปี 2553
วันที่ 11 - 12 มีนาคม 2553

The Science Forum 2010
Faculty of Science
Chulalongkorn University

Adsorption of light gases in MOF-5 studied by molecular dynamic simulations

Tanawut Ploymeerusmee[1], Oraphan Saengsawang[2], Duangamol Nantasri[3] and Supot Hannongbua[2,3]

[1]Petrochemical Program, Faculty of Science,
[2]Computational Chemistry Unit cell (CCUC), Department of Chemistry, Faculty of Science,
[3]Department of Chemistry, Faculty of Science, Chulalongkorn University;
Tel: 0-2218-7602, e-mail: supot.h@chula.ac.th

As known, seeking for new materials with high surface area and capacity becomes a effective area for scientists in the developing of gas storage applications. Metal organic frameworks (MOFs) which consist of zinc oxo acetate clusters and different organic aromatic linkers provide a diversity sort of MOFs in isoreticular metal organic frameworks (IRMOFs) series. IRMOF-1, specifically, MOF-5 was introduced by Yaghi with surface area of approximately 2900 m^2/g and was found to fulfill such requirement of a primary target for gas storage. In this study, adsorption behavior and structural properties of light gases, i.e., the CO_2 and C_2H_4, were investigated using molecular dynamic (MD) simulations. The MD box of $51.78 \times 51.78 \times 51.78$ $Å^3$ of the MOF-5 lattice with the loading of 8, 64, 128, 256, 512 of guest molecules per simulation cube (MPC) were performed at 300 K. The obtained structural data of CO_2 are in agreement with those found from quantum calculations in which CO_2 prefers to absorb at the MOF-5 metal cluster site. Interestingly, at MPC=512, the CO_2 was found to form second layer coordinated weakly to fill the rest space around the MOF-5 corner. In addition, the CO_2 and C_2H_4 molecules were observed to point their molecular axis to the metal cluster site of the MOF-5.

Keywords: MOF-5, molecular dynamic simulations, adsorption of light gases

Poly(acrylic acid) brushes: synthesis via ARGET ATRP and biomolecule immobilization for their application in cell culture

Sasithon Rodtamai[1,2], Suttinee Poolsup[3], Nipan Israsena Na Ayudhaya[4] and Voravee P. Hoven[1*]

[1]Organic Synthesis Research Unit, Department of Chemistry, Faculty of Science, Chulalongkorn University;
[2]Center for Petroleum, Petrochemicals and Advanced Materials, Chulalongkorn University;
[3]Program in Biotechnology;
[4]Stem Cells and Cell Therapy Research Unit, Department of Pharmacology, Faculty of Medicine, Chulalongkorn University;
Tel: +66-2218-7627 ext 102,
e-mail: poadea@hotmail.com,
vipavee.p@chula.ac.th

Despite its great potential as a controlled living polymerization, the conventional atom transfer radical polymerization (ATRP) still suffers from the demand for rigorously deoxygenated condition as well as the catalyst removal. Such limitation has been recently overcome by an addition of minute quantity of an inactive copper catalyst (Cu(II)) with an excess amount of appropriate reducing agent. Since the activators (Cu(I)) can be continuously regenerated from the inactive catalyst, this approach is thus named ARGET ATRP. In this research, surface-tethered poly(acrylic acid) (PAA) brushes were synthesized by surface-initiated polymerization of tert-butyl acrylate via ARGET ATRP process followed by acid hydrolysis. The success of polymer brushes formation was monitored by water contact angle measurements, GPC and ATR-FTIR. The covalent immobilization of N-cadherin mimic cyclic peptide to the carboxyl groups of PAA brushes was subsequently performed in order to determine the applicability of the surface-functionalized PAA brushes towards cell culture applications.

Keywords: PAA, polymer brushes, ARGET ATRP, surface modification

VITAE

Miss Sasithon Rodtamai was born on November 2th, 1984 in Samutsakhon, Thailand. She received a Bachelor Degree of Science, majoring in Chemistry from Faculty of Science, Chulalongkorn University in 2006. Since 2007, she has been a graduate student studying Organic Chemistry as her major course at Department of Chemistry, Faculty of Science, Chulalongkorn University. During her studies towards the Master's degree, she was awarded by Chulalongkorn University Graduate Scholarship to Commemorate the 72nd Anniversary of His Majesty King Bhumibol Adulyadej during 2007-2008 and Center for Petroleum, Petrochemicals and Advanced Materials in during November 2009 – February 2010.

Her present address is 613/1 Paekong Rd., Kratumban, Samutsakhon, Thailand 74110, Tel. (03)-4472152.

Presentation in Conference:

May 2009	The 2nd Polymer Graduate Conference of Thailand, Faculty of Science, Chulalongkorn University, Bangkok, Thailand, Poster Presentation
December 2009	The 11th Pacific Polymer Conference, Cairns, Australia, Poster Presentation
March 2010	The 18th Science Forum, Faculty of Science, Chulalongkorn University, Bangkok, Thailand, Oral Presentation